UNIVERSITÀ DI PARMA

UNIVERSITA' DEGLI STUDI DI PARMA

DOTTORATO DI RICERCA IN

Scienza e Tecnologia dei Materiali

CICLO XXXVI

Design and Development of Eco-sustainable Biomaterials for Healthcare Applications

Coordinatore:
Chiar.mo Prof. Enrico Dalcanale

Tutore:
Monica Sandri, PhD

Co-tutore:
Elisabetta Campodoni, PhD

Dottoranda: *Chiara Artusi*

Anni Accademici 2020/2021 – 2022/2023

Nothing is created,
nothing is destroyed,
everything is transformed.

Antoine-Laurent de Lavoisier

Design and Development of Eco-sustainable Biomaterials for Healthcare Applications

All or part of this work has been or will be published as scientific papers in peer-reviewed scientific journals.

Table of Contents

Aim

This work has been focused on the design and development of polymeric and hybrid biomaterials applicable in the healthcare sector following the principles of eco-sustainability and circular economy. Nowadays there is a growing need to develop healthcare devices composed of renewable resources that are inexpensive, but above all easy to dispose of and which do not harm the environment, as well as being safe and effective for humans. In this context, the aim of this work was to exploit biocompatible and biodegradable materials from natural sources and green biomimetic processes to develop new multifunctional biomaterials capable of responding to specific healthcare needs. Specifically, two eco-sustainable biomaterials have been developed, one fully polymeric and the other of hybrid composition, which have highlighted considerable potential in the fields of mechanical ventilation and of cosmetics with low environmental impact.

The first material is a polymeric aerogel made of gelatin and chitosan, developed through a green-chemistry process optimized to obtain an eco-sustainable medical device capable of guaranteeing, during intensive care or anesthesia, the normal levels of humidity, heat and filtration of the trachea, when the patient's upper airways are by-passed. In detail, raw materials derived from food waste were selected to create a biodegradable disposable filter with reduced environmental impact and low cost. Furthermore, the freeze-drying and cross-linking processes were optimized to develop a stable 3D material with high filtration efficiency that is scalable for industrialization.

The second material is a hybrid compound consisting of a mineral phase, a hydroxyapatite doped with titanium ions, nucleated on a biopolymeric matrix of alginate through a nature-inspired biomineralization process, demonstrating reflecting properties adapt for the formulation of eco-sustainable sunscreens. In particular, in addition to adequately protecting the skin from UV radiation and eliminating the undesirable effects caused by the typical components of commercial sunscreens (photocatalytic effect, irritation, penetration of nanoparticles, etc.), we focused on the development of a biocompatible UV filter which once formulated into a cream and applied to the skin, does not release substances harmful for marine ecosystems or humans.

Finally, an all-round characterization of the key aspects of each material was carried out, highlighting the main achievements and obstacles, as well as the main overall aspects that could be improved.

CHAPTER 1

Introduction

Part of the content of this chapter has been published as Phd Thesis of Savini E. "Design and Development of Biomineralized Nanostructured Devices from natural sources for Biomedical Application" 2016, Phd Thesis of Campodoni E. "Design and development of bio-hybrid multifunctional material for regenerative medicine" 2018, PhD Thesis of Montanari M. "Design and Development of Printable and Injectable Bio-Hybrid Inks for Tissue Engineering and Regeneration" 2022, PhD Thesis of Carella F. "Synthesis and Characterization of Nanostructured Calcium Phosphate Matrices for Biomedical and Environmental Applications" 2022.

1.1. Biomaterial in the context of circular economy

In the twenty-first century, where technological progress coordinates our lives, the main economic and social challenge is to counteract the negative effects of the progressive industrialization on natural ecosystems. The economic development that accompanies this trend is linked to the increased production not only of consumer goods, but also of specialized equipment that are difficult to remanufacture, such as medical equipment. The necessary actions to reduce the production of industrial materials whose waste is difficult to recycle are increasingly evident, especially in the face of the serious environmental and financial crisis that the whole world is going through. Studying and researching innovative eco-sustainable materials, especially for biomedical applications, is now a priority goal of our age to increasingly orient industry and society towards a circular economy context.[1]

Although it is a concept recently applied by our society, already in 1960, the term *circular economy* began to appear with Kenneth Boulding, a famous English economist who wrote: "Man must find his place in a cyclical ecological system which is capable of continuous reproduction of material form even though it cannot escape having inputs of energy".[2]

The term circular economy is used to describe an economy that has no impact on the environment; rather, it restores the damage done in the extraction of resources, while ensuring that there is little waste throughout the production process and the life of the product. It can be described as a closed energy system in which economy and environment are in close contact, where the principles of reducing, reusing, and recycling materials are emphasized to minimize waste generation, environmental impact and maximize the value of resources.[3,4] The aim of the circular economy is to treat waste as a valuable raw material and incorporate it into the life cycle of subsequent products to minimize the consumption of materials and energy during production processes and avoid the use of potentially dangerous substances for the consumer

and the environment. Giving "another life" to products thanks to their reintroduction into the production cycle is the founding principle of the circular economy (Figure 1.1).[5]

Figure 1.1. Schematic process of circular economy.

The current energy system is collapsing due to the inequality in the distribution of resources, the increase in global population and the depletion of petroleum-based resources on earth, all prompted by the alarming increase in greenhouse gas emissions that are destroying the environment. Fossil fuels still remain the main source of energy supply for the whole world, but it is estimated that world energy demand will increase by up to 48% by 2040, making it increasingly difficult to satisfy the demand with non-renewable sources. Furthermore, the environmental concern associated with their use has prompted research towards eco-friendly and sustainable alternative energy sources, in order to get out of the only dependence on fossil resources and satisfy global energy demand without damaging the ecosystem.[6]

Among the various sources of renewable energy that we all know such as the sun, wind, water, etc., which are offered to us directly by nature, the attention was focused on the exploitation of the biodegradable fraction of biological industrial and urban waste (animal and vegetable origin) to generate new materials with zero impact. In fact, in line with the principles of the circular economy, bio-based products are made from recycled natural materials and are disposed of by decomposition without emitting CO_2, since CO_2 produced during their use and disposal is offset by the CO_2 absorbed by the plants during photosynthesis. This phenomenon is identified with the term "*carbon neutrality*" to describe an almost zero impact on the

environment, not applicable to materials derived from fossil fuels.[3] In recent decades in fact, one of the sectors that has most accepted the challenge of recycling and eco-sustainability is that of biomaterials.

A biomaterial is defined as a compound that meets the standards of biocompatibility, biodegradability and non-toxicity and it is capable to interact with a living system for a medical purpose, either therapeutic or diagnostic. The properties of biomaterials have evolved over time with the progress that scientific research has made on the subject. In the early 1960s, the term biomaterial identified inert materials that could be used to replace damaged tissues to provide structural support with minimal impact on the patient. Subsequently between 1980 and 1990 we moved on to talking about bioactive materials, capable of promoting a biological reaction in the contact area between the material and the host, increasing the effectiveness of the final medical device. These biomaterials, however, still highlighted significant drawbacks, especially in terms of infections and immunological reactions, so to overcome these obstacles, biodegradable materials capable of degrading and being absorbed by the host were created at the beginning of the 2000s, avoiding the disadvantages of not resorbable medical devices.

This new generation paved the way for the creation, in the second decade of the 2000s, of the so-called "smart biomaterials", characterized by the ability to emulate natural structures and mechanisms, repairing, and regenerating damaged tissues through specific interaction with cells. These biomaterials are the ones now called biomimetic materials.[7,8]

Biomaterials include different types of compounds[1], but in the context of the circular economy, greater attention has been paid to biopolymers, bioceramics, and biohybrid materials, because they meet the requirement of the green-economy concepts, they are easier to dispose, less expensive and ecosustainable.[4] In this regard, the study and development of devices for healthcare sectors, from implantable to disposable accessories, composed of bio-based materials is and will increasingly be the primary strategy of the green economy to limit wasted materials, pollution, and by following the concepts of recycling and recovery with the ingeneration of green-chemistry productive processes.

1.2. Synthetic and natural biopolymers

Directive 2019/904[9] of the European Parliament has imposed the complete replacement of traditional non-degradable materials with biodegradable polymers by 2030 to reduce environmental impact to zero. In fact, more and more often, companies are introducing the use of biopolymeric materials into the industrial supply chain to adapt their production strategies to the needs of more sustainable development. If we think about the tons of non-recyclable waste that are produced and disposed of in landfills or through incineration every year, it is increasingly clear that biomaterials, in particular polymeric ones, will become the basic element for the production of innovative green materials, mostly in biomedical field where attention to biocompatibility and degradability are essential. For example, during the Covid-19 pandemic, it was estimated that 3 million disposable masks were used per minute, which resulted in a significant increase in greenhouse gas emissions and non-degradable waste. Therefore, the exploitation of biodegradable polymers can reduce the damage and costs associated with waste disposal and at the same time, constitute a response to global trends in the production of mainly disposable products.[10]

With this evidence, biopolymers are the materials that for excellence cover all the fundamental characteristics for producing eco-sustainable devices. An exhaustive definition of biopolymer was provided in 2002 by the United States Congress in the Farm Security and Rural Investment Act which defines them as compounds easily degraded, obtained totally or in significant part, from biological products or from renewable sources such as agricultural materials (plant, animal and marine) or forest materials.[11,12] They can be obtained directly from plant or animal sources present in nature, but can also be chemically synthesized from fats, amino acids, proteins or vegetable oils, for this reason they show some crucial differences and are distinguished in synthetic and natural polymers (Figure 1.2).

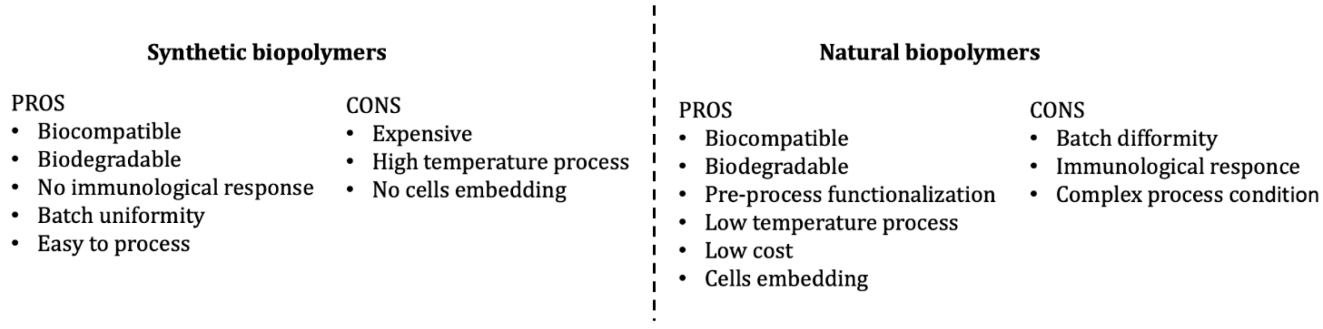

Figure 1.2. Main features of synthetic and natural biopolymers.

Synthetic biopolymers can be obtained through fermentation of microorganisms or chemical synthesis starting from monomers derived from fossil or renewable sources. They have the advantage of being easily workable and showing uniformity between produced batches, but at the same time they are very expensive. They are mainly used in the packaging sector to reduce the use and production of non-degradable plastic waste, but the biomedical and healthcare sectors also make extensive use of them.[13] In particular, synthetic biopolymers show a minimal risk of inducing an immunological response when they come into contact with a tissue, even if their processing at high temperatures limits their functionalization and therefore the incorporation of cells.[14]

The main synthetic biopolymers include polycaprolactone (PCL), an aliphatic and semi-crystalline polymer which has high toughness and mechanical resistance with adequate biocompatibility, very useful in the medical field, polyglycolic acid (PGA) and polylactic acid (PLA), both biodegradable aliphatic polyesters and biocompatible materials used for surgical and packaging devices, as well as polyhydroxyalkanoates (PHA, PHB), thermoplastic polymers widely exploited to generate bioplastics.[15–17]

On the other hand, natural biopolymers are obtained from animal or plant resources present in nature or from industrial waste, therefore they are already born as completely biodegradable and above all low-cost and eco-friendly compounds. However, the problem linked to the extraction of these biopolymers from industrial waste or natural matrices is the difficulty to have homogeneity between different batches of the same product and therefore it is necessary to study different processing methods.[18] Unlike synthetic ones, they require very low processing temperatures but more complex processes, furthermore they can cause an immune response if put into contact with the organism. Even natural biopolymers such as synthetic ones find wide sectors of application from packaging to environmental devices for the purification of water and air, but above all recently they are finding space in the biomedical field, since biocompatibility, biodegradability and low cost are the main characteristics requests for medical devices.[17,19,20]

Natural biopolymers, compared to synthetic ones, constitute an important resource for overcoming the limits linked to the eco-sustainability of biomaterials for healthcare. There are several types of natural polymer, some of animal origin (collagen, gelatin, chitosan) and others of plant origin (alginate, cellulose) largely investigated and applied in this field.

Collagen is the most important and used natural polymer and is the main structural fibrous protein of the extracellular matrix (ECM), the characteristic element of animal connective tissue.[21] It consists of three polypeptide chains arranged in a helix in which the amino acid units glycine, proline and hydroxyproline (Gly-Pro-Hyp) are repeated. The set of these triple helix chains creates a collagen microfibril, which leads to the formation of elongated fibrils, which in turn aggregate to form the final collagen fibers.[22] Collagen is the most widely used material in tissue engineering given its excellent biocompatibility, however being of animal origin, it can lead to some limitations in terms of quality and purity that could affect the final application, and also it is quite expensive given the difficulty in extracting it and of the management of the related documentation for the traceability of the raw material and the product quality assurance (Figure 1.3).[19,23]

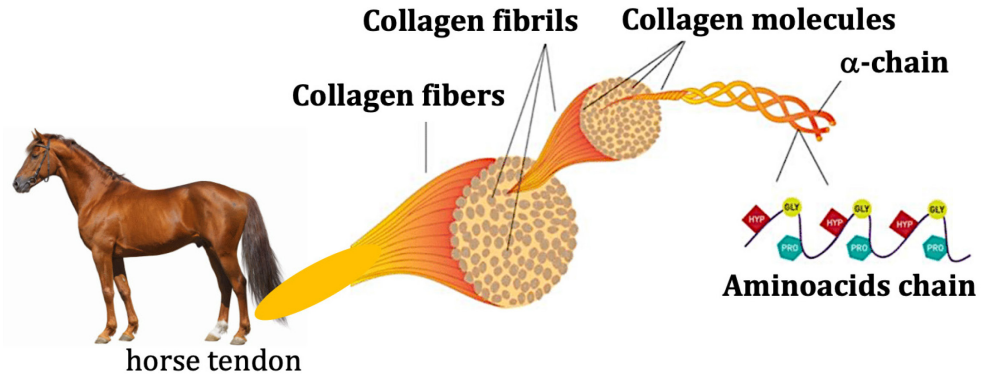

Figure 1.3. Schematic representation of collagen fiber hierarchical structure.

Gelatin is a mixture of proteins consisting mainly of glycine, proline and lysine, obtained through the hydrolysis of collagen and therefore maintains part of its characteristics such as biocompatibility.[24] There are two types of gelatin: type A, which comes from pig skin collagen by acid treatment, and type B, which comes from cow skin or bone collagen by alkali process. Although mainly of animal origin, there are also vegetable gelatins obtained from algae such as Agar Agar or from fruits (pectin) which are gaining ground in the food and cosmetics markets, mainly for ethical reasons related to the reduction of the use of animal sources.[25]

In addition to its exceptional biodegradability, gelatin has various functional groups which therefore allow it to interact easily with other polymers. It is soluble under physiological conditions of pH, temperature and osmolarity, but can form a hydrogel with triple helix structure when the temperature approaches the gel transition temperature of 30°C and can be made irreversible with a crosslinking agent that creates bridges between functional groups of gelatin molecules (Figure 1.4).[26,27]

From an economic/environmental point of view, gelatin is a biopolymer that can be purchased at very low cost from waste from the food industry, easy to handle and work with and which therefore allows the creation of more eco-sustainable biomaterials.[28]

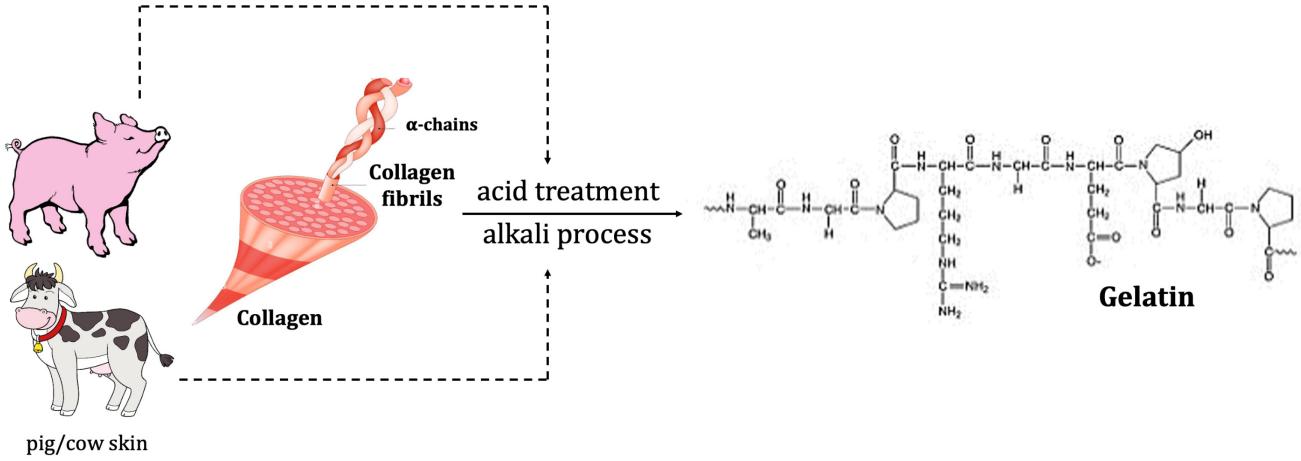

Figure 1.4. Structure of gelatin obtained through denaturation treatment of collagen.

Chitosan is a natural polymer coming from the polysaccharide family, obtained by the partial deacetylation of chitin, a structural element of the crustacean exoskeleton (Figure 1.5). It is a biodegradable and biocompatible cationic polymer, composed of randomly distributed β-(1-4)-D-glucosamine (deacetylated unit) and N-acetyl-D-glucosamine (acetylated unit).[29]

It has great versatility of use, in fact it can be used in agricultural, pharmaceutical as well as biomedical applications, the latter above all thanks to its antimicrobial properties and pH sensitivity.[30] In particular, above the pH range 6.2-7, the amino groups undergo deprotonation, while in solutions with a pH lower than 6.2 the chitosan manages to dissolve making the amino and hydroxyl groups available for possible cross-linking.[31] It can also be considered an eco-sustainable polymer, as it is obtained starting from the reuse of crustacean shells and above all easy to dispose of.[32] Chitosan, like gelatin, can be obtained from waste material from food industry, in particular from the fishing sector, significantly reducing the costs of the raw material and exploiting, from a sustainable perspective, industrial waste to create easily disposable devices.

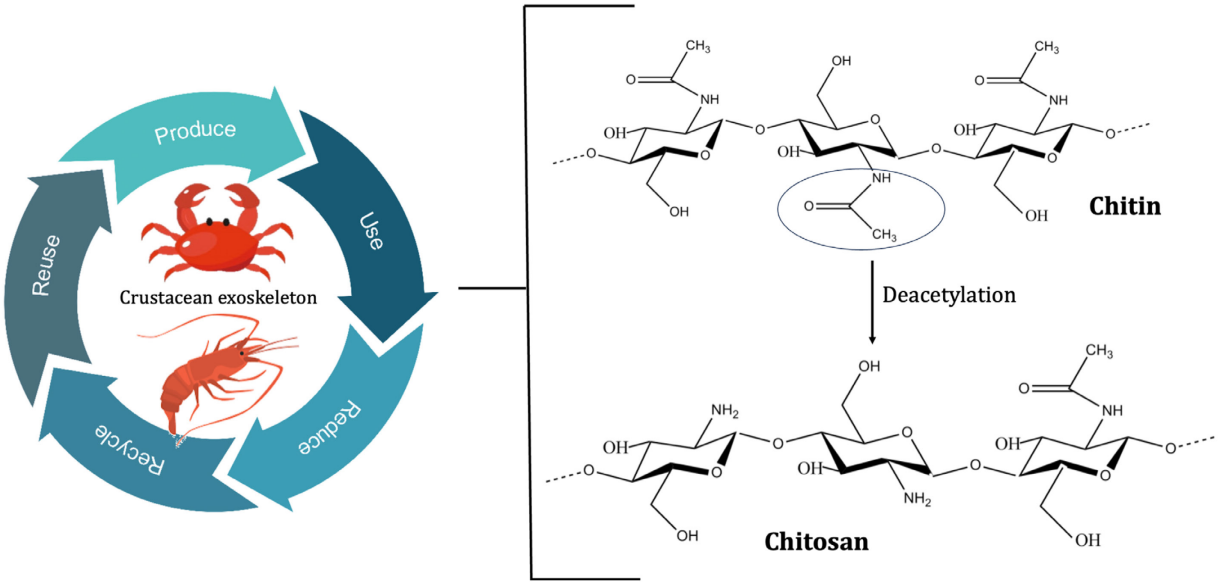

Figure 1.5. Structure of chitosan through the deacetylation of chitin.

Alginate is a natural polysaccharide extracted mainly from marine brown algae and consists of two polymers, D-mannuronate (M) and L-guluronate (G). Its final copolymeric structure consists of consecutive or alternating M and G homopolymeric blocks, covalently linked through –β 1,4 and –α 1,4 glycosidic bond. The different ratio between the G and M polymers characterizes the type of alginate.[33]

Sodium salt alginate is soluble in water, but being an anionic polymer, it has the ability to bind divalent cations (typically Ca^{2+} ions) and form ionically crosslinked hydrogels. In detail, two pairs of two consecutive G units, each belonging to different polymer chains, pack together with the calcium ions located between them, causing the polymer chain to assume a zig-zag shape defined as the egg-box model (Figure 1.6).[34,35] It is biodegradable under normal physiological conditions, moreover, coming from algae it is easily available at low cost and more appreciated for cosmetic and biomedical uses.

In fact, its vegetal origin allows it not only to reduce costs in the choice of raw materials, but to avoid the use of animal sources which on an ethical and industrial level are increasingly less taken into consideration for the production of new materials, especially in healthcare sector.

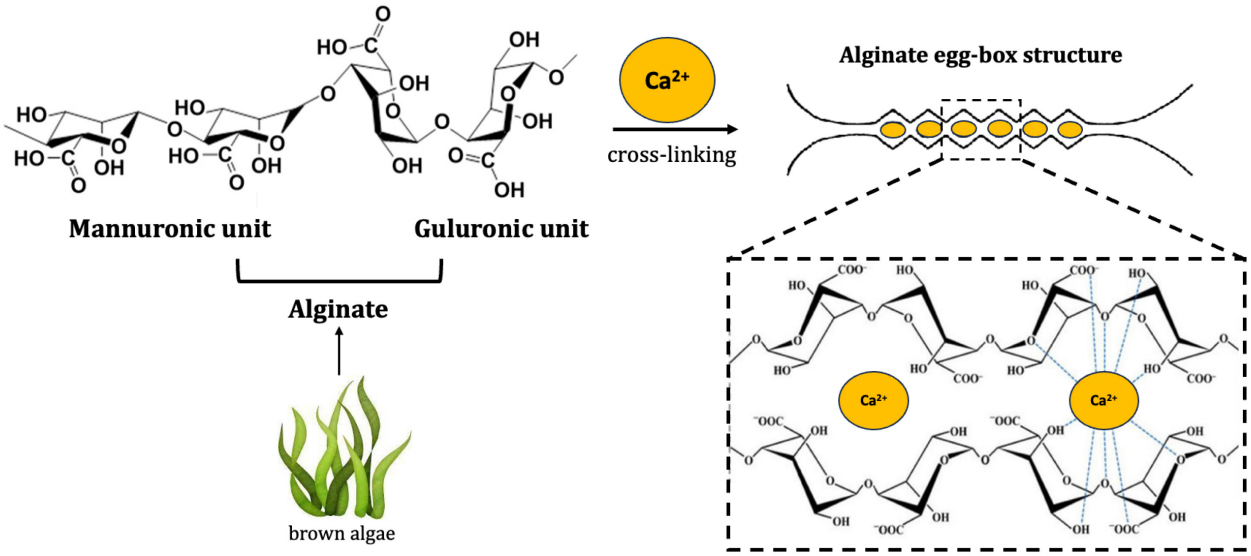

Figure 1.6. Structure of alginate and egg-box model after cross-linking with calcium ions.

Cellulose is the most widespread polymeric material in nature, obtained from numerous sources, such as cotton, paper, wood, sugar cane and for this reason it is also characterized by its high cost-effectiveness.[36] From cellulose it is possible to extract its nanometric component, i.e. nanocellulose, through physical/chemical/enzymatic treatments to isolate the individual fibrils from the general structure, obtaining cellulose nanofibrils (CNF) or cellulose nanocrystals (CNC) (Figure 1.7).[37]

It is a water-insoluble biodegradable polysaccharide with excellent mechanical properties, which can be functionalized with different chemical compounds, which allow it to be exploited for different applications.[38,39] Cellulose, like alginate, is widely exploited for its plant origin, but above all because it is obtained from industrial waste materials, thus facilitating its disposal and recycling.

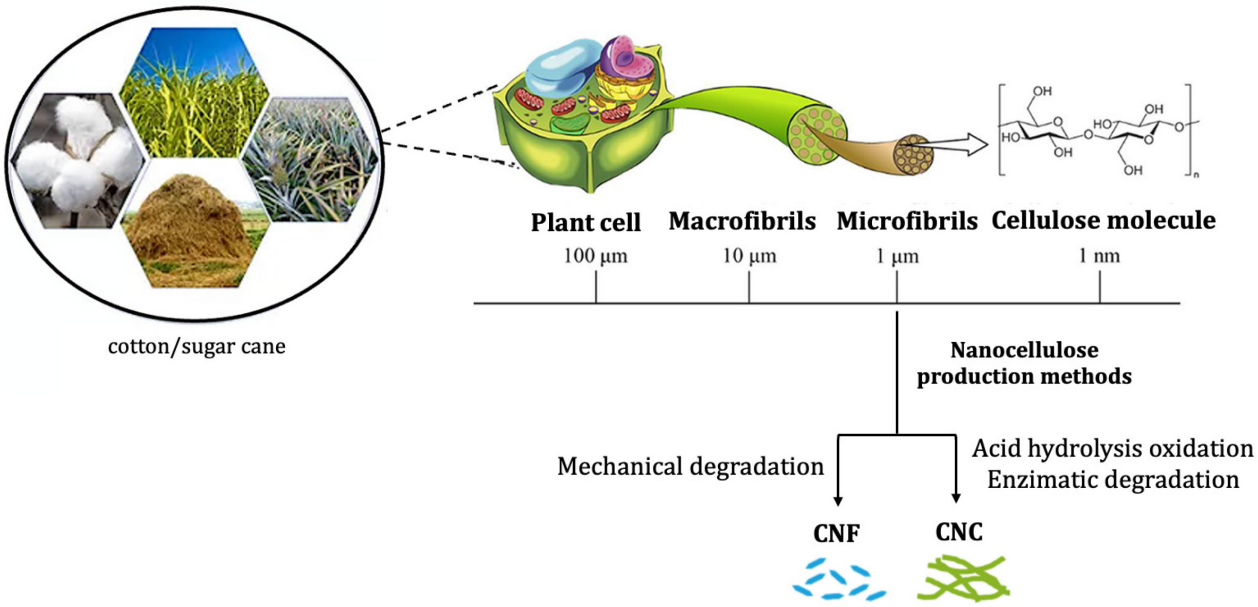

Figure 1.7. Structure of cellulose and methods for obtaining nanocellulose.

1.3. Bioceramics materials

In the context of ecosustainable biomaterials for healthcare applications, polymeric materials, discussed previously, play a fundamental role due to their easy degradation, disposal and reuse, however among the various known biomaterials, the use of bioceramic compounds appears to be a valid ecosustainable option.

The term "bioceramics" refers to biocompatible ceramic materials, applicable for biomedical or clinical uses. These biomaterials are usually classified in terms of behavior in the body environment, morphology or according to fields of application as bioinert, bioactive and bioresorbable. Bioinert ceramics are defined as stable bioceramics that do not show any harmful effects or responses in the body and are usually identified as Alumina, Zirconia and Carbon. However, if we talk about bioactive ceramic, we are referring to a material that creates an interaction or stimulates a reaction with the organism, without undergoing structural changes over time, as bioglass does for example. Finally, moving on to bioabsorbable ceramics, in addition to being bioactive, they have the added value of being able to be gradually reabsorbed by the body or easily degraded in the environment, as happens with the calcium phosphate (CaP) family.[40–43]

Thinking back to the circular economy concepts defined in the initial chapter with application in the healthcare sector, a biocompatible ceramic material, which generates an interaction with the body and at the same time can be easily degraded and disposed, reflects all the necessary characteristics required. In this regard, calcium phosphates appear to be the most suitable

bioceramic phase to develop innovative eco-sustainable biomaterials for healthcare applications.

CaPs are minerals that predominantly form the inorganic component of hard tissues in vertebrates (e.g., bones and teeth) and are often used as biomaterials in biomedical field, in detail for regenerative medicine to recreate or replace bone tissue or as drug delivery systems.[44] By modifying the synthesis parameters to develop CaPs, different crystalline phases can be obtained, with different morphology, crystallinity, Ca/P ratio etc., which influence the characteristics and functions of the ceramic phase (Figures 1.6). The most relevant CaPs phases are four and appear as amorphous calcium phosphate (ACP), octacalcium phosphate (OCP), tricalcium phosphate (TCP), and hydroxyapatite (HA).[45] Each of them shows different properties, which are exploited for specific applications in the healthcare field, but among all the CaP phases, HA is the bioceramic phase mostly used for its high biomimetics and excellent thermodynamic stability in physiological conditions.[46,47]

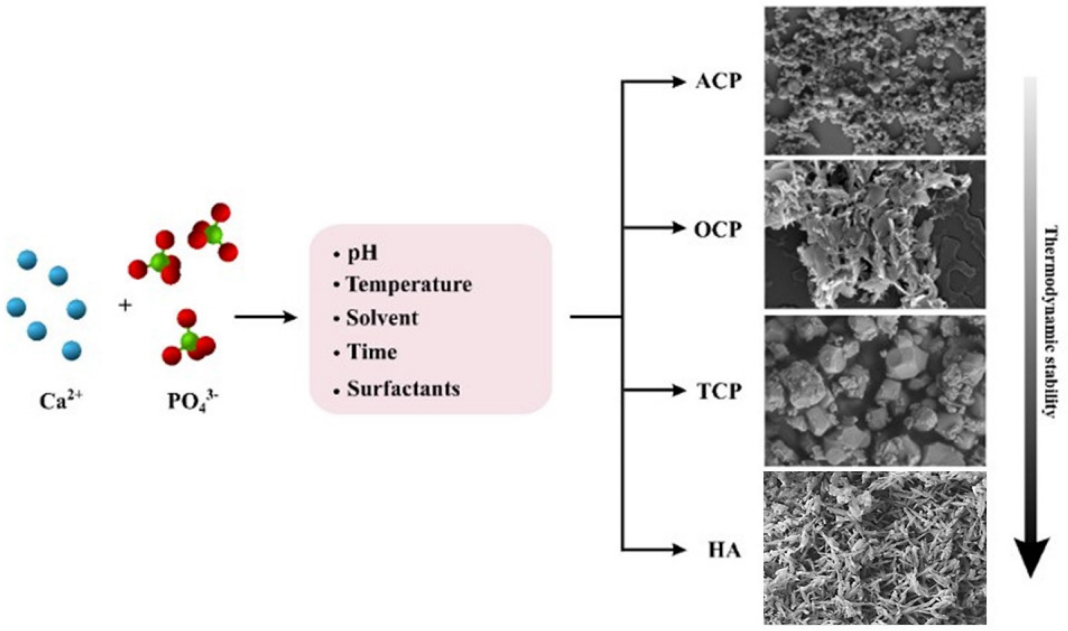

Figure 1.6. Principal synthesis parameters that influence the formation of different CaP phases.

1.3.1. Hydroxyapatite

Hydroxyapatite is the mineral phase of vertebrate bones, mammalian teeth and fish scales and is the most common of the apatite family with chemical formula $Ca_{10}(PO_4)_6(OH)_2$. Its hexagonal crystalline structure visible in Figure 1.7, beyond to containing PO_4^{3-} and OH^- ions, presents calcium ions in two crystallographically different sites of symmetry. Ca(I) ions are identified in columns along the three axes and each is nine coordinated with O atoms, while Ca(II) ions are seven coordinated, with six O atoms and one OH^- ion.[46]

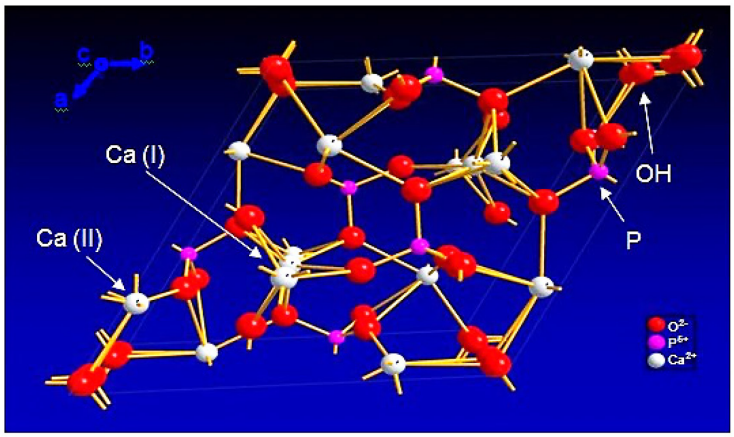

Figure 1.7. HA hexagonal crystal structure with the position of Ca^{2+} divided in the two different symmetry sites.

When talking about hydroxyapatite, however, it is necessary to make a clear distinction between the two existing types: stoichiometric or biological. Stoichiometric hydroxyapatite is composed of Ca^{2+}, PO_4^{3-} and OH^-, corresponding to the chemical formula described previously, with a Ca/P ratio of 1.67. It has a high crystallinity, low reactivity and a very ordered structure with difficulty in being functionalized. On the contrary, the biological one, i.e. the one present in our bones, is not stoichiometric as in addition to Ca^{2+}, PO_4^{3-} and OH^- ions, it has a very flexible crystalline lattice capable of exchanging and incorporating in its crystal structure numerous ions (e.g. CO_3^{2+}, Mg^{2+}, Sr^{2+}), which modify the Ca/P ratio and their chemical-physical characteristics according to the needs of the constituent bone tissue. Furthermore, the biological hydroxyapatite, allowing the entry of different ions, has poor crystallinity, modifiable if subjected to external stimuli and the ability to interact and transfer important biological signals with cells.[48]

In the field of biomaterials for healthcare, the need to have the availability of apatite as similar as possible to the natural one has always been a crucial point for the development of bioactive particles and devices. In this regard, over the last twenty years a synthetic method has been developed to mimic in laboratory what normally happens in hard human tissue and produce a biomimetic hydroxyapatite. Precisely, by synthesising a non-stoichiometric apatite, a very elastic crystalline lattice is generated, capable of exchanging a high number of ions (Na^+, K^+, Mg^{2+}, Sr^{2+}, $Fe^{2+/3+}$, Zn^{2+}, CO_3^{2+}, Cl^-, Ti^{4+}) with the external environment, managing to mimic the continuous chemical remodelling that occurs in bones with ion substitution. The entry of new ions can significantly change the properties of HA, such as Ca/P ratio, solubility, bioactivity,

stability and confer unique features such as superparamagnetic behavior or modification of its reflectance, with an expansion of its possible fields of application (Figure 1.8).[49–51]

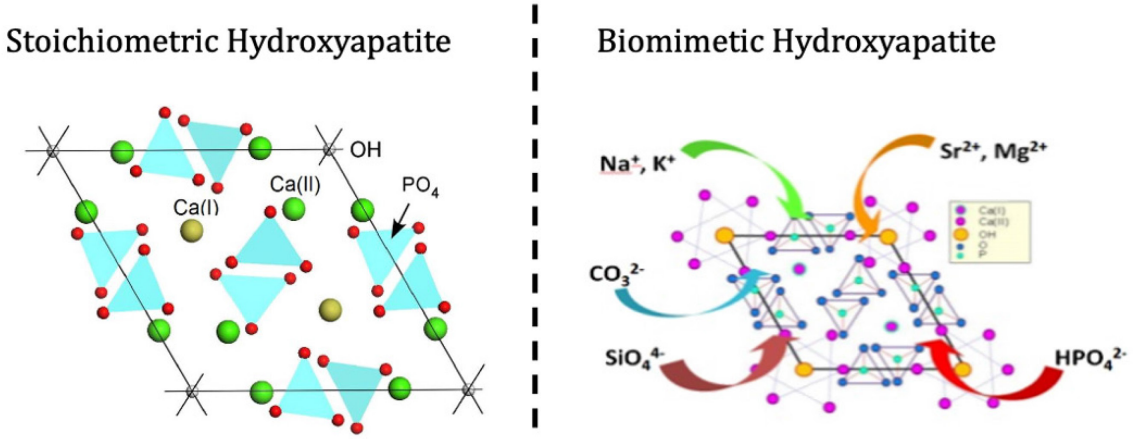

Figure 1.8. Cristal structure of stoichiometric and biomimetic hydroxyapatite.

Biomimetic HA is characterized by unique peculiarities, such as excellent bioactivity, non-toxicity, non-immunogenicity, and biocompatibility compared to other bioceramics materials.[52] Furthermore, another important characteristic is its pH-dependent solubility. This material, in fact, is poorly soluble at neutrality and soluble at acid and alkaline pH.[53] In addition, being composed of ions already present in our body, when it degrades it does not release harmful substances in the surrounding environment and the decomposition products are easily disposed of, thus proving to be a biocompatible as well as eco-sustainable material.[54]

Finally, the HA, as previously reported, is also widely present in nature in the bones of vertebrates, in the teeth of mammals and in the scales of fish. Therefore, at this time when for social, economic and environmental reasons, the principles of the circular economy are fundamental, the use of HA from biogenic sources is an opportunity that must be exploited.[55,56] In particular, biowaste from the food industry, such as animal bones, fish scales and shells can be thermally treated to obtain HA, recycling organic waste and converting it into green products with high added value.[57] Due to its great versatility, HA can be used as a biomaterial for numerous applications, primarily in the biomedical and healthcare field, but recently also in the environmental one.[58,59]

1.4. Biohybrid materials

Until now, the characteristics and advantages of polymeric and ceramic biomaterials have been highlighted, underlining their use from an eco-sustainable perspective. Being materials with completely different chemical-physical properties, their role within the final device also differs considerably, but this is not always a negative aspect. In fact, a biomaterial can be increasingly engineered by combining different functional elements to create a biocomposite material with different potentialities.

The term biocomposite refers to a biocompatible and environmental friendly material composed of two or more components, with significantly different chemical and physical properties, which merged create a new composite material with features unlike the individual elements, influencing the behavior and the final application of the product itself.[60,61] In particular, when the two components are neither distinguishable nor dissociable it is possible to identify the biocomposite as biohybrid material, where usually an organic and an inorganic phase interact with each other stably.[62]

When it comes to biomaterials for healthcare, the organic phase can be made up of a biomimetic, biodegradable, and biocompatible polymeric matrix, which turns out to be a fundamental resource for creating more ecological and low-cost materials. On the other hand, the inorganic phase can include the exploitation of biocompatible ceramic compounds, also biomimetic in case of bioceramics phases, capable of best mimicking the characteristics already present in nature of a specific element and exploiting them to develop innovative materials. Since our body is primarily a hybrid compound, where different components with specific characteristics and functions coexist, biohybrid materials are increasingly proving to be an effective solution for developing healthcare devices. In fact, by observing the nature of the organism, it is possible to create a single multifunctional material, which allows the limits posed by the single polymeric or ceramic component to be overcome, reducing production costs and waste of raw materials.[63]

1.4.1. Biomineralization process

The development of hybrid biomaterials in the biomedical field can take place in different ways[64], but if you want to use an eco-sustainable and at the same time biocompatible process with biomimetic ceramics compound, limiting costs and energy expenditure, the biomineralization process turns out to be a fair compromise.

The term biomineralization refers to the process by which organisms in nature form the minerals that are the basis of load-bearing structures such as bones, teeth, shells and exoskeletons.[65] Through a complex cascade of phenomena, organic and inorganic components interact with each other to give life to nanostructured hybrid materials organized hierarchically from the nanometric to the macroscopic scale and which are difficult to replicate in the laboratory. In detail, taking bones as example, the polymer matrix of collagen acts as a template on which the bioceramic phase, i.e hydroxyapatite, is able to grow and nucleate. Through multiple mechanisms, the organic phase exerts a rigid control on the formation of the mineral crystal: it coordinates the ionic transport, the spatial arrangement and size of the inorganic phase, promotes the nucleation of specific crystalline faces along the collagen matrix and the assembly into higher order. The result is a mineralized collagen fiber which represents the building block of hard tissue (Figure 1.9).[66]

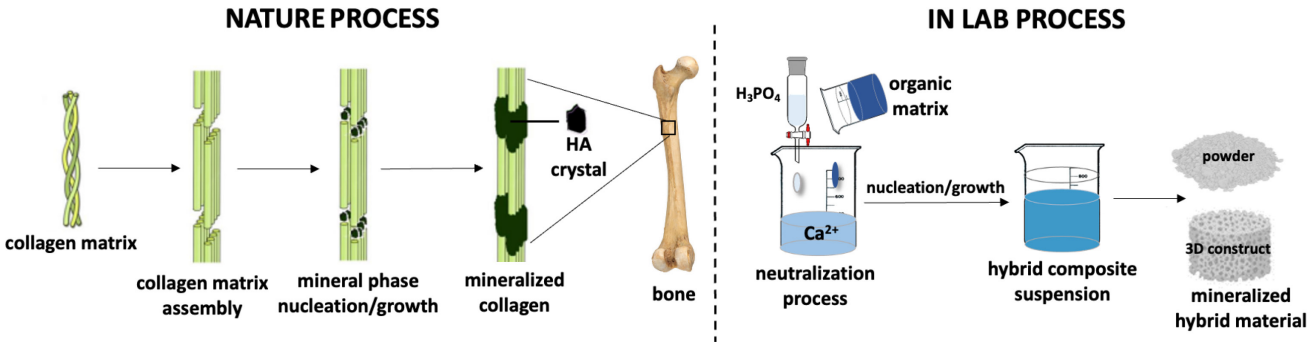

Figure 1.9. Comparison between the biomineralization process that naturally occurs in bones and the biomineralization process mimicked in the laboratory allowing to obtain biomimetic hybrid powders o 3D constructs.

Biomineralization is therefore capable of generating, depending on the different context, a hybrid material with chemical, physical and structural complexity and exceptional properties, that confer to the final product the ability to interact and respond intelligently to environmental stimuli and the capacity for self-renewal/self-regeneration. In the early 2000s, scientific research exploited this process to generate several forms of hybrid biomaterials, from porous 3D constructs to nanostructured powder, for applications in the biomedical and environmental fields.[67,68]

As shown in Figure 1.9, to reproduce in lab-scale what happens in nature, a neutralization process was optimized in which an acidic solution containing PO_4^{3-} ions and the organic phase, was slowly added to a basic solution containing Ca^{2+} ions. During the process the pH of the solution is neutralized, triggering two mechanisms: the assembly of the organic phase in a

complex matrix and the simultaneous nucleation of nanostructured mineral particles above and within it. This nature-inspired process offers the possibility of developing biohybrid materials, in which hydroxyapatite nanoparticles, present small dimensions and low crystallinity, therefore capable of easily degrading releasing ions that are harmless to humans and the environment. Furthermore, thanks to the ability of the apatite lattice to host external ions, it is possible to synthetize compounds with unique properties and therefore multiple applications and functions depending on the nature of ions inserted.[69,70]

Regarding the organic phase, natural polymers, such as chitosan, gelatin, alginate etc., thanks to their active functional groups, allow the nucleation of the hydroxyapatite, producing composites with different structures, in form of particles or 3D structures depending from their polymerization ability. Those materials highlighted very important features and behaviour and their applications can range from regenerative medicine to healthcare products.[54,71,72] In addition, being a process taken inspiration from nature, it is able to develop eco-sustainable products made up of easily disposable and biodegradable natural substances with high added value for the industrial sector.[73]

1.5. Features and design of polymeric and hybrid biomaterials

A biomaterial shows diverse physical, chemical and structural characteristics, which can be modulated by the type of polymeric/hybrid compound selected or by prototyping techniques. The multiple applications of these materials are obviously influenced by the different features that distinguish them.

In particular, biomaterials for healthcare, encountering tissues and body fluids, must have specific properties in order to fully carry out their functions without being a risk to our body. From 3D constructs to powders, each biomaterial is designed and developed to measure based on the needs of the chosen sector, trying to give it the properties necessary to guarantee its functionality.

1.5.1 Biocompatibility

The term biocompatible has been in use for many years now, but a continuous reevaluation of its definition is necessary given the rapid evolution of the sector and above all the different application contexts which can range from tissue engineering to cosmetics up to personal care devices. Biocompatibility is the characteristic of any biomaterial that is well tolerated by the biological system with which it comes into contact. It is important to note that biocompatibility is specific to the chosen application and linked to other characteristics: a material deemed biocompatible in one specific use case may not be so in another. A biocompatible material in turn can present itself as bioinert or bioactive. Bioinert is a material that does not produce a physiological reaction on the part of the organism. If it is bioactive, however, a physical or chemical reaction is triggered in the body to produce a local physiological response.

For example, biohybrid materials used for bone regeneration are bioactive compounds capable of nucleating the ceramic phase on the organic bone tissue matrix, generating a chemical bond between the tissue and the material without the presence of fibrous tissue. In the healthcare sector therefore, a biomaterial, being a substance designed to interact with biological systems must have high biocompatibility and even better bioactivity to make possible an adequate response from the body.[63,74]

1.5.2 Biodegradability

Among the various characteristics of a biomaterial to take into consideration, in addition to biocompatibility, it is essential that the final device is biodegradable. The term "biodegradable"

can refer to various aspects: when talking about regenerative medicine, biodegradability means that the material used must be partially or completely resorbable in a time functional to the regeneration of the tissue; when we refer instead to biomedical devices that are not inserted into the body, biodegradability concerns the environmental concept of eco-sustainability, in which a material must be easily disposable or recyclable at the end of its use. In both cases, however, being biodegradable is closely connected with being stable of a material, as in order to allow its function to be carried out, the compound must fully maintain its properties in the humidity and temperature conditions of usage, at the end of which it may deteriorate. In this regard, once the appropriate components have been selected, during the prototyping phase of a biomaterial, it is essential to carefully choose the cross-linking method necessary to give it stability and greater resistance in the conditions of use, while remaining biodegradable.[14,75]

1.5.2.1 Cross-linking processes

The structure of a polymeric or hybrid biomaterial requires strong stability to maintain its morphology and function during different applications, especially in the healthcare sector, where the materials are often in contact with fluids and cells. Natural polymers have a high biodegradability, which if from an environmental point of view represents an advantage, in the case of structural stability it can constitutes a problem. To overcome this drawback, among the biomaterial design techniques it is necessary to resort to cross-linking processes.

Cross-linking can occur in different ways, i.e. by exploiting chemical or natural molecules or through physical treatments capable of creating strong intermolecular bonds between polymeric fibres, improving the packing of the molecules and reducing the collapse of the polymer structure. Therefore, depending on the type and composition of the biomaterial, these cross-linking techniques have been refined to modulate its resistance, i.e. its stability in conditions of high humidity and physiological environment.[76]

There are several cross-linking methods, normally divided into chemical and physical cross-linking. The most significant and used are: i) 1,4-Butanediol diglycidyl ether (BDDGE) ii) Genipin iii) tannic acid (TA) like chemical cross-linker; i) Ultraviolet radiation (UV) ii) Dehydrothermal Treatment (DHT) as physical cross-linker.

Starting from chemical cross-linking methods, this occurs thanks to the interaction of different lateral functional groups of the molecule which can easily form chemical bonds, making the structure more stable and resistant to adverse conditions.

<u>1,4-butenediol diglycidyl ether</u> (**BDDGE**) is a cross-linking agent widely used to cross-link polymers that contain amine or carboxyl groups in their structure as they immediately react with epoxy groups present at both ends of the cross-linking molecule. Depending on the pH of the solution, BDDGE prefers to react with different functional groups: alcohols or carboxylic acids in the basic state and primary amino groups in acidic conditions.

It is exploited in the biomedical field due to its lower toxicity compared to other cross-links through ethereal bonding and being biodegradable, it falls within an environmental sustainability perspective (Figure 1.10).[77]

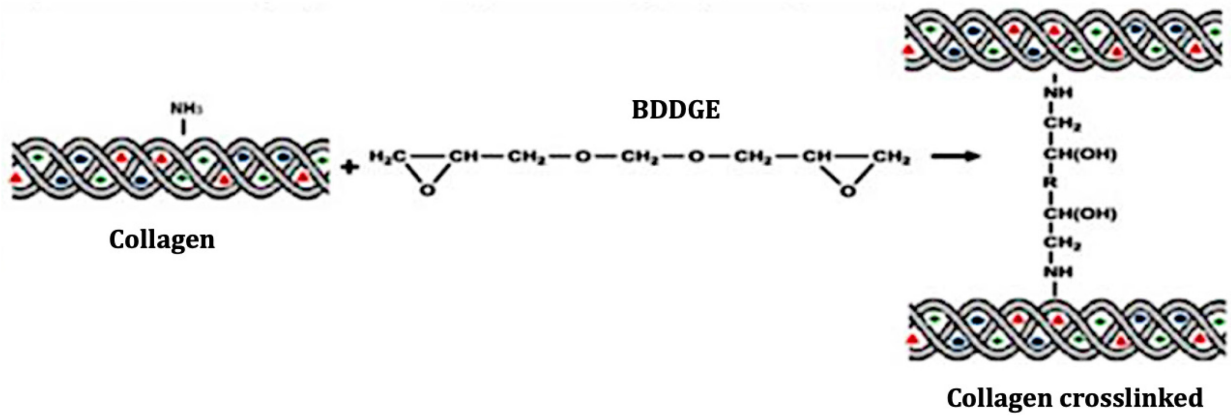

Figure 1.10. Reaction mechanism involving BDDGE and amino functional groups of Collagen**.**

<u>Genipin</u> derives from the Gardenia fruit (Gardenia Jasminoides Ellis) and is a natural, water-soluble cross-linking agent. It reacts spontaneously with biopolymers such as collagen, gelatin, chitosan where amino groups are present within the structure. In this way, a new amide bond is formed between amino acids and proteins, which is also visible by the color change from light to blue. Cross-linking of genipin is promoted at pH greater than or equal to 5.5. Its cytotoxicity, as reported in various studies, is much lower than other cross-linkers used, but from an economic point of view it is rather expensive and can have quite long reaction times (Figure 1.11).[78]

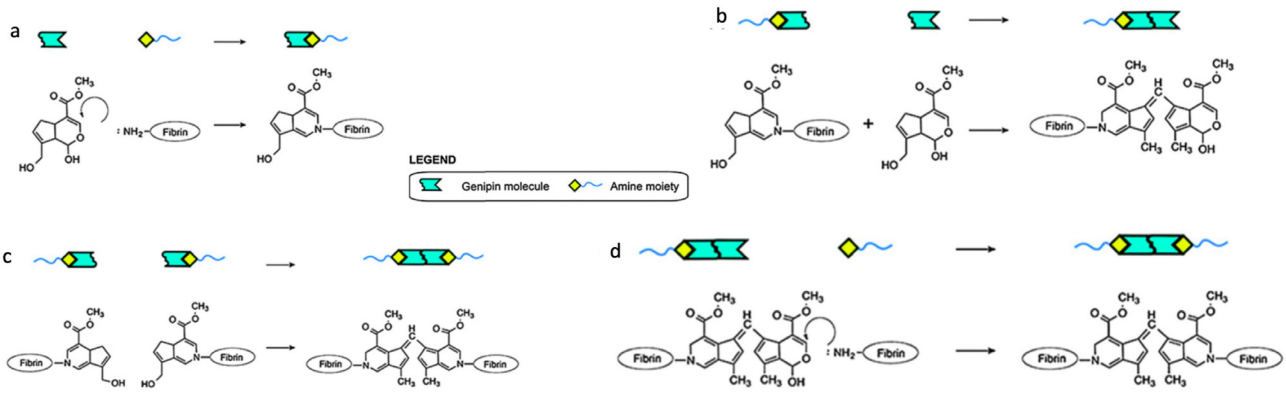

Figure 1.11. Different reaction mechanism involving genipin and amino functional groups of polymers.

Tannic acid (**TA**) is a natural compound of the polyphenol's family found in wood and in the leaves of various plants. Its structure is characterized by a glucose molecule condensed with five molecules of digallic acid, this generates a molecule rich of numerous hydroxyl and phenolic groups which are able to cross-link the structure of different polymers such as gelatin, chitosan, cellulose via hydrogen bonding or exploiting the phenolic groups for covalent bonds. Furthermore, this cross-linker, coming from natural sources, falls within the principles of eco-sustainability and biocompatibility, fundamental for biomaterials with healthcare applications (Figure 1.12).[79]

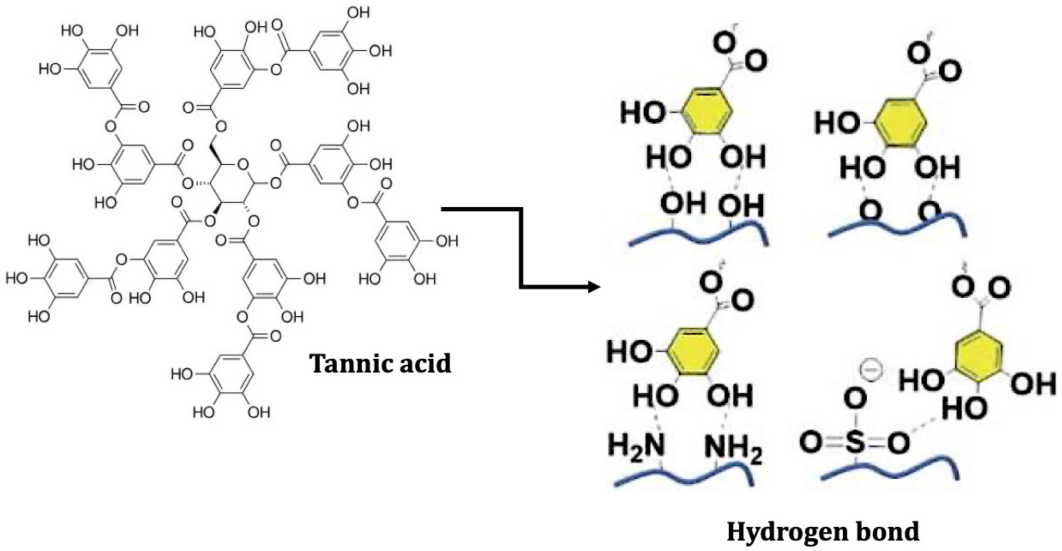

Figure 1.12. Chemical structure of tannic acid and its reaction mechanism with hydrogen bond of polymers.

Regarding physical cross-linking methods, they include treatments, which allow, without the use of external molecules, to make the material more stable and resistant without the risk of toxicity, as sometimes happens with chemical cross-linking.

UV radiation it can be used as a physical catalyst to activate cross-linking, leading to the formation of a covalent bond between adjacent molecules of one or more polymers. The reaction can be mediated via a photon initiator which activates the deprotonation of the polymer functional groups and an auxiliary crosslinker which acts as a bridge, like a free radical, attacking the deprotonated filaments by interposing itself between them. Otherwise, the functional groups of the polymer chains themselves, stressed by UV radiation, can generate the bond between them (Figure 1.12).[80]

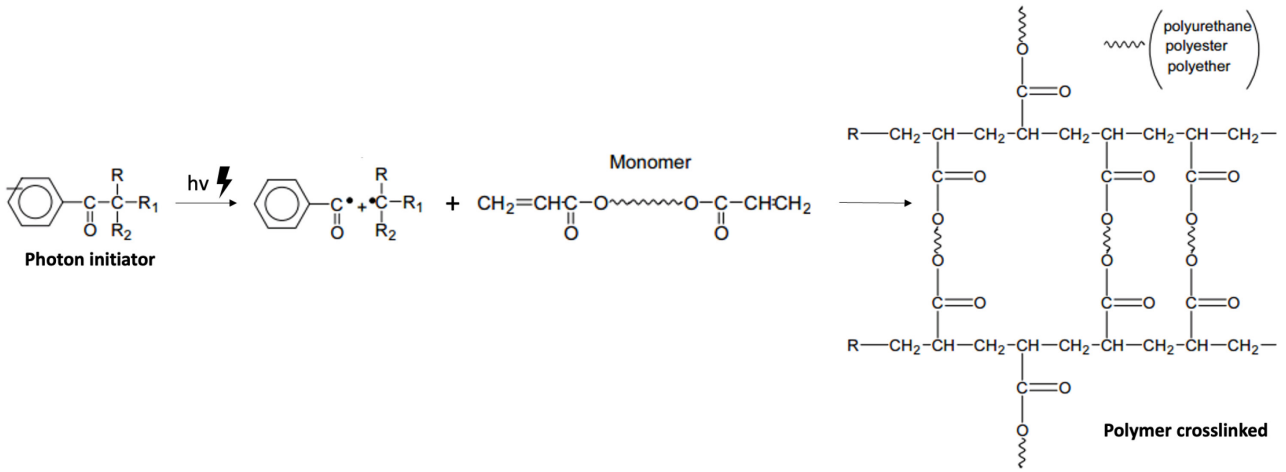

Figure 1.12. Reaction mechanism of UV crosslinking.

<u>Dehydrothermal treatment</u> (**DHT**) is a specific treatment in which, by exploiting temperature and vacuum, intermolecular bonds are generated between the polymeric functional groups (amino and carboxyl groups) of the material itself which allow its structure to be strengthened. It is a method without risk of toxicity and by opportunely selecting the temperature to use (120-160 °C), at low vacuum, it is possible to control the partial elimination of water from the structure e therefore the stability and wettability of the material of interest (Figure 1.13).[81,82]

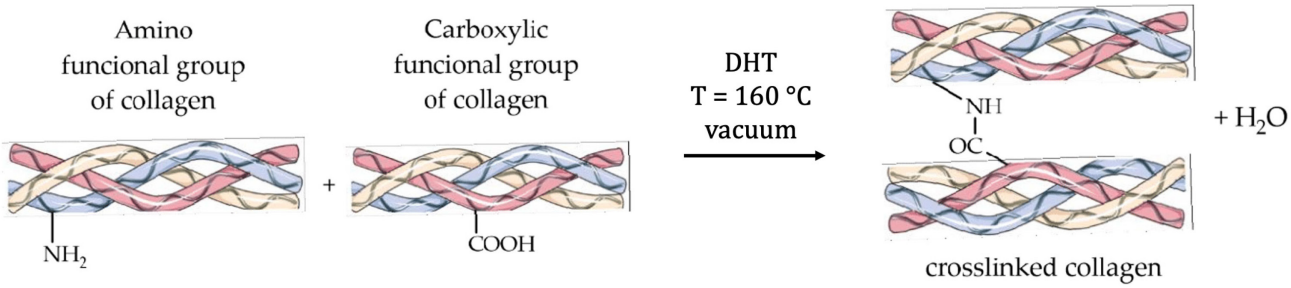

Figure 1.13. Schematic representation of DHT treatment.

Physical cross-linking methods like this, when are applicable, are preferred, because allow, without the use of external molecules, to modulate the stability and the resistance of the material without the risk of toxicity, sometimes associated with chemical cross-linkers.

1.5.3 Porosity

When talking about materials for healthcare applications, it is essential to consider their biocompatibility, biodegradability and wettability, which we have seen previously, but equally important is the morphology of the device in terms of size, geometry, density and porosity, which must be closely connected to the type of task that the biomaterial will have to perform.

Porosity can be defined as the presence of voids and interconnected cavities within the material which allow the infiltration of cells, the passage of fluids or gases, the encapsulation of drugs, in other words they allow the body's response to take place in the presence of the biomaterial. Precisely for this reason the presence of pores is a determining factor in having a compound that is as bioactive, biocompatible and wettable as possible. The porosities, in fact, allow a better adaptation of the material in contact with the tissue and more retention/exchange of biological fluids, therefore to have a material with a high wettability cannot fail to be porous.
Porosity is not an intrinsic property of the material, but is achieved by prototyping techniques, which allow the formation and control of pores with different sizes, geometry, and distribution depending on the type of application required. Modulating the porosity of the 3D structure of a biomaterial not only means making it more attractive for the organism, but also improving other peculiarities necessary for its use.[83]

1.5.3.1 Prototyping methods

Currently the need to have a porous 3D architecture is a key point in the design of a biomaterial to have a better interaction with tissues or body fluids. Nowadays there are numerous techniques for prototyping polymeric or hybrid biomaterials with high porosity, many though do not allow adequate control over the final microstructure, require too much time or expense and are not very sustainable. Among the most cited are solvent casting, gas foaming, electrospinning, three-dimensional printing (3D printing), and freeze-drying reported below.[84]

Solvent casting-particulate leaching is a technique composed of two phases, in which extra-solid particles are incorporated directly into the material solution/suspension, to form pores in the final product. First of all, the polymer is dissolved in a special solvent (solvent casting) and the solution is then poured into a mould containing porogen particles (e.g NaCl, gelatin, soluble fibres). When the solvent evaporates, extra-particles are still inside the bulk of material solidified but are subsequently removed by dissolution with distilled water or organic solvents, or through their thermal degradation (particulate leaching). In this way it is possible to obtain materials with interconnected porosities and a high surface/volume ratio (Figure 1.14).[85]

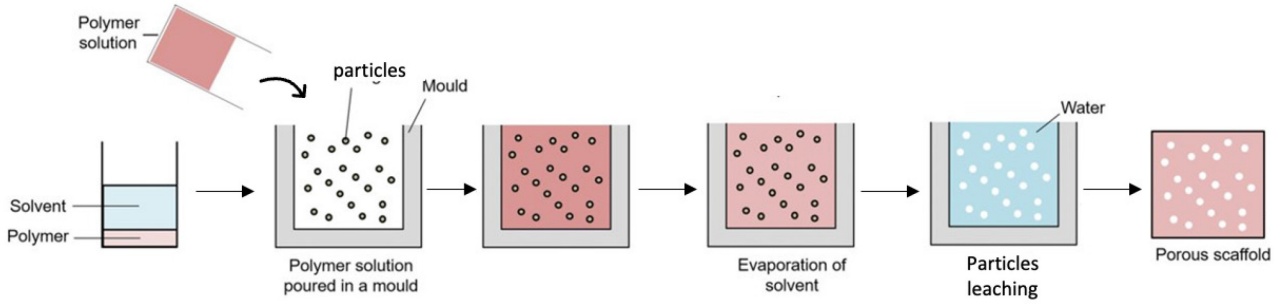

Figure 1.14. Schematic illustration of solvent casting technique.

Gas foaming makes it possible the development of 3D scaffolds, using carbon dioxide of air bubble as a foaming agent. In this technology, viscosity increases by trapping gas bubbles in the structure that grow directly within the material matrix (Figure 1.15).[86]

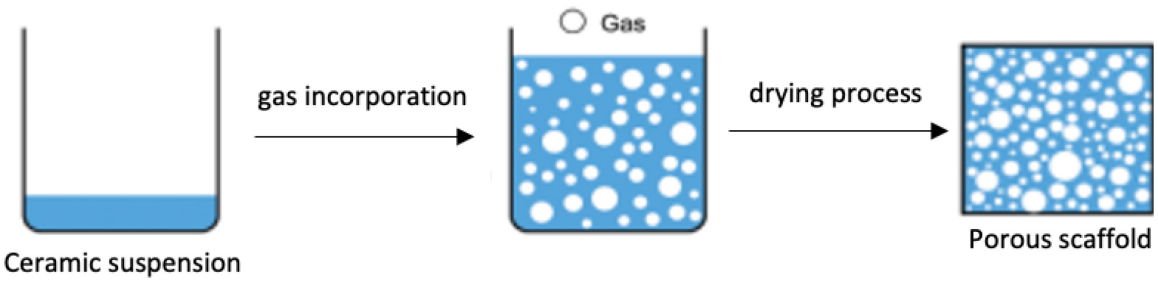

Figure 1.15. Schematic illustration of gas foaming technique.

Electrospinning is a versatile technique, capable of developing highly porous micrometric fiber mats. The instrumentation is composed of a metal capillary from which the solution of the final material is expelled and a collector on which this solution is deposited. When a high voltage is applied between the capillary and the collector and the electrostatic force exceeds the cohesive force of the solution, the fibrous mat with a certain porosity is formed. Fiber size and sheet morphology can be monitored by varying solution characteristics and spinning variables (Figure 1.16).[87]

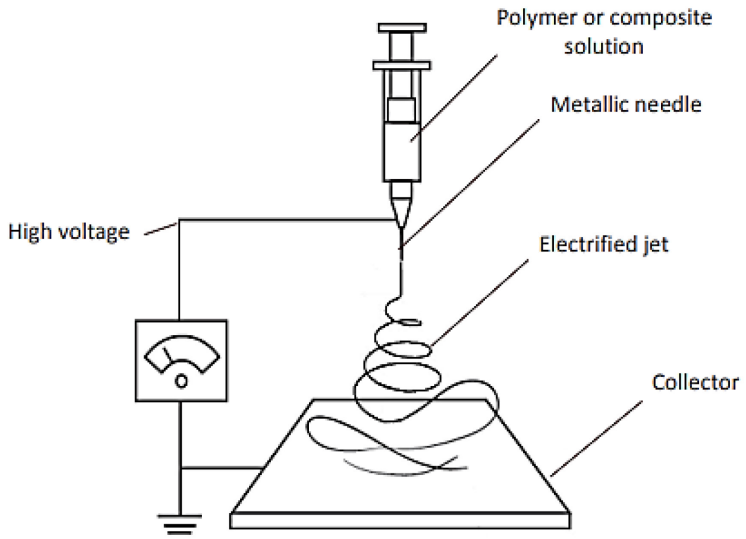

Figure 1.16. Schematic illustration of the electrospinning technique**.**

Three-dimensional printing (3D printing) is a widely used prototyping method for designing complex 3D porous matrices. Thanks to a computerized control of specifications such as temperature, pressure, speed etc., the layer-by-layer deposition of the material takes place to obtain a final device with specific geometry (Figure 1.17).[88,89]

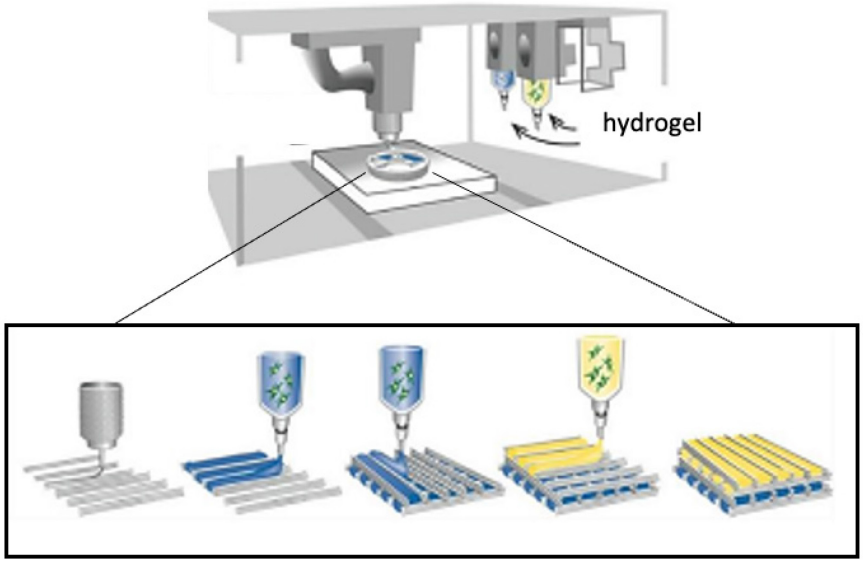

Figure 1.17. Schematic illustration of 3D printing.

Freeze-drying process is the manufacturing technique that best allows the design of biomaterials with high and controlled porosity morphology. This is made possible by two different consecutive phases: the freezing of the material, in form of solutions, hydrogels or dispersions and the slow drying of the material by sublimation of the solvent through low vacuum. Starting from the freezing process, the hybrid or polymeric wet material is subjected

to vertical cooling from bottom to top, also influenced by the sample holder whether conductive or insulating. Subsequently, the frozen solvent (typically water) is removed from the rigid structure of the material through its sublimation, applying a low vacuum and a very slow heating rate. During this last step, cavities are formed which will characterize the porous morphology of the final material (Figure 1.18).

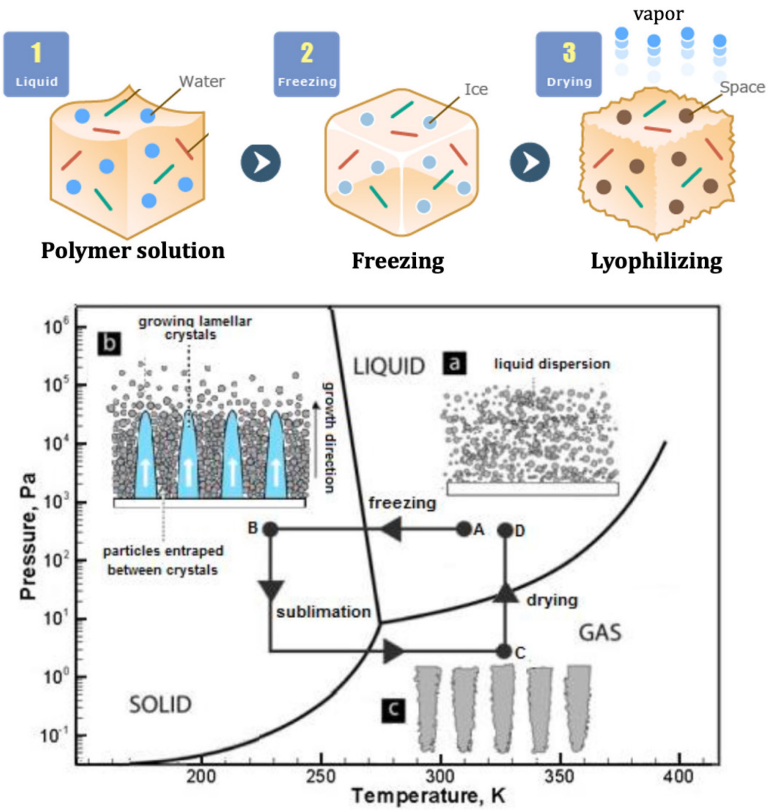

Figure 1.18. Schematic illustration of the freeze-drying process.

Both phases of the freeze-drying process are fundamental to obtain specific porosities, but the most important to control the final structure is the freezing step. In fact, the growth and the orientation of ice crystals within the material, formed during the freezing phase, define the structural characteristics of the final pores. Modifying the final temperature and the freezing speed, the characteristics of the pores can be modulated. For example, a rapid freezing until low temperatures produces the fast formation of a large number of small crystals, which leads to a material with many small pores, on the contrary, a slow freezing lead to a material with fewer larger pores.[90–92]

1.5.4 Wettability

Biomaterials, as previously mentioned, being biocompatible and biodegradable, come into contact with biological systems, making their surface properties a critical factor for the final

performance of the material. One of the most important surface properties that can influence the functionality of a biomaterial is its wettability. Wettability generally refers to the ability of a liquid to spread on the surface of a solid material and this phenomenon is governed by the balance between the adhesive forces between the liquid and solid and cohesive forces within the liquid itself. Depending on the type of wettability that a biomaterial presents, it can be classified as hydrophilic or hydrophobic: the first has a high affinity to water, causing liquids to spread easily on surfaces, while the second repels water, accumulating droplets on the surface and causing them to slide off.

Being more or less able to retain liquids plays a crucial role in the performance of a biomaterial, especially in the medical field. In fact, biomaterials must interact effectively with biological systems and for this reason they must have high wettability to have better cellular adhesion and avoid adverse reactions. It is possible to manipulate the wettability of a compound through chemical and structural modifications, improving interaction with the organism and long-term performance, in particular through techniques such as freeze-drying and cross-linking processes.[93]

1.6. Ecosustainable biomaterials in healthcare applications

By varying the materials, and the synthesis and forming parameters, it is possible to obtain biomaterials with different chemical and physical properties, and different behaviour and function, therefore usable for different types of applications. It is well noted that biomaterials play a fundamental role in the biomedical field[7,23], from tissue regeneration to nanomedicine, but their versatile capabilities have made these materials also exploitable in other healthcare fields. In particular, among the many known applications, it is attracting a growing interest the development of biomaterials for cosmetics and for breathing through mechanical ventilation following the concepts of eco-sustainability and circular economy, to respond not only to the needs of human health and well-being, but also to the economic and environmental ones (Figure 1.15).

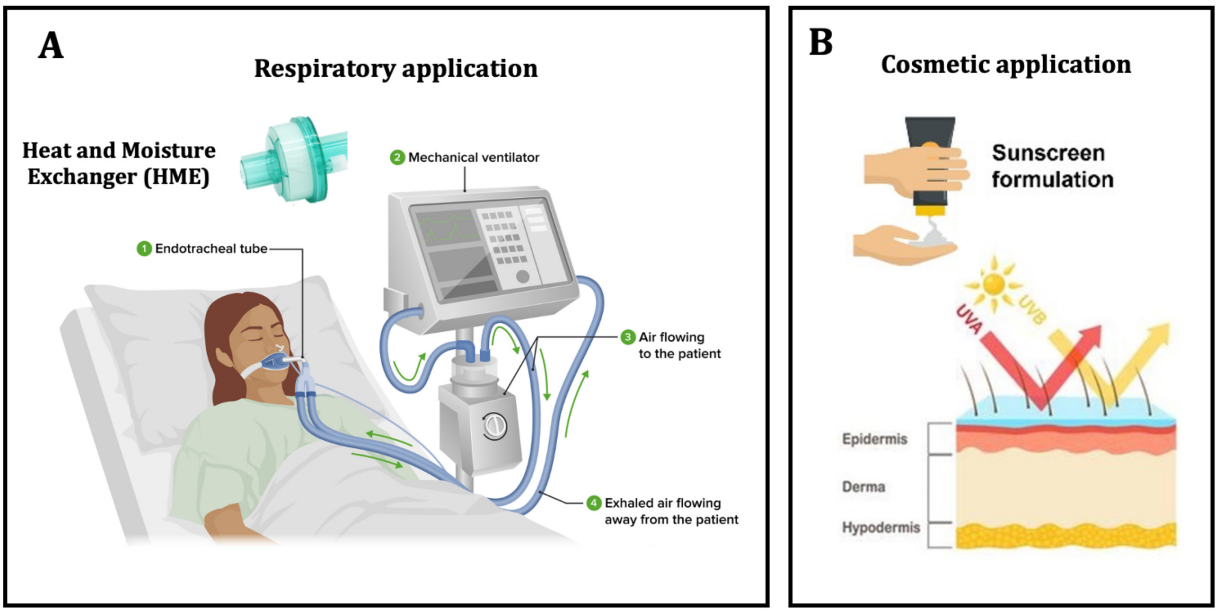

Figure 1.15. Schematic illustration of ecosustainable biomaterial applications: A) respiratory and B) cosmetic.

1.6.1 Respiratory application

The increase in life expectancy and advances in the medical field have led over the last 50 years to an exponential increase in patients requiring respiratory support, i.e. mechanical ventilation. According to a study reported by the America Association for Surgery of Trauma, there are an estimated 2.7 hospitalizations requiring mechanical ventilation per 1000 inhabitants per year, including 0.86% who present acute respiratory tract damage with an estimated national cost equal to 12% of total hospital costs.[94]

Mechanical ventilation, in fact, represents one of the most common interventions in intensive care units, when the patient cannot be able to maintain the airways adequately oxygenated, for example due to respiratory insufficiency or compromised lung function and during anesthetic treatments. Therefore, during the mechanical ventilation process, the steps that are naturally carried out by our body to allow us to breathe are replaced by hospital devices.[95]

However, although it is the classic method used to help patients with breathing difficulties, mechanical ventilation presents a series of disadvantages which can in turn have repercussions on the patient. If it is "non-invasive" ventilation, i.e. through the supply of air through a face mask, the problem is marginal, but when there is a need to use invasive instruments such as the endotracheal tube or tracheostomy to allow breathing, various complications can arise, primarily the risk of pneumonia. In particular, tracheal intubation bypasses the natural filter of the respiratory tract, which physiologically heats and humidifies the inspired gases and blocks the entry of bacteria, directly subjecting the tracheal/bronchial mucosa to air that is too dry and cold. This can cause hyperactivity of the mucous membranes up to lung infections and other disorders such as cough and dyspnea, moreover the equipment is often contaminated by infections from the patients themselves who, breathing through the tube, create an infectious nucleus that can be spread.[96,97]

Given the need to remedy these problems, in the 1950s, filtering devices, known as Heat and Moisture Exchangers (HME), were studied and developed, to be placed between the patient and the tube connecting the technical gases, capable of capturing part of the heat and humidity exhaled by the patient, and then returned to the cold technical gases during ventilation, as if they were "artificial noses". In this way, the air that reaches the trachea is no longer cold and dry but heated and humidified by the heat released by the HME filter during the passage of gases. The characteristics that these devices must respect to be effective in their operation are a high exchange of heat and humidity and low pressure drops during the air flow according to specific regulations.[98]

The current HME filters used for mechanical ventilation satisfy these requests, but the main disadvantage is linked to their composition, as they are made of expensive and non-degradable materials, which do not reflect the circular economy principles that the industrial sector is looking for to reach. In particular, these devices have a mainly "disposable" use, which involves a high economic expense as well as a considerable accumulation of waste.[99]

In this regard, given the need to develop more ecological and high-performance HME filters, in line with environmental recycling policies, the mechanical ventilation sector has exploited the potential of biomaterials.

In fact, thanks to their biocompatibility, biodegradability and origin from natural sources, biomaterials can be used for respiratory applications, in particular for mechanical ventilation devices, since they represent an excellent solution to their economic and environmental problems while maintaining high efficiency. More specifically, the research has led to the development of biopolymeric compounds such as eco-sustainable HME filters, made from industrial waste raw materials, completely biodegradable and economical. Biopolymers such as gelatin and chitosan have chemical characteristics that can easily adapt to the needs of the respiratory system, mimicking the nasal mucosa and ensuring a high exchange of heat and humidity.[100] A new generation of HME filters was created, effective for protecting the respiratory tract during mechanical ventilation, but above all ecological, as they are made of completely recyclable and degradable materials with zero impact and limited production costs.

1.6.2 Cosmetic application

The US Food and Drug Administration (FDA) has defined cosmetics as substances to be applied to the human body to clean, beautify or protect the skin without altering its physiology or functions.[101] Unfortunately, however, in a world where we still rely heavily on petroleum-based resources, current cosmetic products are full of synthetic substances that are applied to the skin every day, causing damage not only to our health but also to the environment.[102] For example, during the 20th century, toxic heavy metal contamination such as cadmium, arsenic and lead was found in cosmetics and was linked to health problems such as skin sensitivity, respiratory and cardiovascular disorders, fertility problems, cancer and even death. The safety of cosmetics therefore, even before their effectiveness and application, is of fundamental importance.[103,104]
Among the many cosmetic products that we find in our homes every day, research is having particular interest in the solar products sector. Everyone knows that exposure to solar radiation can bring benefits to our body. In details, the solar rays stimulate the production of vitamin D, necessary for bone growth, and serotonin, which allows correct regulation of the metabolism, as well as strengthening the immune system.[105,106] However, if we do not protect ourselves adequately, avoiding excessive exposure, the effect obtained is the opposite, not to mention harmful. In fact, when the skin is hit by UV radiation, sunburn, dermatitis, erythema up to melanoma can occur, but can be drastically reduced with sun protection.[107,108]
Commercial sunscreens are composed of UV filtering components: organic type (Benzophenones, Octinoxate etc.), capable of adsorbing the UV radiation and/or inorganic type

(ZnO, TiO_2), able to reflect the solar radiation, shielding it before it come into contact with the skin.[109]

Despite the excellent protective efficacy of current solar filters, several studies have shown how these substances can be harmful to human health and the environment. For example, the photocatalytic activity, generated by an inorganic filter often used, as TiO_2, in contact with the sun, can lead to the generation of free radicals and other reactive species (ROS) responsible for damaging collagen. Furthermore, inorganic filters, when used in nanometric dimensions, increase the risk of skin deeper layers penetration, causing phototoxic reaction and skin irritations.[110] On the other hand, powerful organic filters such as Benzophenones and Octocrylene, can penetrate the subcutaneous layers and interfere with the endocrine system as well as causing photosensitivity reactions.[111] In addition, from an environmental point of view, both types of UV filters, dispersed in water, cause countless problems for the marine environment, damaging fragile and precious ecosystems such as coral reefs, eliminating biodiversity and bioaccumulating in the fish species caught and consumed by man.[112,113]

In this regard, given the need to develop safer sunscreens and the increasingly strong incentives in the use of environmentally friendly and biocompatible materials, the cosmetics sector has exploited the potential of biomaterials.

In fact, thanks to their biocompatibility, biodegradability and origin from natural sources, biomaterials can be used for cosmetic applications, particularly in sunscreen products, as they are an excellent solution to the health and environmental safety problems of commercial sunscreens. More specifically, the research led to the development of hybrid compounds as eco-sustainable solar filters with SPF booster capacity, formed by nanostructured hydroxyapatite (HA) mineral particles nucleated on biopolymeric matrix. The apatite component, which easily incorporates foreign ions into its lattice, can be doped with ions as Fe^{3+}, Fe^{2+}, Zn^{2+} and Ti^{4+}, which give the material reflective properties in the UV region, eliminating the risk of photocatalytic activity and environmental pollution linked to the use of TiO_2 and others similar filters.[114,115] Furthermore, it is possible to functionalize apatite with active molecules, such as antioxidants, antiaging etc., to increase its functions in the cosmetic field.[116,117]

A new generation of sunscreens was created, effective for sun protection, but above all safe and eco-friendly, since containing a reduced quantity of commercial filters thanks to booster effect and is composed of natural materials which contact with the skin and dissolved in the environment do not cause phototoxicity or damage to the marine ecosystem.

References

(1) Dziuba, R.; Kucharska, M.; Madej-Kiełbik, L.; Sulak, K.; Wiśniewska-Wrona, M. Biopolymers and Biomaterials for Special Applications within the Context of the Circular Economy. *Materials* **2021**, 14, 7704-7721.

(2) Murray, A.; Skene, K.; Haynes, K. The Circular Economy: An Interdisciplinary Exploration of the Concept and Application in a Global Context. *Journal of Business Ethics* **2017**, 140, 369–380.

(3) Gupta, M.; Savla, N.; Pandit, C.; Pandit, S.; Gupta, P. K.; Pant, M.; Khilari, S.; Kumar, Y.; Agarwal, D.; Nair, R. R.; Thomas, D.; Thakur, V. K. Use of Biomass-Derived Biochar in Wastewater Treatment and Power Production: A Promising Solution for a Sustainable Environment. *Science of the Total Environment* **2022**, 825, 153892.

(4) Van Der Meer, Y.; France, B. Sustainable Bio-Based Materials: Opportunities and Challenges. *The International Conference for Biotechnology* **2006**.

(5) Aguilar, A.; Twardowski, T.; Wohlgemuth, R. Bioeconomy for Sustainable Development. *Biotechnology Journal* **2019**, 14, 1800638.

(6) Adeleye, A. T.; Louis, H.; Akakuru, O. U.; Joseph, I.; Enudi, O. C.; Michael, D. P. A Review on the Conversion of Levulinic Acid and Its Esters to Various Useful Chemicals. *AIMS Energy* **2019**, 7, 165–185.

(7) Festas, A. J.; Ramos, A.; Davim, J. P. Medical Devices Biomaterials – A Review. *Proceedings of the Institution of Mechanical Engineers, Part L: Journal of Materials: Design and Applications* **2020**, 234, 218–228.

(8) Montanari Margherita "Design and Development of Printable and Injectable Bio-Hybrid Inks for Tissue Engineering and Regeneration" (University of Parma, **2022**).

(9) Directive (EU) 2019/904 of the European Parliament and of the Council of 5 June **2019** on the Reduction of the Impact of Certain Plastic Products on the Environment.

(10) Yin, G. Z.; Yang, X. M. Biodegradable Polymers: A Cure for the Planet, but a Long Way to Go. *Journal of Polymer Research* **2020**, 27, 38-52.

(11) Zhu, Y.; Romain, C.; Williams, C. K. Sustainable Polymers from Renewable Resources. *Nature* **2016**, 540, 354–362.

(12) Schmid, O.; Padel, S.; Levidow, L. ISSN Xxxx-Xxxx (Print) The Bio-Economy Concept and Knowledge Base in a Public Goods and Farmer Perspective. *Bio-based and Applied Economics* **2012**, 1, 47–63.

(13) Liu, X.; Holzwarth, J. M.; Ma, P. X. Functionalized Synthetic Biodegradable Polymer Scaffolds for Tissue Engineering. *Macromolecular Bioscience* **2012**, 12, 911–919.

(14) Tian, H.; Tang, Z.; Zhuang, X.; Chen, X.; Jing, X. Biodegradable Synthetic Polymers: Preparation, Functionalization and Biomedical Application. *Progress in Polymer Science (Oxford)* **2012**, 37, 237–280.

(15) Dong, Q.; Zhang, M.; Zhou, X.; Shao, Y.; Li, J.; Wang, L.; Chu, C.; Xue, F.; Yao, Q.; Bai, J. 3D-Printed Mg-Incorporated PCL-Based Scaffolds: A Promising Approach for Bone Healing. *Materials Science and Engineering C* **2021**, 129, 112372.

(16) Kunam, P. K.; Ramakanth, D.; Akhila, K.; Gaikwad, K. K. Bio-Based Materials for Barrier Coatings on Paper Packaging. *Biomass Conversion and Biorefinery* **2022**.

(17) Bharadwaz, A.; Jayasuriya, A. C. Recent Trends in the Application of Widely Used Natural and Synthetic Polymer Nanocomposites in Bone Tissue Regeneration. *Materials Science and Engineering C* **2020**, 110, 110698.

(18) Pires, P. C.; Mascarenhas-Melo, F.; Pedrosa, K.; Lopes, D.; Lopes, J.; Macário-Soares, A.; Peixoto, D.; Giram, P. S.; Veiga, F.; Paiva-Santos, A. C. Polymer-Based Biomaterials for Pharmaceutical and Biomedical Applications: A Focus on Topical Drug Administration. *European Polymer Journal* **2023**, 187, 111868.

(19) Murphy, C. A.; Costa, J. B.; Silva-Correia, J.; Oliveira, J. M.; Reis, R. L.; Collins, M. N. Biopolymers and Polymers in the Search of Alternative Treatments for Meniscal Regeneration: State of the Art and Future Trends. *Applied Materials Today* **2018**, 12, 51–71.

(20) Gupta, R. K.; Guha, P.; Srivastav, P. P. Natural Polymers in Bio-Degradable/Edible Film: A Review on Environmental Concerns, Cold Plasma Technology and Nanotechnology Application on Food Packaging- A Recent Trends. *Food Chemistry Advances* **2022**, 1 100135.

(21) Luo, T.; Kiick, K. L. Collagen-like Peptides and Peptide-Polymer Conjugates in the Design of Assembled Materials. *Eur Polym J* **2013**, 49, 2998–3009.

(22) Grigore, M. E.; Grumezescu, A. M.; Holban, A. M.; Mogoşanu, G. D.; Andronescu, E. Collagen-Nanoparticles Composites for Wound Healing and Infection Control. *Metals* **2017**, 7, 516-529.

(23) Pina, S.; Oliveira, J. M.; Reis, R. L. Natural-Based Nanocomposites for Bone Tissue Engineering and Regenerative Medicine: A Review. *Advanced Materials* **2015**, 27, 1143–1169.

(24) Hoque, E.; Nuge, T.; Tshai, K. Y.; Nordin, N.; Hoque, M. E.; Yeow, T. K.; Prasad, R. G. S. V. Gelatin Based Scaffolds For Tissue Engineering-A review. *Polymers Research Journal* **2015**, 9, 16-32.

(25) Bello, A. B.; Kim, D.; Kim, D.; Park, H.; Lee, S.-H. Engineering and Functionalization of Gelatin Biomaterials: From Cell Culture to Medical Applications. *Tissue Eng Part B Rev* **2020**, 26, 164–180.

(26) Spencer, A. R.; Shirzaei Sani, E.; Soucy, J. R.; Corbet, C. C.; Primbetova, A.; Koppes, R. A.; Annabi, N. Bioprinting of a Cell-Laden Conductive Hydrogel Composite. *ACS Appl Mater Interfaces* **2019**, 11, 30518–30533.

(27) Bigi, A.; Cojazzi, G.; Panzavolta, S.; Roveri, N.; Rubini, K. Stabilization of Gelatin Films by Crosslinking with Genipin. *Biomaterials* **2002**, 23, 4827-4832.

(28) Vázquez, J. A.; Menduíña, A.; Durán, A. I.; Nogueira, M.; Fraguas, J.; Pedreira, A.; Valcarcel, J. Microbial Bioconversion of Chemical Waste Effluents from Marine Gelatin Isolation: Production of Probiotics under Circular Economy Philosophy. *J Clean Prod* **2023**, 416, 137952.

(29) Ul-Islam, M.; Alabbosh, K. F.; Manan, S.; Khan, S.; Ahmad, F.; Ullah, M. W. Chitosan-Based Nanostructured Biomaterials: Synthesis, Properties, and Biomedical Applications. *Advanced Industrial and Engineering Polymer Research* **2023**, 1-21.

(30) Pulieri, E.; Chiono, V.; Ciardelli, G.; Vozzi, G.; Ahluwalia, A.; Domenici, C.; Vozzi, F.; Giusti, P. Chitosan/Gelatin Blends for Biomedical Applications. *J Biomed Mater Res A* **2008**, 86, 311–322.

(31) Yan, L. P.; Wang, Y. J.; Ren, L.; Wu, G.; Caridade, S. G.; Fan, J. B.; Wang, L. Y.; Ji, P. H.; Oliveira, J. M.; Oliveira, J. T.; Mano, J. F.; Reis, R. L. Genipin-Cross-Linked Collagen/Chitosan Biomimetic Scaffolds for Articular Cartilage Tissue Engineering Applications. *J Biomed Mater Res A* **2010**, 95, 465–475.

(32) Issahaku, I.; Tetteh, I. K.; Tetteh, A. Y. Chitosan and Chitosan Derivatives: Recent Advancements in Production and Applications in Environmental Remediation. *Environmental Advances* **2023**, 11, 100351.

(33) Weng, Y.; Yang, G.; Li, Y.; Xu, L.; Chen, X.; Song, H.; Zhao, C. X. Alginate-Based Materials for Enzyme Encapsulation. *Advances in Colloid and Interface Science* **2023**, 318, 102857.

(34) Daemi, H.; Barikani, M. Synthesis and Characterization of Calcium Alginate Nanoparticles, Sodium Homopolymannuronate Salt and Its Calcium Nanoparticles. *Scientia Iranica* **2012**, 19, 2023–2028.

(35) Basu, S.; Mandal, S.; Senthil Kumar, S.; Krishnamoorthy, B.; Kumar Basu, S. Development and Evaluation of Calcium Alginate Beads Prepared by Sequential and Simultaneous Methods. *Brazilian Journal of Pharmaceutical Sciences* **2010**, 46, 786-793.

(36) Rashad, A.; Mustafa, K.; Heggset, E. B.; Syverud, K. Cytocompatibility of Wood-Derived Cellulose Nanofibril Hydrogels with Different Surface Chemistry. *Biomacromolecules* **2017**, 18, 1238–1248.

(37) Leng, C.; Li, K.; Tian, Z.; Si, Y.; Huang, H.; Li, J.; Liu, J.; Huang, W.-Q.; Li, K. Theoretical Study of Cellulose II Nanocrystals with Different Exposed Facets. *Sci Rep* **2021**, 11, 21871.

(38) Aziz, T.; Farid, A.; Haq, F.; Kiran, M.; Ullah, A.; Zhang, K.; Li, C.; Ghazanfar, S.; Sun, H.; Ullah, R.; Ali, A.; Muzammal, M.; Shah, M.; Akhtar, N.; Selim, S.; Hagagy, N.; Samy, M.; Al Jaouni, S. K. A Review on the Modification of Cellulose and Its Applications. *Polymers* **2022**, 14, 3206-3240.

(39) Vlaia, L.; Coneac, G.; Olariu, I.; Vlaia, V.; Lupuleasa, D. Cellulose-Derivatives-Based Hydrogels as Vehicles for Dermal and Transdermal Drug Delivery. *Emerging Concepts in Analysis and Applications of Hydrogels* **2016**, chapter 7.

(40) Kumar, R.; Pattanayak, I.; Dash, P. A.; Mohanty, S. Bioceramics: A Review on Design Concepts toward Tailor-Made (Multi)-Functional Materials for Tissue Engineering Applications. *J Mater Sci* **2023**, 58, 3460–3484.

(41) Heness, G.; Ben-Nissan, B.; Heness, G.; Ben-Nissan, B. *Innovative Bioceramics* **2004**, 27, 104-114.

(42) Chen, P.; Liu, L.; Pan, J.; Mei, J.; Li, C.; Zheng, Y. Biomimetic Composite Scaffold of Hydroxyapatite/Gelatin-Chitosan Core-Shell Nanofibers for Bone Tissue Engineering. *Materials Science and Engineering C* **2019**, 97, 325–335.

(43) Gerhardt, L.-C.; Boccaccini, A. R. Bioactive Glass and Glass-Ceramic Scaffolds for Bone Tissue Engineering. *Materials* **2010**, 3, 3867–3910.

(44) Eliaz, N.; Metoki, N. Calcium Phosphate Bioceramics: A Review of Their History, Structure, Properties, Coating Technologies and Biomedical Applications. *Materials* **2017**, 10, 334-438.

(45) Bose, S.; Tarafder, S. Calcium Phosphate Ceramic Systems in Growth Factor and Drug Delivery for Bone Tissue Engineering: A Review. *Acta Biomaterialia* **2012**, 8, 1401–1421.

(46) Riviera Munoz, E. M. Hydroxyapatite-Based Materials: Synthesis and Characterization. *Biomedical Engineering - Frontiers and Challenges* **2011**, 79-95.

(47) Carella Francesca "Synthesis and Characterization of Nanostructured Calcium Phosphate Matrices for Biomedical and Environmental Applications" (University of Parma, **2022**).

(48) Tampieri, A.; Celotti, G.; Landi, E. From Biomimetic Apatites to Biologically Inspired Composites. *Analytical and Bioanalytical Chemistry* **2005**, 381, 568–576.

(49) Šupová, M. Substituted Hydroxyapatites for Biomedical Applications: A Review. *Ceramics International* **2015**, 41, 9203–9231.

(50) Landi, E.; Logroscino, G.; Proietti, L.; Tampieri, A.; Sandri, M.; Sprio, S. Biomimetic Mg-Substituted Hydroxyapatite: From Synthesis to in Vivo Behaviour. *J Mater Sci Mater Med* **2008**, 19, 239–247.

(51) Panda, S.; Biswas, C. K.; Paul, S. A Comprehensive Review on the Preparation and Application of Calcium Hydroxyapatite: A Special Focus on Atomic Doping Methods for Bone Tissue Engineering. *Ceramics International* **2021**, 47, 28122–28144.

(52) Szcześ, A.; Hołysz, L.; Chibowski, E. Synthesis of Hydroxyapatite for Biomedical Applications. *Advances in Colloid and Interface Science* **2017**, 249, 321–330.

(53) Wagner, M.; Hess, T.; Zakowiecki, D. Studies on the PH-Dependent Solubility of Various Grades of Calcium Phosphate-Based Pharmaceutical Excipients. *J Pharm Sci* **2022**, 111, 1749–1760.

(54) Campodoni, E.; Montanari, M.; Artusi, C.; Bergamini, L.; Bassi, G.; Destro, E.; Fenoglio, I.; Panseri, S.; Tampieri, A.; Sanson, A.; Sandri, M. Biomineralization: A New Tool for Developing Eco-Sustainable Ti-Doped Hydroxyapatite-Based Hybrid UV Filters. *Biomaterials Advances* **2023**, 151, 213474.

(55) Agbeboh, N. I.; Oladele, I. O.; Daramola, O. O.; Adediran, A. A.; Olasukanmi, O. O.; Tanimola, M. O. Environmentally Sustainable Processes for the Synthesis of Hydroxyapatite. *Heliyon* **2020**, 6, e03765.

(56) Mohd Pu'ad, N. A. S.; Koshy, P.; Abdullah, H. Z.; Idris, M. I.; Lee, T. C. Syntheses of Hydroxyapatite from Natural Sources. *Heliyon* **2019**, 5, e01588.

(57) Bee, S. L.; Hamid, Z. A. A. Hydroxyapatite Derived from Food Industry Bio-Wastes: Syntheses, Properties and Its Potential Multifunctional Applications. *Ceramics International* **2020**, 46, 17149–17175.

(58) Ibrahim, M.; Labaki, M.; Giraudon, J. M.; Lamonier, J. F. Hydroxyapatite, a Multifunctional Material for Air, Water and Soil Pollution Control: A Review. *Journal of Hazardous Materials* **2020**, 383, 121139.

(59) Terzioğlu, P.; Öğüt, H.; Kalemtaş, A. Natural Calcium Phosphates from Fish Bones and Their Potential Biomedical Applications. *Materials Science and Engineering C* **2018**, 91, 899–911.

(60) Trivedi, A. K.; Gupta, M. K.; Singh, H. PLA Based Biocomposites for Sustainable Products: A Review. *Advanced Industrial and Engineering Polymer Research* **2023**, 6, 382-395.

(61) Campodoni, E.; Montanari, M.; Dozio, S. M.; Heggset, E. B.; Panseri, S.; Montesi, M.; Tampieri, A.; Syverud, K.; Sandri, M. Blending Gelatin and Cellulose Nanofibrils: Biocomposites with Tunable Degradability and Mechanical Behavior. *Nanomaterials* **2020**, 10, 1–18.

(62) Wang, C.; Zhang, Z.; Wang, J.; Wang, Q.; Shang, L. Biohybrid Materials: Structure Design and Biomedical Applications. *Mater Today Bio* **2022**, 16, 100352.

(63) Witte, F.; Bartsch, I.; Willbold, E. Designing the Biocompatibility of Biohybrids. **2011**, 126, 285–296.

(64) Ruiz-Hitzky, E.; Darder, M.; Aranda, P.; Ariga, K. Advances in Biomimetic and Nanostructured Biohybrid Materials. *Advanced Materials* **2010**, 22, 323–336.

(65) Suga, S.; Nakahara, H. Mechanisms and Phylogeny of Mineralization in Biological Systems. **1991**.

(66) Hong, M; Heon Lee, J; Suk Jung, H; Shin, H; Shin, H. Biomineralization of bone tissue: calcium phosphate-based inorganics in collagen fibrillar organic matrices. *Biomaterials Research* **2022**, 26, 42-61.

(67) Chen, Y.; Feng, Y.; Deveaux, J. G.; Masoud, M. A.; Chandra, F. S.; Chen, H.; Zhang, D.; Feng, L. Biomineralization Forming Process and Bio-Inspired Nanomaterials for Biomedical Application: A Review. *Minerals* **2019**, 9, 68-89.

(68) Campodoni Elisabetta "Design and Development of Bio-Hybrid Multifunctional Materials for Regenerative Medicine" (University of Parma, **2018**).

(69) Tampieri, A.; Celotti, G.; Landi, E.; Sandri, M.; Roveri, N.; Falini, G. Biologically Inspired Synthesis of Bone-like Composite: Self-Assembled Collagen Fibers/Hydroxyapatite Nanocrystals. *J Biomed Mater Res A* **2003**, 67, 618–625.

(70) Campodoni, E.; Montanari, M.; Artusi, C.; Bassi, G.; Furlani, F.; Montesi, M.; Panseri, S.; Sandri, M.; Tampieri, A. Calcium-Based Biomineralization: A Smart Approach for the Design of Novel Multifunctional Hybrid Materials. *Journal of Composites Science* **2021**, 5, 278-302.

(71) Lei, Y.; Xu, Z.; Ke, Q.; Yin, W.; Chen, Y.; Zhang, C.; Guo, Y. Strontium Hydroxyapatite/Chitosan Nanohybrid Scaffolds with Enhanced Osteoinductivity for Bone Tissue Engineering. *Materials Science and Engineering C* **2017**, 72, 134–142.

(72) Tampieri, A.; Sandri, M.; Landi, E.; Celotti, G.; Roveri, N.; Mattioli-Belmonte, M.; Virgili, L.; Gabbanelli, F.; Biagini, G. HA/Alginate Hybrid Composites Prepared through Bio-Inspired Nucleation. *Acta Biomater* **2005**, 1, 343–351.

(73) Gomes, S. I. L.; Guimarães, B.; Campodoni, E.; Sandri, M.; Sprio, S.; Blosi, M.; Costa, A. L.; Scott-Fordsmand, J. J.; Amorim, M. J. B. Safer and Sustainable-by-Design Hydroxyapatite Nanobiomaterials for Biomedical Applications: Assessment of Environmental Hazards. *Nanomaterials* **2022**, 12, 4060-4072.

(74) Williams, D. F. Specifications for Innovative, Enabling Biomaterials Based on the Principles of Biocompatibility Mechanisms. *Front Bioeng Biotechnol* **2019**, 7.

(75) Fernandez-Yague, M. A.; Abbah, S. A.; McNamara, L.; Zeugolis, D. I.; Pandit, A.; Biggs, M. J. Biomimetic Approaches in Bone Tissue Engineering: Integrating Biological and Physicomechanical Strategies. *Advanced Drug Delivery Reviews* **2015**, 84, 1–29.

(76) Krishnakumar, G. S.; Gostynska, N.; Dapporto, M.; Campodoni, E.; Montesi, M.; Panseri, S.; Tampieri, A.; Kon, E.; Marcacci, M.; Sprio, S.; Sandri, M. Evaluation of Different Crosslinking Agents on Hybrid Biomimetic Collagen-Hydroxyapatite Composites for Regenerative Medicine. *Int J Biol Macromol* **2018**, 106, 739–748.

(77) Nicoletti, A.; Fiorini, M.; Paolillo, J.; Dolcini, L.; Sandri, M.; Pressato, D. Effects of Different Crosslinking Conditions on the Chemical–Physical Properties of a Novel Bio-Inspired Composite Scaffold Stabilised with 1,4-Butanediol Diglycidyl Ether (BDDGE). *J Mater Sci Mater Med* **2013**, 24, 17–35.

(78) Yan, L.; Wang, Y.; Ren, L.; Wu, G.; Caridade, S. G.; Fan, J.; Wang, L.; Ji, P.; Oliveira, J. M.; Oliveira, J. T.; Mano, J. F.; Reis, R. L. Genipin-cross-linked Collagen/Chitosan Biomimetic Scaffolds for Articular Cartilage Tissue Engineering Applications. *J Biomed Mater Res A* **2010**, 95A, 465–475.

(79) Chen, C.; Yang, H.; Yang, X.; Ma, Q. Tannic Acid: A Crosslinker Leading to Versatile Functional Polymeric Networks: A Review. *RSC Advances* **2022**, 12, 7689–7711.

(80) Fu, Y.-W.; Sun, W.-F.; Wang, X. UV-Initiated Crosslinking Reaction Mechanism and Electrical Breakdown Performance of Crosslinked Polyethylene. *Polymers (Basel)* **2020**, 12, 420-434.

(81) Kozlowska, J.; Sionkowska, A.; Osyczka, A. M.; Dubiel, M. Stabilizing Effect of Carbodiimide and Dehydrothermal Treatment Crosslinking on the Properties of Collagen/Hydroxyapatite Scaffolds. *Polym Int* **2017**, 66, 1164–1172.

(82) Madaghiele, M.; Calò, E.; Salvatore, L.; Bonfrate, V.; Pedone, D.; Frigione, M.; Sannino, A. Assessment of Collagen Crosslinking and Denaturation for the Design of Regenerative Scaffolds. *J Biomed Mater Res A* **2016**, 104, 186–194.

(83) Hernandez, J. L.; Woodrow, K. A. Medical Applications of Porous Biomaterials: Features of Porosity and Tissue-Specific Implications for Biocompatibility. *Advanced Healthcare Materials* **2022**, 11, 2102087.

(84) Savini Elisa "DESIGN AND DEVELOPMENT OF BIOMINERALIZED NANOSTRUCTURED DEVICES FROM NATURAL SOURCES FOR BIOMEDICAL APPLICATIONS" (University of Bologna, **2016**).

(85) Mondragon, G.; Peña-Rodriguez, C.; González, A.; Eceiza, A.; Arbelaiz, A. Bionanocomposites Based on Gelatin Matrix and Nanocellulose. *Eur Polym J* **2015**, 62, 1–9.

(86) Sprio, S.; Sandri, M.; Iafisco, M.; Panseri, S.; Adamiano, A.; Montesi, M.; Campodoni, E.; Tampieri, A. Bio-Inspired Assembling/Mineralization Process as a Flexible Approach to Develop New Smart Scaffolds for the Regeneration of Complex Anatomical Regions. *J Eur Ceram Soc* **2016**, 36, 2857–2867.

(87) Gomes, S. R.; Rodrigues, G.; Martins, G. G.; Roberto, M. A.; Mafra, M.; Henriques, C. M. R.; Silva, J. C. In Vitro and in Vivo Evaluation of Electrospun Nanofibers of PCL, Chitosan and Gelatin: A Comparative Study. *Materials Science and Engineering: C* **2015**, 46, 348–358.

(88) Montanari, M.; Sangiorgi, A.; Campodoni, E.; Bassi, G.; Gardini, D.; Montesi, M.; Panseri, S.; Sanson, A.; Tampieri, A.; Sandri, M. Additive-Free Gelatine-Based Devices for Chondral Tissue Regeneration: Shaping Process Comparison among Mould Casting and Three-Dimensional Printing. *Polymers (Basel)* **2022**, 14, 1036.

(89) Lewis, P. L.; Green, R. M.; Shah, R. N. 3D-Printed Gelatin Scaffolds of Differing Pore Geometry Modulate Hepatocyte Function and Gene Expression. *Acta Biomater* **2018**, 69, 63–70.

(90) Arora, A.; Kothari, A.; Katti, D. S. Pore Orientation Mediated Control of Mechanical Behavior of Scaffolds and Its Application in Cartilage-Mimetic Scaffold Design. *J Mech Behav Biomed Mater* **2015**, 51, 169–183.

(91) Campodoni, E.; Heggset, E. B.; Rashad, A.; Ramírez-Rodríguez, G. B.; Mustafa, K.; Syverud, K.; Tampieri, A.; Sandri, M. Polymeric 3D Scaffolds for Tissue Regeneration: Evaluation of Biopolymer Nanocomposite Reinforced with Cellulose Nanofibrils. *Materials Science and Engineering C* **2019**, 94, 867–878.

(92) Bai, H.; Chen, Y.; Delattre, B.; Tomsia, A. P.; Ritchie, R. O. Bioinspired Large-Scale Aligned Porous Materials Assembled with Dual Temperature Gradients. *Sci Adv* **2015**, 1, e1500849.

(93) Sun, L.; Guo, J.; Chen, H.; Zhang, D.; Shang, L.; Zhang, B.; Zhao, Y. Tailoring Materials with Specific Wettability in Biomedical Engineering. *Advanced Science* **2021**, 8, 2100126.

(94) Wunsch, H.; Linde-Zwirble, W. T.; Angus, D. C.; Hartman, M. E.; Milbrandt, E. B.; Kahn, J. M. The Epidemiology of Mechanical Ventilation Use in the United States*. *Crit Care Med* **2010**, 38, 1947–1953.

(95) Scheenstra, R. J.; Muller, S. H.; Vincent, A.; Sinaasappel, M.; Zuur, J. K.; Hilgers, F. J. M. Endotracheal Temperature and Humidity Measurements in Laryngectomized Patients: Intra- and Inter-Patient Variability. *Med Biol Eng Comput* **2009**, 47, 773–782.

(96) GALLAGHER, J.; STRANGEWAYS, J. E. M.; ALLT-GRAHAM, J. Contamination Control in Long-term Ventilation: A Clinical Study Using a Heat- and Moisture-exchanging Filter. *Anaesthesia* **1987**, 42, 476–481.

(97) Ahmed, A.; Mewes, J. C.; Boot, I. W. A.; Vrijhoef, H. J. M. New Heat and Moisture Exchangers for Laryngectomized Patients in Germany: Mixed Methods Study on the Expected Effectiveness. *JMIR Form Res* **2023**, *7*, e36401.

(98) ISO 9360-2:2001 Anaesthetic and Respiratory Equipment -- Heat and Moisture Exchangers (HMEs) for Humidifying Respired Gases in Humans -- Part 2: HMEs for Use with Tracheostomized Patients Having Minimum Tidal Volumes of 250 Ml **2001**.

(99) Plotnikow, G. A.; Accoce, M.; Navarro, E.; Tiribelli, N. Humidification and Heating of Inhaled Gas in Patients with Artificial Airway. A Narrative Review. *Revista Brasileira de Terapia Intensiva* **2018**, 30, 86–97.

(100) Campodoni, E.; Artusi, C.; Vazquez Iglesias, B.; Nicosia, A.; Belosi, F.; Vandini, A.; Monticelli, P.; Tampieri, A.; Sandri, M. Nature-Inspired Heat and Moisture Exchanger Filters Composed of Gelatin and Chitosan for the Design of Eco-Sustainable "Artificial Noses." *ACS Appl Polym Mater* **2023**, 5, 3468–3479.

(101) *FDA Cosmetic Guidelines-Regulations https://www.fda.gov/industry/regulated-products/cosmetics-overview*.

(102) Zhao, L.; Zhu, H. The Research Status of Cosmetics and the Establishment of Biological Beautiology. *Life Science Journal* **2020**, 17, 5-11.

(103) Bilal, M.; Iqbal, H. M. N. An Insight into Toxicity and Human-Health-Related Adverse Consequences of Cosmeceuticals — A Review. *Science of the Total Environment* **2019**, 670, 555–568.

(104) Lim, D. S.; Roh, T. H.; Kim, M. K.; Kwon, Y. C.; Choi, S. M.; Kwack, S. J.; Kim, K. B.; Yoon, S.; Kim, H. S.; Lee, B.-M. Non-Cancer, Cancer, and Dermal Sensitization Risk Assessment of Heavy Metals in Cosmetics. *J Toxicol Environ Health A* **2018**, 81, 432–452.

(105) Engelsen, O. The Relationship between Ultraviolet Radiation Exposure and Vitamin D Status. *Nutrients* **2010**, 2, 482–495.

(106) Hart, P. H.; Gorman, S.; Finlay-Jones, J. J. Modulation of the Immune System by UV Radiation: More than Just the Effects of Vitamin D? *Nat Rev Immunol* **2011**, 11, 584–596.

(107) Narayanan, D. L.; Saladi, R. N.; Fox, J. L. Ultraviolet Radiation and Skin Cancer. *International Journal of Dermatology* **2010**, 49, 978–986.

(108) Lindqvist, P. G.; Epstein, E.; Landin-Olsson, M. Sun Exposure - Hazards and Benefits. *Anticancer Research* **2022**, 42, 1671–1677.

(109) Serpone, N.; Dondi, D.; Albini, A. Inorganic and Organic UV Filters: Their Role and Efficacy in Sunscreens and Suncare Products. *Inorganica Chim Acta* **2007**, 360, 794–802.

(110) Monteiro-Riviere, N. A.; Wiench, K.; Landsiedel, R.; Schulte, S.; Inman, A. O.; Riviere, J. E. Safety Evaluation of Sunscreen Formulations Containing Titanium Dioxide and Zinc Oxide Nanoparticles in UVB Sunburned Skin: An In Vitro and In Vivo Study. *Toxicological Sciences* **2011**, 123, 264–280.

(111) Battistin, M.; Pascalicchio, P.; Tabaro, B.; Hasa, D.; Bonetto, A.; Manfredini, S.; Baldisserotto, A.; Scarso, A.; Ziosi, P.; Brunetta, A.; Brunetta, F.; Vertuani, S. A Safe-by-Design

Approach to “Reef Safe” Sunscreens Based on ZnO and Organic UV Filters. *Antioxidants* **2022**, 11, 2209-2214.

(112) Moeller, M.; Pawlowski, S.; Petersen-Thiery, M.; Miller, I. B.; Nietzer, S.; Heisel-Sure, Y.; Kellermann, M. Y.; Schupp, P. J. Challenges in Current Coral Reef Protection – Possible Impacts of UV Filters Used in Sunscreens, a Critical Review. *Frontiers in Marine Science* **2021**, 8, 665548.

(113) Corinaldesi, C.; Marcellini, F.; Nepote, E.; Damiani, E.; Danovaro, R. Impact of Inorganic UV Filters Contained in Sunscreen Products on Tropical Stony Corals (Acropora Spp.). *Science of the Total Environment* **2018**, 637–638, 1279–1285.

(114) De Araujo, T. S.; De Souza, S. O.; De Sousa, E. M. B. Effect of Zn2+, Fe3+ and Cr3+ Addition to Hydroxyapatite for Its Application as an Active Constituent of Sunscreens. In *Journal of Physics: Conference Series* **2010**, 249, 012012.

(115) Adamiano, A.; Sangiorgi, N.; Sprio, S.; Ruffini, A.; Sandri, M.; Sanson, A.; Gras, P.; Grossin, D.; Francès, C.; Chatzipanagis, K.; Bilton, M.; Marzec, B.; Varesano, A.; Meldrum, F.; Kröger, R.; Tampieri, A. Biomineralization of a Titanium-Modified Hydroxyapatite Semiconductor on Conductive Wool Fibers. *J Mater Chem B* **2017**, 5, 7608–7621.

(116) Bikiaris, N. D.; Koumentakou, I.; Hatzistamatiou, K.; Lykidou, S.; Barmpalexis, P.; Nikolaidis, N. Preparation and Investigation of the SPF and Antioxidant Properties of O/W and W/O Emulsions Containing Vitamins A, C and E for Cosmetic Applications. *Cosmetics* **2023**, 10, 76-90.

(117) Adli, S. A.; Ali, F.; Azmi, A. S.; Anuar, H.; Nasir, N. A. M.; Hasham, R.; Idris, M. K. H. Development of Biodegradable Cosmetic Patch Using a Polylactic Acid/Phycocyanin–Alginate Composite. *Polymers (Basel)* **2020**, 12, 1669-1680.

CHAPTER 2

Development and Validation of Eco-friendly Designed Heat and Moisture Exchanger (HME) for the Safeguard of the Respiratory Tract and the Environment

Part of the content of this chapter has been published as Campodoni E., Artusi C., et al. "Nature-Inspired Heat and Moisture Exchanger Filters Composed of Gelatin and Chitosan for the Design of Eco-Sustainable "Artificial Noses"" ACS Applied Polymer Materials 2023.

2.1. Introduction

For more than 50 years, HMEs (Heat and Moisture Exchanger) filters have been used in hospital to ensure that the air arriving in the trachea of patients, under anaesthesia or in intensive care, maintain normal levels of humidity, heat and filtration when the upper airways are by-passed.[1] In particular, during mechanical ventilation, it is fundamental to maintain a suitable level of heat and moisture to avoid damages to the respiratory epithelium and increased secretions.

Taking a closer look, the respiratory system is made up of hollow organs in which gaseous substances are transported to or from the lungs and can be divided into upper and lower airways. The upper tract includes the nose and nasal passages, the paranasal sinuses, the pharynx and the part of the larynx above the vocal cords. This has various functions such as humidification and heating of the air, as well as the capture of dust and microorganisms derived from the outside. The lower section, on the other hand, includes the lower part of the larynx, the trachea, the bronchi, the bronchioles and the alveoli, the latter enclosed within the lungs, and is essential for carrying out the exchange of carbon dioxide and oxygen and therefore completing the own respiratory act.[2]

Focusing on the upper airways (Figure 2.1 respectively a and b), the nasal cavity is the main component extending approximately 12-14 cm in length with a total volume of 15-20 mL. It consists of three small bone folds, defined as turbinates (upper, middle and lower), which have the fundamental task of humidifying, filtering and heating the air inspired through the nostrils. Furthermore, inside it, it is possible to identify three areas, namely the respiratory section, the olfactory section and the nasal vestibule, all covered by the respiratory mucosa which covers 90% of the nasal cavity.[3]

The respiratory mucosa is made up of various types of cells and glands that are essential for protecting the upper, but particularly the lower, airways from infections and bacteria. In fact, they secrete mucus, a sticky substance composed of mucin (high molecular weight glycoproteins), water, salts, proteins and lipids, which acts as a first line of defense by trapping and expelling harmful or irritating substances, which can be inhaled from the outside. during breathing.[4,5]

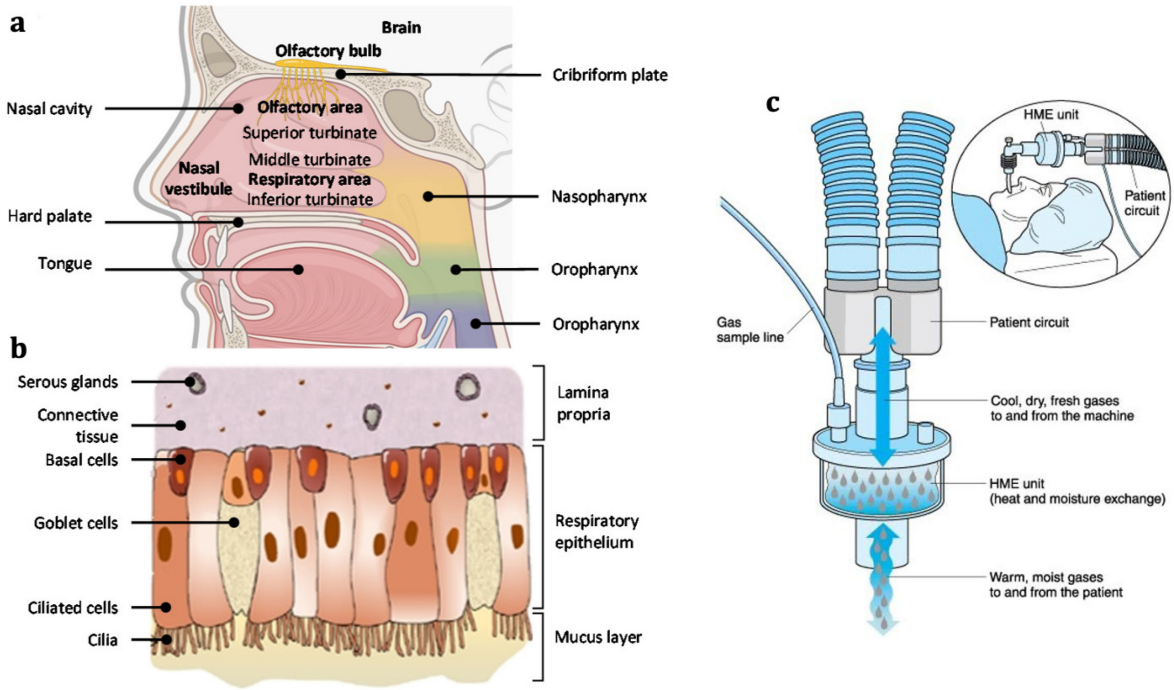

Figure 2.1. a) Anatomy of the nasal cavity; b) Anatomy of the respiratory mucosa;[2] c) Schematic representation of the use of the HME filter within the mechanical ventilation system.

Patients under anesthesia or in intensive care do not have the ability to breathe independently, therefore it is necessary to mechanically ventilate them through the mouth bypassing the upper airways, responsible for maintaining a constant level of heating and humidification necessary to avoid drying out of the mucous membranes and filtering the incoming air from possible pathogens.

In this regard, the use of HMEs aim to maintain normal physiological conditions in the lower respiratory tract, holding back part of the heat and moisture of the exhaled air by the patient during breathing and releasing them to warm and humidify the inhaled gas such as an "artificial nose". In fact, observing and taking inspiration from the superior respiratory system, HME filters have the ability to replace the functions of the nasal cavity to allow normal breathing of

the patients, heating the dry and cold medical gases with the heat and humidity recycled from the breath of the patient and filtering the air from possible bacteria (Figure 2.1c).

Currently, the HMEs commercially adopted have to ensure adequate filtration efficiency and moisture exchange for the patient, as well as show hydrophilicity and antibacterial capacity. They have also excellent mechanical properties in both dry and wet conditions and an adequate porous structure to allow easy passage of air through the device and therefore comfortable breathing.[6] However, the current HME devices have considerable limitations regarding production costs and sustainability and, in times of global warming and diminishing petroleum oil reserves, it is essential to tend towards the concept of circular economy where a reduced use of synthetic raw materials and therefore lower CO_2 production is the priority.[7–9] Furthermore, HME filters, are applied as disposable devices, generating about 100 tons of difficult-to-dispose waste every year. In this regard, making filter disposal more sustainable and limiting the productive process costs are essential points for the economy of the industries and for the environment.[10]

With this evidence, recently has been invested in replacing the employing of synthetic materials with biodegradable raw materials to develop a new generation of eco-sustainable HME devices that are more efficient and less expensive, to assist patients with tracheostomy or difficulty breathing, than those currently on the market.

It is known that natural polymers are able to mimic the biochemical composition of human body structures[11], in this case nasal mucus, a slippery secretion constituting a large part of our respiratory tract. As already mentioned, it is composed of immunoglobulins, inorganic salts, protein, glycoprotein and antiseptic enzymes and it is responsible to protect the respiratory system by trapping allergens, pollutants, bacteria and to moisturize and warm the inhaled air.[12] Among various natural polymers[13–15] (collagen, nanocellulose, alginate, fibroin, etc.), gelatin[16] (Gel) and chitosan[16] (Chit) have highlighted good chemico-physical characteristics suitable to mimic the chemistry and the moisturizing function of our natural mucus and to develop 3D porous structure able of functioning an effective HME filter.

In particular, Gel is a protein polymer derived from the denaturation of collagen, completely biocompatible, biodegradable, capable of mimicking the main protein chain of glycoproteins and thanks to its plentiful alimentary use it is available at low cost and in high quantity. It is able to create stable and porous 3D structures showing good mechanical properties and high permeability to water vapour, ideal for exchanging heat and humidity.[17] Chit instead, is a natural cationic polysaccharide, coming from the deacetylation of chitin, present in the exoskeleton of crustaceans. It can mimic polysaccharide side chains of glycoprotein and, like

gelatin, besides being biocompatible and biodegradable, it is inexpensive and easily available, being a waste material from the food industry. This natural polymer has a higher hydrophobicity respect gelatine, but above all it is capable of easily giving a resistant porous structure, which is essential for ensuring the passage of air inside the filter for the entire duration of use. Moreover, it has an intrinsic antimicrobial activity, able to counteract the proliferation of pathogens.[18]

Using an optimized and specific freeze-drying and cross-linking process, the Gel/Chit polymeric blend allow to create a resistant and effective porous 3D structure with low pressure drops and efficient heat and moisture exchange, necessary to meet commercial specifications required by an HME filter through a green-chemistry process based on raw materials from food industry waste.[19]

Following these evidences, the next strategic step is to make this new generation of medical filters marketable, making the synthesis process easily scalable, limiting production costs and reducing the percentage of polluting emissions without losing the high efficiency of the device. For this reason, this research is focused on the development and validation of an eco-sustainable, bioinspired and biodegradable HME filter composed of a Gel/Chit aerogel, with excellent filtration and bacterial inhibition properties, able to increase the exchange performance of moisture, limiting the production costs through a green-circular process based on low-cost raw materials deriving from food waste. By optimizing the production process, it was possible to reduce the environmental and economic impact of the filter and test the final prototype on a hospital equipment to promote its marketing.[20]

Analysing the process steps, the freeze-drying process is crucial for the obtaining of an aligned porous structure through the vertical freezing and subsequent the sublimation of the water contained into the material. By optimizing the freezing temperature and cooling rate[21], responsible for the size and orientation of the pores, it was possible to obtain high heat and moisture exchange, with imperceptible pressure drops, reducing the freeze-drying time. Furthermore, the cross-linking process is essential to guarantee the structural resistance of the aerogel, which tends to collapse on itself when in contact with the warm and humid aerosol during breathing.[22] In this regard, with a view to an ecological and low-cost process, two different cross-linking processes were evaluated, the dehydrothermal treatment (DHT)[23] and the treatment with tannic acid[24] (TA). Both interact with the amino groups of both polymers creating irreversible covalent bonds which increase the mechanical and chemical properties of the material, especially the preservation of the aerogel structure in water. The DHT treatment acts thermally through a vacuum oven applied after freeze-drying, while tannic acid is a natural

compound that chemically reacts with the polymeric blend during the synthesis, modifying its chemical structure. Compared to other crosslinkers[25,26], they have the advantage of being, in addition to their safety and eco-sustainability, very cheap and more immediate to use within the process, important requirements for a low cost and low time-consuming production. In addition, TA exhibits antibacterial properties, increasing the inhibitory capacity of the device against bacteria.[27]

By optimizing the freeze-drying and cross-linking process, it was possible to overcome the drawbacks of commercial HME filters, developing an innovative HME filter with increased heat and moisture exchange efficiency through a highly scalable and less expensive process.

The filtration efficiency and the antibacterial inhibition tests with the main nosocomial pathogens[28] were carried out demonstrating the ability of the filtering device to be able to counteract the presence of bacteria both by blocking them to the air passage and inhibiting their growth inside the filter. More specifically, it was tested in a hospital respiratory equipment to evaluate the HME filter in a relevant environment and to promote its possible commercialisation increasing the TRL (Technology Readiness Level) of the device. Furthermore, the improved and easily scalable process steps, together with the excellent bacterial filtration and inhibition, especially in hospital environment, highlighted the promising industrial production of a new HME device for the prevention of respiratory tract infections.

Finally, the insertion of a diagnostic component has been investigated (HMEDs filter). It is composed of liposomal vesicles functionalized with chromatic molecules to allow fast microbial detection[29] against the main bacterial strains and therefore obtaining a proof of concept to assist and facilitate the de-hospitalization of patients reducing the costs of hospital medical assistance. In this way, patients could continue their healthcare in a familiar and comfortable place, easily monitoring the presence of infections even outside the healthcare facility.

2.2. Materials&Methods

2.2.1 Biopolymers

Gelatin (Gel) was purchased from Italgelatine (Cuneo, Italy). It was extracted from pig skin and produced with mesh 4 and bloom 280. Chitosan (Chit) of medium molecular weight) was purchased by CD Bioparticles (Shirley, New York, USA) and by Sigma Aldrich (Saint Louis, Missouri, USA). Tannic acid (TA) and Acetic acid were purchased by Sigma Aldrich (Saint Louis, Missouri, USA). Rhodamin-B and sorbitol was received from Merck-Sigma (Germany), Soybean lecithin given by Lipoid (Ludwigshafen am Rhein, Germany).

2.2.2 Synthesis of HMEs filters

A biopolymer blend, with a concentration of 2 wt% was obtained by mixing an aqueous solution of Gel and an acidified aqueous solution of Chit in order to obtain Gel:Chit weight ratios of 70:30. In detail, Gel solution was prepared by dissolving gelatin in water at 45 °C under magnetic stirring, while Chit solution was prepared by dissolving Chit in acetic solution 0.1 wt% respect polymer (pH=5.5) at room temperature and stirring till its complete dissolution. In the meantime, TA water solution was prepared by dissolution under stirring at room temperature. Afterwards, Gel and Chit solutions were mixed and after homogenization TA solution (8 wt% respect biopolymer blend) was added to perform a chemical cross-linking. The stirring was maintained at room temperature until a complete homogenization of the blend (about 15 min). Finally, the mixture was casted into a 100 mL mold with copper bottom of 5x5 cm^2 and plastic walls. After four hours at room temperature the light-yellow solution jellifies thanks to the polymer/tannic acid cross-linking reaction. The hydrogel was freeze-dried (freeze-drier 5 Pascal Lio 3000 PLT) applying different freezing temperatures, reported afterwards (Table 2.1), and a heating ramp of 5 °C/h up to -10 ° C followed by a ramp of 1 °C/h up to 25 °C. After freeze-drying, the upper and the lower surfaces were cut off about 2 mm of thickness and the 3D construct (aerogel) obtained was further cross-linked with dehydrothermal treatment (DHT) (vacuum oven VDL 53 Binder) (Figure 2.2).

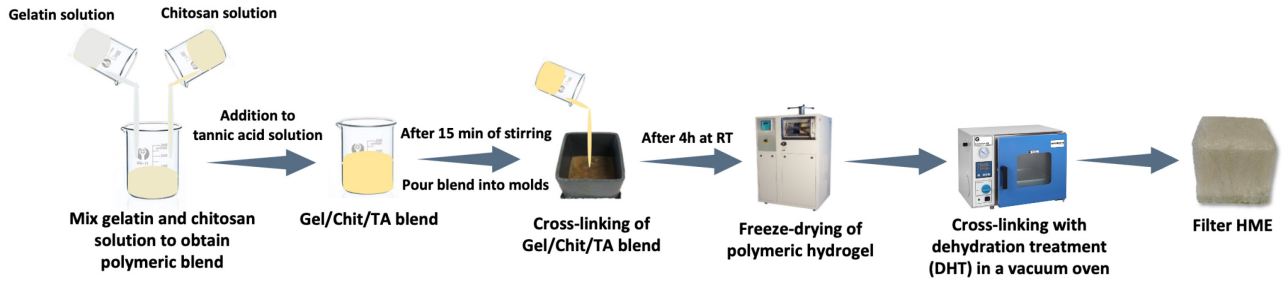

Figure 2.2. Synthesis and forming process steps to develop the Gel/Chit/TA aerogel as an HMEs filter device.

Different process parameters such as freeze-drying and cross-linking were experimented in order to optimize the features related to the specific functions that lead the device to be suitable as HME. All the parameters tested are resumed in the Table 2.1 below.

Table 2.1. Freeze-drying and cross-linking parameters of the developed Gel/Chit based HMEs.

Samples	Freeze-drying condition		Cross-linking condition	
	Freezing T	Cooling rate	DHT condition	TA
A	-40 °C	50 °C/h		
B	-40 °C	30 °C/h		
C	-40 °C	10 °C/h		
D	-30 °C	10 °C/h		
E	-20 °C	10 °C/h		
F	-20 °C	10 °C/h	0,01 mbar; 160 °C; vacuum; 48h	---
G			0,01 mbar; 160 °C; vacuum; 24h	---
H			0,01 mbar; 120 °C; vacuum; 48h	---
I			0,01 mbar; 120 °C; vacuum; 24h	---
L			0,01 mbar; 120 °C; vacuum; 24h	8wt%
M			0,01 mbar; 80 °C; vacuum; 24h	8wt%
N			---	8wt%

2.2.3 Morphological characterization

Biocomposite morphology was evaluated after freeze-drying by Environmental Scanning Electron Microscopy (ESEM, Quanta 200 FEG, FEI Company, Hillsboro, OR USA). The samples were prepared by fixing them onto aluminum stubs using carbon tape, and then Au coated using the coating unit Polaron Sputter Coater E5100 (Polaron Equipment, Watford, Hertfordshire, UK). The dimensional analysis was performed by means of ImageJ software.

2.2.4 Chemico-physical characterization

The **degradation** of the filters was measured through a weight-loss test. It was performed by soaking the samples in distilled water at 37 °C while shaking.[30] After 1 and 3 days, being the maximum life-time of an HME filter of 2-3 days, the samples were taken out from the medium, washed three times in distilled water and freeze-dried. The samples were then weighed and the weight loss (%) was calculated through the following equation 2.1:

$$\boldsymbol{Weight\ loss_{\%}} = \frac{\boldsymbol{W_i - W_f}}{\boldsymbol{W_f}} \times \mathbf{100} \qquad \textbf{Eq. 2.1}$$

where W_i was the dried sample's initial weight while W_f was the freeze-dried sample weight at a specific time point.

The **cross-linking degree** (CD%) were evaluated by TNBS (2,4,6-trinitrobenzenesulfonic acid) assay, reported by Balakrishnan et al.[31] TNBS test spectrophotometrically evaluated the amount of free primary amines ($-NH_2$) of the Gel that decreased after blending with Chit through physical or chemical cross-linking process.

Briefly, to perform the CD% tests, 1 mL of $NaHCO_3$ solution (4% w/v) was added to 5 mg of cross-linked materials and non-cross-linked materials. After 30 min, a freshly prepared TNBS (0. 5% w/v) solution was added. The reaction mixture was heated at 40 °C for 2 h and then 3 mL of 6 M HCl were added. The reaction mixture was heated at 60 °C for 90 min and then diluted 1:1 with milliQ water and cooled to room temperature. The absorbance at 415 nm was recorded using a UV–vis spectrophotometer (Perkin-Elmer Lambda 35, Milano, Italy). For each sample, the measurements were run in triplicates and a composite-free blank was prepared under the same conditions. The cross-linking degree (CD%) was evaluated through the following equation 2.2:

$$CD_{\%} = \left(1 - \frac{Cross\text{-}linked\ biocomposite\ absorbance}{Not\ cross\text{-}linked\ biocomposite\ absorbance}\right) \times 100 \qquad \textbf{Eq. 2.2}$$

Three replicates were assessed (n = 3) and the results are expressed as mean ± standard error.

For the **moisture recovery** tests, the test apparatus used was based on the lung model described in ISO 9360 and consisted of two separate circuits (Figure 2.3).[32]

The performance of the sample (moisture output) was determined with equation 3 by measuring the mass of water lost from the patient model. Moisture loss, expressed in milligrams of water per liter of air (mg H_2O/L), was assessed from the weight differences of the test apparatus over a certain period. Therefore, knowing the value of absolute humidity of the expired air assuming flow was fully saturated with water vapor (AHexp), it is possible to calculate the moisture output:

$$\textit{Moisture output = AHexp – moisture loss} \qquad \textbf{Eq. 2.3}$$

The limit value of moisture output accepted by the ISO 9360 standard is 33 mg H_2O/L.[7,33]

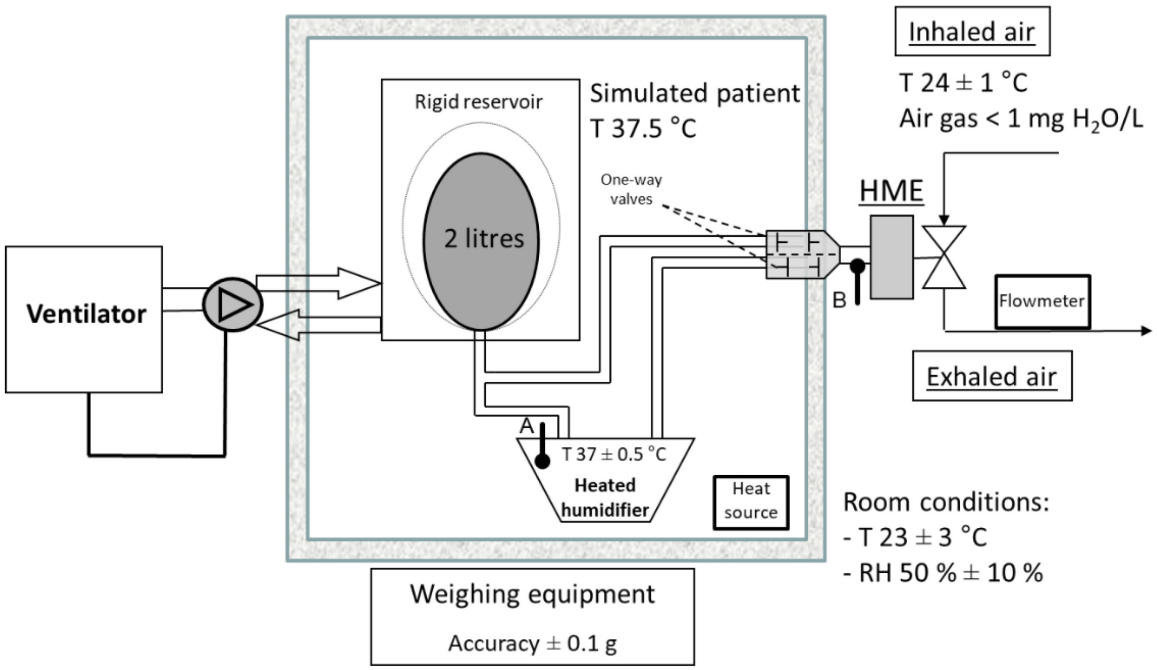

Figure 2.3. Schematic diagram of the experimental test apparatus based on ISO 9360.

The **pressure drop** of each sample was recorded before and after preconditioning the sample in the previous test apparatus for two hours. One flowrate was used with dry air according to

the ISO standard 9360: 60 L/min. Resistance across the sample holder was measured by an electronic differential manometer (2080P, Digitron, United Kingdom). The value limit of pressure drops accepted by the ISO 9360 standard is 5 mbar.[7,33]

2.2.5 Bacterial filtration and Bacteriostatic activity

To evaluate the bacterial filtration capacity of HME devices, the three most common bacterial strains, *Escherichia coli* (Gram-negative enterobacteria), *Pseudomonas aeruginosa* (Gram-negative bacteria of environmental origin), *Staphylococcus aureus* (Gram-positive bacteria belonging to the human-derived genus), were selected and tested with optimized HME filter through microbiological analyses.

Initially the bacterial solutions were prepared. Each bacterial strain was revitalized in Tryptone Soya Broth (TSB) medium at 35 °C for 24 h and seeded by loop seeding in Tryptone Soya Agar (TSA) medium. Subsequently an incubation of 72 h at 36 °C was carried out to allow the correct development of the colonies. Each bacterial culture obtained was collected and dispersed in 5 mL of sterile sodium chloride physiological solution (0,9%), until a concentration of 10^8 Colony Forming Units (CFU, unit by which the culturable number of microorganisms is expressed) per mL. Finally, each bacterial suspension in liquid culture was diluted to obtain a known title high concentration of 10^6 CFU/mL to be used to test the filtration efficiency and both a low concentration of 10^3 CFU/mL and a higher concentration of 10^6 CFU/mL to evaluate the bacteriostatic capacity of test HME filter.

Subsequently, the HME filter under examination was placed on a support connected to a vacuum pump for the filtration of 5 mL of each bacterial culture in suspension to determine its efficiency and effectiveness in reducing the initial bacterial concentration corresponding to both the percentage bacterial filtration capacity and the bacteriostatic activity of the optimized HME filter N.

2.2.6 Bacterial Filtration Efficiency (BFE)

The Bacterial Filtration Efficiency (BFE) was carried out based on the standard EN14683:2019[34] and involves the evaluation of the filtering efficiency of a filter against a nebulized bacterial suspension in the form of an aerosol. The bacterial load used is made up of *Staphylococcus Aureus*, which is nebulized inside an aerosol chamber. The droplets produced then come into contact with the filter to be tested placed at the inlet of a 6-stage cascade

impactor (Andersen) under vacuum where they are sampled for the subsequent bacterial count and therefore filtration efficiency.[35]

Initially, the bacterial suspension at a known concentration (3.0x103 CFU) is introduced into the nebulizer where the particles formed have a size of around 3.0 ± 0.3 μm. Before carrying out the test on the filter, a test was carried out without a specimen as a positive control, the bacterial aerosol was then passed through the impactor for two minutes. Subsequently, 5 samples of optimized HME filter of size 5x5 cm were tested, previously conditioned at 21 ± 5 °C and 85 ± 5% of relative humidity for at least 4 hours to bring them into equilibrium with the atmosphere. They were then placed at the inlet of the impactor in contact with the bacterial aerosol for two minutes. Finally, the last positive control was performed by flushing the bacterial suspension inside the impactor without sample.

Each stage of the impactor consists of a plate which is incubated at 37 °C for 50h to then count the bacterial colonies which have deposited on each plate and which therefore have not been filtered by the device.

For each sample, the bacterial filtration efficiency B is calculated as a percentage using equation 2.4:

$$\boldsymbol{B = \frac{(C-T)}{C}\, x\, 100} \qquad \textbf{Eq. 2.4}$$

Where C is the average of the bacterial colonies found on the plates for the positive controls, i.e. without any filtering barrier; T is the total bacterial colony count deposited on the plates following the HME specimen test. In this way it was possible to analyze how much the HME filter is able to block a bacterial aerosol.

2.2.7 Validation in hospital environment

In order to make possible the commercialization of the optimized HME filter and thus reduce the gap from Research to Market, the efficiency of the device was evaluated in a real environment. In detail, the tests were carried out directly on hospital instrumentation inside Montecatone Rehabilitation Hospital (Bologna, Italy) without connection with the patient.

The optimized filter was compared with a commercial one normally used in hospitals, placed in parallel between an AMBU (Auxiliary Manual Breathing Unit) flask and the machine connected to the medical gas line (Figure 2.4).

Two tests were performed, one by keeping the two filters connected for 4 hours to an AMBU flask coming from a patient infected with *Acinetobacter species*, opportunistic pathogenic Gram-

negative bacteria and the other for 6 hours connected to a flask coming from a patient with a significant infection with *Klebsiella New Delhi*, Gram-negative enterobacteria. The initial bacterial load (T0) was directly quantified from the two infected AMBU flasks.

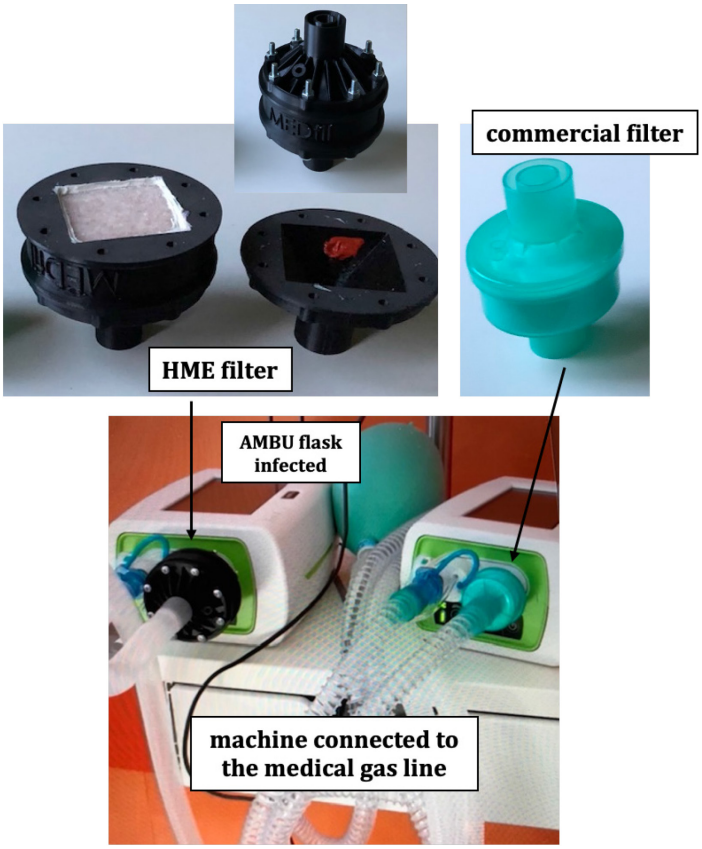

Figure 2.4. Set-up of bacterial filtration test to compare commercial filter and optimized HME filter in hospital environment.

After the respective hours in intensive care in contact with the bacterial aerosol from the different infected AMBUs, each HME prototype was taken and tested in the microbiological laboratory. The bacterial count was carried out using a selective culture medium (Cetrimide Agar) and two differential culture mediums, such as MacConkey Agar and Cled (Cysteine-Lactose-Electrolyte-Deficient) Agar, incubated for 4 days at 36 °C, to evaluate the difference between the two types of device and demonstrate the percentage filtering efficiency of the optimized HME filter in the hospital field.

In addition to the comparison between commercial filter and HME filter, the bacterial filtration efficiency of HME prototype was tested again, in this case placing it between the respiratory mask (in the absence of a patient) and respectively three AMBU flask that had come into contact with patients infected with different bacterial strains for 4 hours each, i.e. *Acinetobacter species/KCP, Pseudomonas species* and mixed bacterial culture (Figure 2.5). The initial bacterial

concentration (T0) was obtained by calculating the bacterial load present in the commercial HME filter which was connected to the three infected patients.

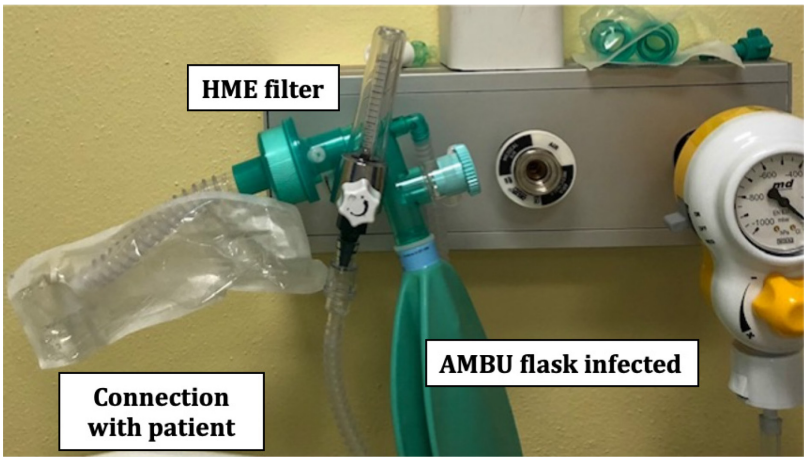

Figure 2.5. Set-up of bacterial filtration test with optimized HME filter in contact to three different bacterial strains in hospital environment.

As the previous test, after the respective hours in intensive care in contact with the bacterial aerosol from the different infected AMBUs, each HME filter tested was sampled and analyzed in the microbiological laboratory to confirm the bacterial filtration capacity of the HME filter and therefore its use as a filter device in the hospital. The bacterial count was carried out using selective culture mediums, incubated for 4 days at 36 °C, depending on the bacterial type: Mac Conkey Agar for *Acinetobacter species/KCP,* Cetrimide Agar for *Pseudomonas species* and Cled Agar for mixed bacterial culture.

2.2.8 Stability test

To evaluate the stability of the HME filter over time and therefore the possibility of producing and storing it on an industrial level, the sterilized (gamma radiation) and validated prototype was tested inside the apparatus at different time points, precisely 1-3-6-9-12 months, to demonstrate that the pressure drops and moisture exchange measures remain constant over time.

2.2.9 Diagnostic component (HMEDs filter)

To evaluate and control the onset of respiratory infections and have a proof of concept of the possible de-hospitalization of patients thanks to the use of HME filters, thus reducing healthcare costs, a diagnostic component has been inserted within the material, creating HMEDs device.

This component is made of soybean lecithin vesicles functionalized with the chromatic molecules of Rhodamine-B. The interaction of these liposomes with microbial toxins is known to effect liposome permeability or produce membrane breakage with rhodamine leakage. This phenomenon allows the fast-chromatic detection of the microbial presence. Tests were affected with *Staphylococcus aureus*, *Pseudomonas aeruginosa* and *Escherichia coli*.

2.2.9.1 Synthesis of liposome

The lipid vesicles containing Rhodamine-B in the ratio of 20:1 and 10:1 (lipid:dye) were prepared using the hydration technique.[36,37] Briefly a homogeneous and well dried lipid film of soybean lecithin (1 gr, 1.2 mmol) was hydrated with an aqueous solution (20 ml) containing Rhodamine B (27.74, 0.06 mmol) or (57.48 mg, 0.12 mmol), according to the ratio, and sorbitol (100 mg, 0.005 mmol) as cryoprotectant. The suspension was vortexed for 10 min obtaining the liposomes as multi-lamellar vesicles. The non-encapsulated Rhodamine-B was removed by sequential centrifugations (15000 rpm g × 4 °C × 30 min) and washed with fresh tri-distilled water until a transparent and colourless supernatant was obtained. The absence of Rhodamine-B in the transparent supernatant phase was also confirmed by UV (550 nm maximum value of absorbance for Rhodamine-B). The size of the MLVs, determinate DLS (dynamic light Scattering) was equal to 930±30 nm (polydispersity of 0.2). The encapsulated efficacy (EE%) of Rhodamine-B contained in the lipid vesicles was equal to 57% and determined by UV, analysing the ethanolic aqueous solution (30%) used to induce the disruption of the liposomes with consequent release of the dye. The derivatized vesicles as pellets were stored at 4 °C and used for the needed experiments.

2.2.9.2 HMEs filters impregnation with liposome/Rhodamine-B solution

To obtain the most effective impregnation of the HME filters with the solution of synthesized liposomes loaded with Rhodamine-B, tests were carried out to evaluate which was the best combination between the size of the filter area and the volume of solution to be impregnated. 3 different areas (4, 2, 1 cm^2) with different volumes (4, 2, 1, 0.5, 0.25 mL) were tested and the complete absorption and homogeneous distribution of the solution on the HME filter were observed. The best result obtained was highlighted with an area of 1 cm^2 impregnated with 0.25 mL of solution. Obviously being a proof of concept, small areas and volumes have been used.

2.2.9.3 Bacterial detection

Two different solutions were tested with concentration of liposome/Rhodamine-B 10:1 and 20:1, respectively, by impregnating 0.25 mL of each solution directly on a small area of the device (1 cm^2). Subsequently, the sample impregnated was placed on a Whatman hydrophilic membrane and 200 μL of the mix of bacterial suspension at known concentration ($3.2x10^5$ CFU/mL) was dripped and filtered over it to evaluate through visual analysis the colour variation following contact with the bacteria. The chromatic variation obtained was defined on the basis of a colour intensity scale from 0 to 1.

2.3. Results&Discussion

2.3.1 Chemico-physical characterization

2.3.1.1 Freeze-drying process evaluation

Gel/Chit wt% ratio at 70:30 and hydrogel concentration at 2%, as literature suggests[12], the suitable freeze-drying cycle which influences pore size and orientations, was evaluated to create an HME device with reduced pressure drop. In particular, freezing temperature and cooling rate are the two main process steps, which control the growth of crystals inside the hydrogel and therefore the final pores size and orientation. Cooling rate and freezing T have been modified in order to observe how the porous structure changes accordingly (Figure 2.6).

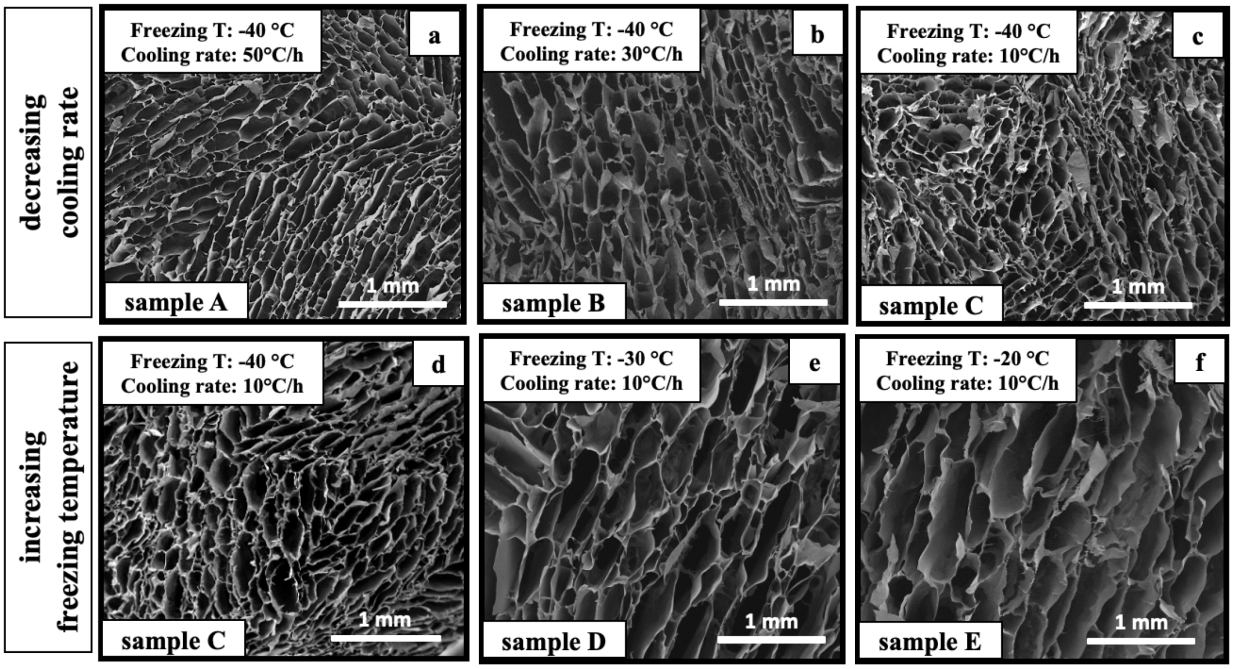

Figure 2.6. SEM morphologies of samples freeze-dryed with different freezing temperature and cooling rate.

As can be seen from Figures 2.6 (a-c), the freezing temperature at -40 °C was kept constant in these samples and the cooling rate varied, respectively at 50 °C/h, 30 °C/h and 10 °C/h. As the cooling rate increases, the short axis of ellipsoidal pores decreases from 108 to 73 ± 0,05 μm with a more heterogeneous structure and no effective preferential orientation (sample A), because an excessive freezing rate causes the formation of very small ice crystals. On the other hand, increasing the freezing temperature, the size of ice crystals increases from 108 to 252 ± 0,03 μm approximately (Figures 2.6 d-f).[38]

Freeze-drying, by acting on the pores' size, influences the pressure drops of the device, which play one of the most important roles for the effectiveness of HME filters. As Figure 2.7 shows, the pressure drops decrease with the increase of the pores' size. Comparing pores' size and pressure drop, small and heterogeneous pores caused by freeze-drying process with too rapid cooling rate (samples A, B, C), lead to high pressure drops; on the other hand, as observed in samples D and E, channels with pore sizes around 250 µm show pressure drops almost undetectable by the instrument, which is below the 5 mbar value limit of the ISO 9360 standard.

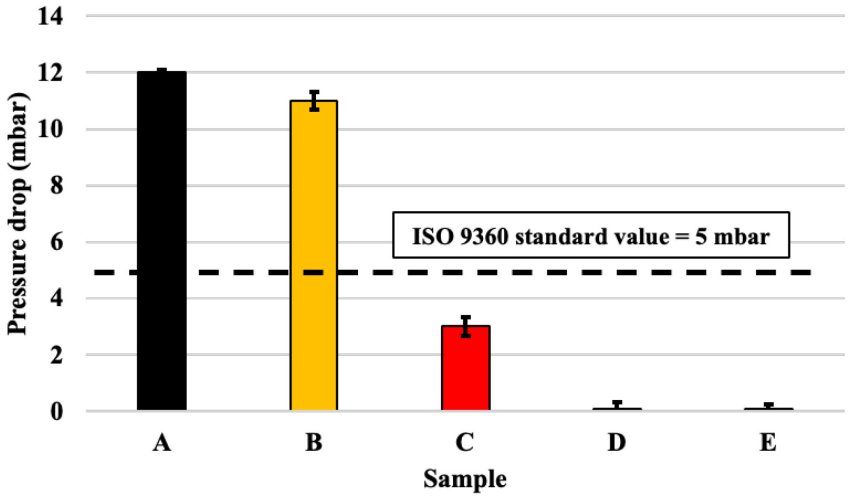

Figure 2.7. Pressure drop of samples freeze-dryed with different freezing temperature and cooling rate: A) freezing temperature of -40 °C, cooling rate of 50 °C/h, pore dimensional range of 73-76 µm B) freezing temperature of -40 °C, cooling rate of 30 °C/h, pore dimensional range of 82-86 µm C) freezing temperature of -40 °C, cooling rate of 10 °C/h, pore dimensional range of 103-108 µm D) freezing temperature of -30 °C, cooling rate of 10 °C/h, pore dimensional range of 198-206 µm E) freezing temperature of -20 °C, cooling rate of 10 °C/h, pore dimensional range of 248-252 µm.

According to the results reported in Figure 2.7, although both freezing temperatures at -30 °C (sample D) and -20 °C (sample E) were effective for the specifications required by an HME device, the use of a higher freezing temperature (sample E), requires less use of energy and process time, preferable in terms of cost reduction.

With this evidence, the freeze-drying cycle at -20 °C for 10 °C/h (sample E) was selected as the best choice because shows undetectable pressure drops and low energy consumption due to its morphology, that highlight highly aligned and big pores' size (Figure 2.8).

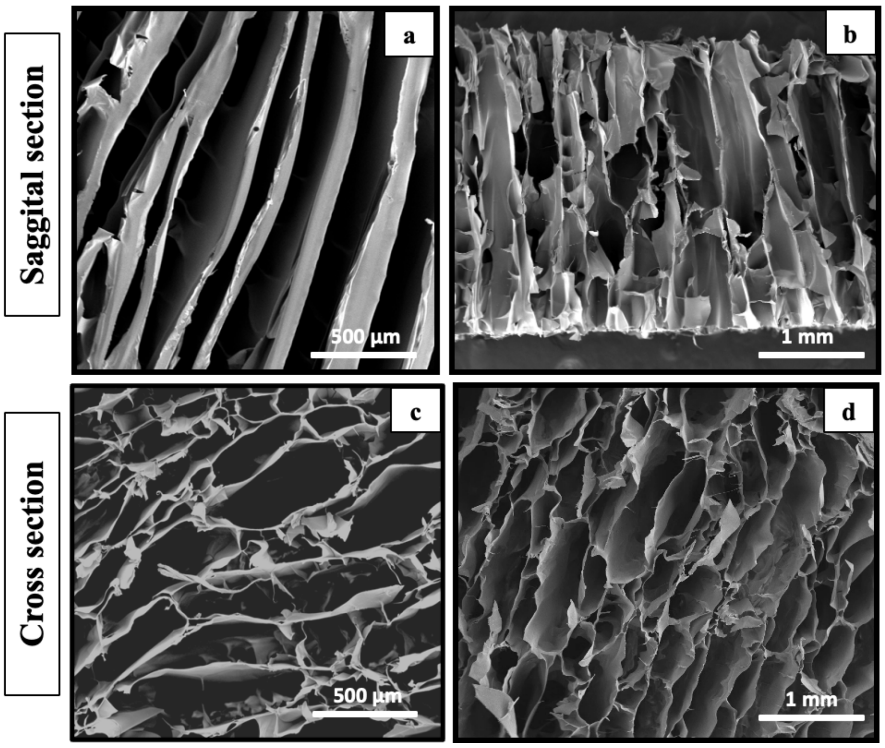

Figure 2.8. Sagittal and cross morphology of sample E.

2.3.1.2 Cross-linking process evaluation

Two different cross-linking agents, natural and physical ones, have been tested to evaluate an improvement in the HME structural strength and stability.

Among several cross-linking agents[39], natural ones have been favoured. In particular, Tannic acid (TA) has been selected due to its hydrophilic chemical structure could improve the heat and moisture exchange of the filter, as well as speed up and increase energy savings in the process of HME filers development. TA is derived from tannin, a polyphenol presents in the bark of many plants and in some fruits such as grapes. It is reacting with amine groups allows chemical bonding between Gel and Chit before the freeze-drying process of the filter.[40] In detail, TA is very interesting due to its low cost and it has been preferred to other effective natural cross-linking as genipin, because it is too expensive and requires too long cross-linking times for a disposable device.[12]

On the other hand, dehydrothermal treatment (DHT) has been selected as physical cross-linking process able to induce the formation of amide bonds between carboxyl and amine groups via condensation reactions; in detail, it acts on dried samples through the heat and vacuum generated by an oven.[41] With this evidence, different cross-linking conditions such as temperature, cross-linking time and TA wt% (Table 2.1) were modulated to evaluate the

morphology, material degradation, cross-linking degree, pressure drop and moisture exchange for the optimized HME filter (sample E, freezing T -20 °C, cooling rate 10 °C/h).

ESEM images of cross-linked samples with different cross-linking conditions are shown in Figure 2.9 to observe possible morphological changes.

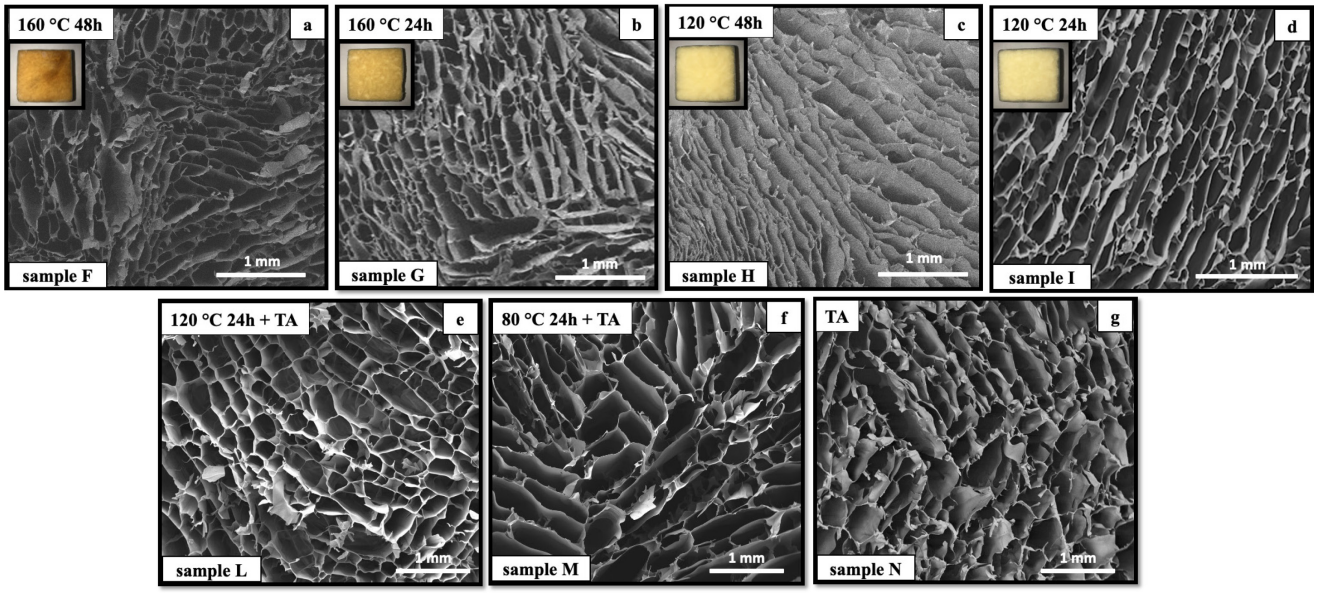

Figure 2.9. SEM morphologies of samples trasversal section cross-linked with different parameters of DHT treatment and/or TA: a) 160 °C for 48h b) 160 °C for 24h c) 120°C for 48h d) 120 °C for 24h e)120°C for 24h with TA f) 80 °C for 24h with TA g) only TA

From the structure and size of the pores it is noted that the temperature and time of DHT do not affect the morphology of the material (Figures 2.9 a-d), and the pore size remains homogeneous, about 240 μm, with an anisotropic interconnected structure featured by vertically aligned channels thanks to freeze-drying process. Furthermore, also the addition of TA does not change the porosity structure (Figures 2.9 e-g), even when it is combined with the DHT treatment (samples L and M), meaning that the cross-linking process acts on the polymeric chains of the compounds, forming new chemical bonds and reinforcing their structure, without modifying their morphology, as opposed to freeze-drying.

On the other hand, focusing on the stability of HMEs (Figure 2.10 a), it is clearly visible that the higher the cross-linking temperature the lower the degradation of the material over time, this is because there is a greater formation of amine bonds which make the final polymeric structure more resistant. In detail, the sample G and F appear to be the most stable compared to the other samples, being those crosslinked with DHT at the highest temperature (160 °C). As the cross-linking temperature decreases, the stability decreases (sample H, I), but it is possible to

compensate for it with the addition of tannic acid (sample L, M, N). In fact, even if the samples with TA show a slightly greater degradation after 1 day than those crosslinked with DHT alone at 160°C, after 3 days the difference is imperceptible, managing to reduce (sample L, M) or eliminate the use of DHT (sample N).

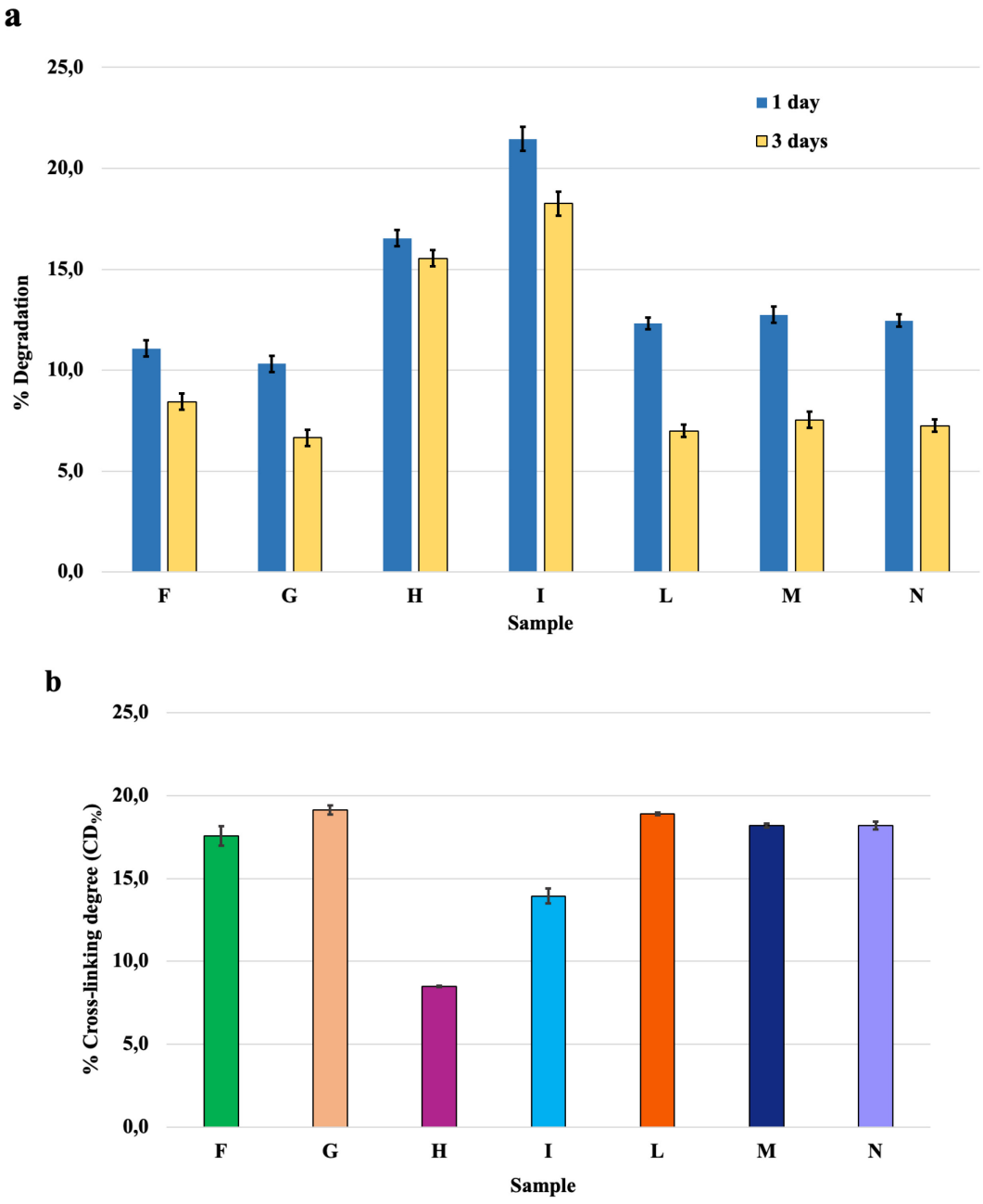

Figure 2.10. a) Wt% Degradation test b) % Crosslinking degree test of samples cross-linked with different parameters of DHT treatment and/or TA: F) 160 °C for 48h G) 160 °C for 24h H) 120°C for 48h I) 120 °C for 24h L) 120°C for 24h with TA M) 80 °C for 24h with TA N) only TA

Indeed, by analysing the cross-linking degree obtained with the TNBS test (Figure 2.10 b), samples H and I crosslinked at lower temperatures show a higher percentage of free amines

and therefore a lower cross-linking degree than the other two samples F and G, confirming the greater resistance of these samples obtained from the degradation test. Observing the crosslinked samples also with the presence of TA, little difference in the degree of cross-linking between the latter and the samples crosslinked with DHT at higher temperatures can be seen. Evidently the DHT treatment allows to create a greater number of amide bonds which lead to a lower degradation of the material in physiological conditions of the breath, but as the crosslinking temperature decreases and TA is inserted, there is a slight increase of stability.
This further confirms that the tannic acid can compensate for the drop in the crosslinking temperature up to eliminating the DHT, while keeping the material stable under the conditions of use and reducing the process time and costs, such as shown by sample N.
Analysing the pressure drop and the moisture exchange of differently cross-linked HME (Figure 2.11), it is possible to observe that in both graphs all samples crosslinked at different temperatures, times and wt% of TA are within or close to the standard specifications.
In particular, the pressure drops (Figure 2.11 a) measured are all below 1 mbar, even if the sample crosslinked with TA (sample N) has a slightly higher-pressure drop compared to the sample F and G crosslinked using only DHT. Evidently, the cross-linking treatments selected by not modifying the morphology of the filter do not create potential obstacles for the passage of air. The moisture exchange graph (Figure 2.11 b), on the other hand, outlines that the crosslinked filters at 120 °C (samples H and I) have a value slightly below the standard limit of 33 mg H_2O/L, while the other samples show a good heat and humidity exchange capacity which is above the standard value. In detail, the sample N cross-linked with TA as single cross-linking, records the highest value equal to 36.5 mg H2O/L confirming that the use of TA in the HME, despite presenting a slight increase in the degradation of the material, improves the effective moisture exchange's performances.

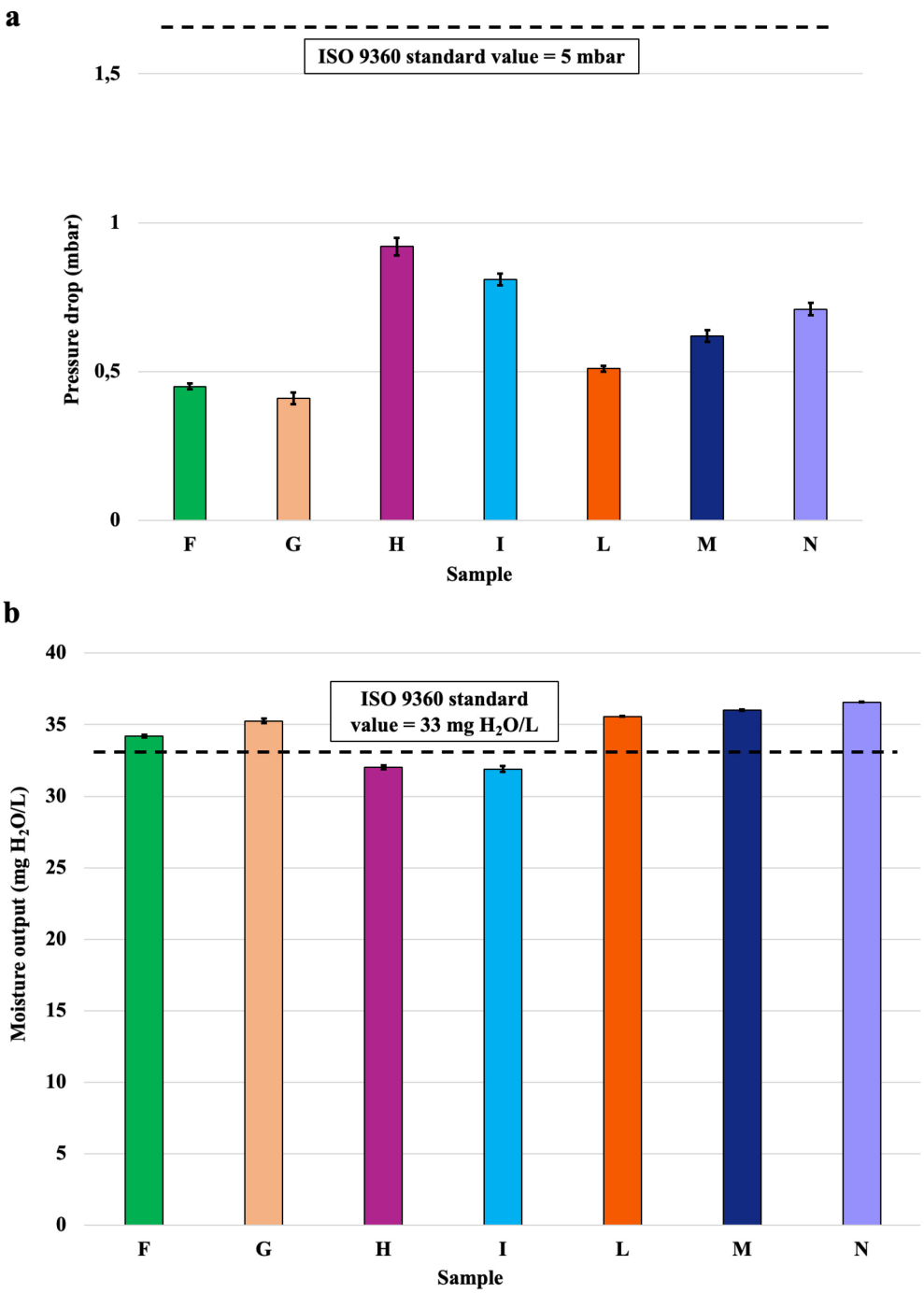

Figure 2.11. a) Pressure drop b) Moisture exchange of samples cross-linked with different temperature and time of DHT treatment: F) 160 °C for 48h G) 160 °C for 24h H) 120°C for 48h I) 120 °C for 24h L) 120°C for 24h with TA M) 80 °C for 24h with TA N) only TA

To sum up the collected results, both DHT treatment and TA are two eco-sustainable and efficient crosslinking methods for developing HME devices according to the regulations; however, TA reaches the same performance as DHT but reduces energy consumption and speeds up the production time, decreasing, thus, the costs of final HME in comparison with that

currently in the market. Furthermore, tannic acid has the added value of being antibacterial, increasing together with chitosan the device's ability to inhibit the onset of infections.[27]
By the end, sample N freeze-dried with freezing temperature of -20 °C and cooling rate of 10 °C/h and cross-linked with tannic acid has been selected as the most promising eco-sustainable, low cost and efficacy HME device. Indeed, being composed of completely biodegradable materials, coming from food waste, leads to final product cheaper and eco-friendly with reduced CO_2 emissions, developed through a circular green process, essential for industrialization.

2.3.2 HME filter optimization for reducing cost and environmental impact

Once selected the suitable polymers and cross-linking agent able to i) mimic the chemical structure of glycoproteins of the mucus; ii) reduce the pressure drop conferring a comfortable breathing; iii) increase moisture exchange maintaining chemical structural stability, a deep investigation was carried out with the aim to reduce the cost of this disposable material and even more the impact on the environment making it more attractive to the industrial market.
The filtering devices currently on the market, as previously specified, are composed of synthetic raw materials, which in addition to increasing production costs, involve a greater expenditure of energy for their industrial processing and more difficulty in disposing of the final product. In this regard, despite the good performance of current synthetic HME filters, in terms of cost reduction and environmental impact they are not comparable with new generation eco-sustainable devices, where raw materials from biodegradable industrial waste are used.
Focusing on being "low-cost", as can be seen from Figure 2.12 a, gelatin, acetic acid and tannic acid are not components that affect the final price of the product since the total cost of a single HME filter is less than 0.10 cents (0,067). Chitosan, on the other hand, is the element that most unbalances the overall expense (94%) with the cost of 1 € to develop a single device (HME 1).

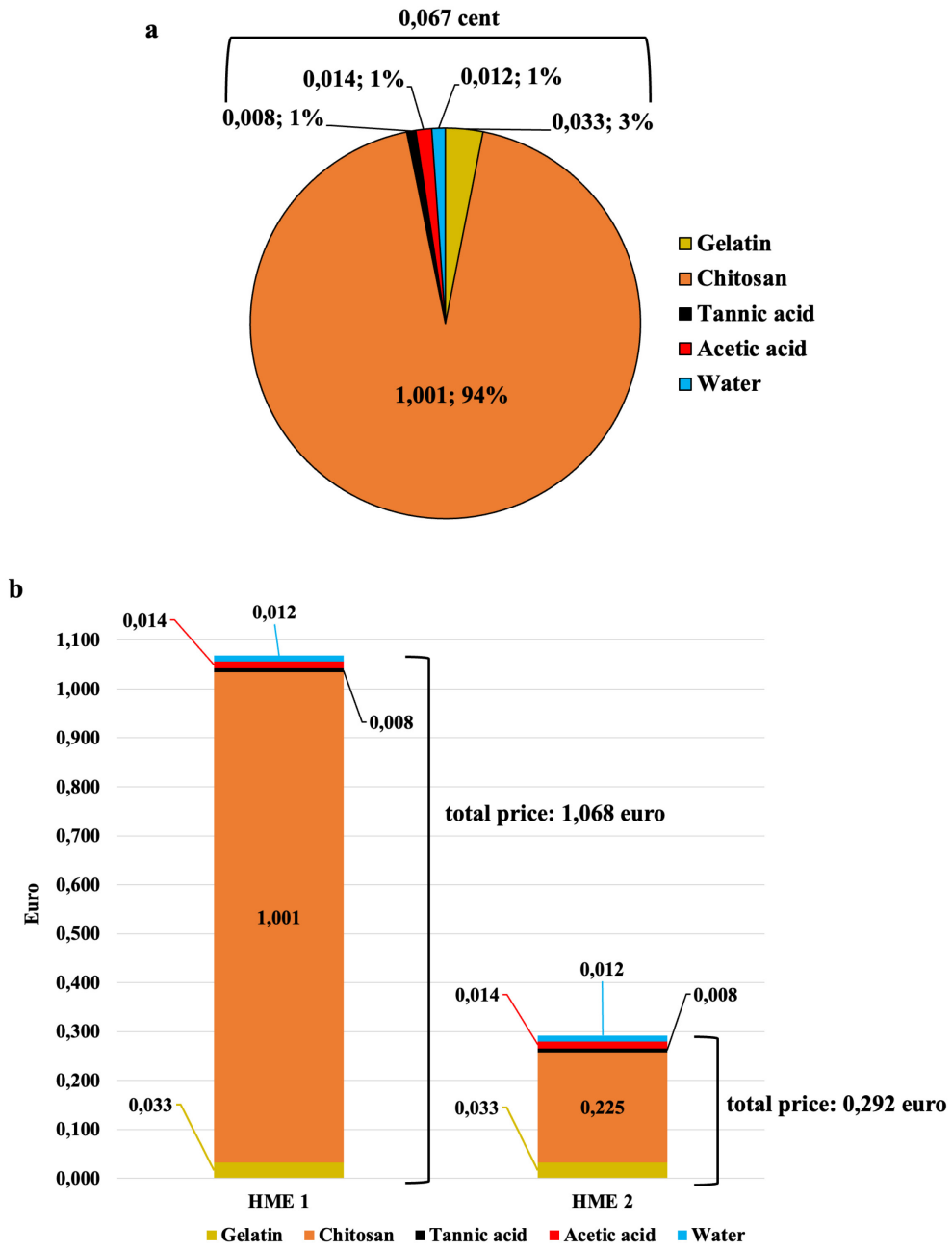

Figure 2.12. a) Cost analysis in € of the individual raw materials to make up an HME filter b) Comparative analysis of the cost in euros of a single HME filter by changing the source of chitosan.

In this regard, we evaluated the use of a different source of chitosan to be able to lower the unit cost of the final device.

In detail, through another company, we bought the same quantity of polymer at a price of about five times less than the previous one, obtaining the same efficient final characteristics of the HME filter shown before. In this way we were able to reduce the final price of the device by 73%, going from 1.068 to 0.292 € for a single filter (HME 2), thus making it more appropriate for a disposable device and more easily marketable (Figure 2.12 b).

As well as the individual polymers that compose the filter, also the filter holder needs to be selected maintaining the claims of HME filter such as biodegradability and high efficiency. In particular, a prototype in polylactic acid (PLA) has been developed by Pollution S.r.l company (Bologna, Italy) with the features of being completely biodegradable and less expensive than commercial ones. However, the disadvantage that the filter holder entails is the increase in dead space during the passage of air and consequently also the pressure drops. The dead space represents an excessive volume that the air must travel inside the filter holder, further hindering its passage. Two-way filter holders[6] are currently used in hospitals, directly connecting the patient and the respirator with an acceptable dead space, but to improve the performance of the final device and reduce the dead space, a three-way filter holder has been designed and developed always by Pollution S.r.l. In this regard, the two-way and three-way filter holders were compared, to evaluate the possible differences in terms of moisture exchange and pressure drops, using the optimized HME filter (sample N) (Figure 2.13).

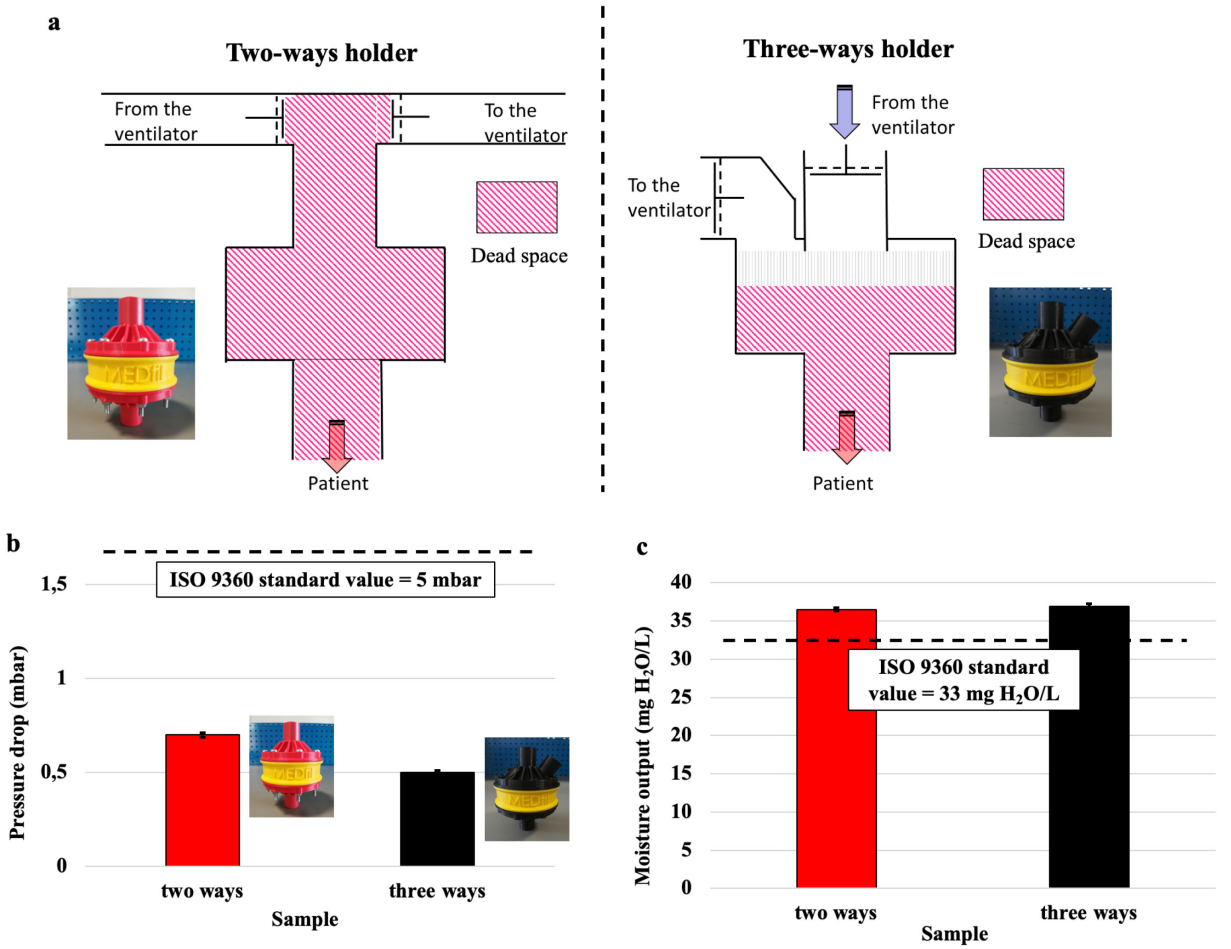

Figure 2.13. a) Schematic rapresentation of dead space of two-ways and three-ways filter holder b) Pressure drop c) Moisture exchange of optimized HME filter with two-way and three-way filter holder. The two images inserted in the graph a correspond to the yellow-red two-way filter holder and the yellow-black three-way filter holder.

Observing Figure 2.13 b, it is possible to note that the three-way filter holder leads to a reduction in pressure drops compared to the use of the two-way one, in which in any case the value already had a value below the regulatory standard of 1 mbar. As regards the moisture exchange (Figure 2.13 c), there is a slight increase in efficiency with the three-way filter holder, from 36.5 to 36.9 mg H_2O/L. Furthermore, from Figure 2.13 a, it is clear that the three-way filter holder leads to a reduction in dead space, limiting the size of the final device and allowing this device to also be considered for pediatric patients.

From the obtained results, therefore, it is possible to deduce that the three-way filter holder does not modify the final performance of the optimized prototype, on the contrary it is able to improve them compared to the use of the classic two-way filter holder, further reducing the dead space. To sum up, the possibility of having the most economical, eco-sustainable, long-lasting and effective complete set-up of HME filter and filter holder increases the approach of this product to the industrial sector.

2.3.3 Bacterial filtration and Bacteriostatic activity

HME filter carefully optimized in terms of stability and morphology has been tested to evaluate its bacterial filtration and bacteriostatic activity, essential features and required in filtration devices for hospital uses to avoid the proliferation of bacteria on the filter surface and inside the filter.

Among several bacteria present in the hospital environment and damaging to human health, three different microorganisms' standard strains derived from the American Type Culture Collection (or ATCC) have been evaluated representing the main nosocomial pathogenic indicators, such as *Escherichia coli* ATCC 8739, *Pseudomonas aeruginosa* ATCC 9027 and *Staphylococcus aureus* ATCC 6538. Firstly, the bacterial filtration efficiency was evaluated with the optimized HME filter N through the filtration of bacterial suspensions in cultures in broth containing the standard strains defined above. Each bacterial suspension was introduced separately into the HME N filter and filtered using a vacuum pump. At the end of the filtration, the residual bacterial concentration was determined and the percentage of filtration effectiveness was calculated as reported in Table 2.2.

Table 2.2. Bacterial filtration efficiency of optimized HME filter.

Bacterial suspension	Bacterial concentration T0	Bacterial concentration after filtration	Bacterial filtration efficacy %
Escherichia coli	1,8x10^6 CFU/ml	1,3x10^3 CFU/ml	**99,97**
Pseudomonas aeruginosa	2,6x10^6 CFU/ml	3,6x10^3 CFU/ml	**99,86**
Staphylococcus aureus	2,4x10^6 CFU/ml	7,2x10^2 CFU/ml	**99,93**

As can be seen in Table 2.2, the results demonstrate that the HME filter is able to effectively filter all three types of bacteria ATCC test, reducing the concentration of each bacterial suspension of 99,9%. Regarding the bacteriostatic activity, however, only two bacterial suspensions at two different concentrations were tested, *Staphylococcus aureus* and *Pseudomonas aeruginosa*, as they were considered more significant for the evaluation of the bacterial growth inhibition capacity by the optimized HME filter.

From Table 2.3 shows *in vitro*, both at lower and higher concentration there is a considerable reduction in the initial bacterial load, especially *Staphylococcus aureus*. The results obtained demonstrate the bacteriostatic capacity of the HME N filter against the most widespread nosocomial pathogenic microorganisms.

Table 2.3. Bacteriostatic activity of optimized HME filter.

Bacterial suspension	Bacterial concentration T0	Bacterial concentration after filtration	Bacteriostatic activity
Staphylococcus aureus	1,3x10^3 CFU/ml	9,5x10^2 CFU/ml	**Confirmed**
Pseudomonas aeruginosa	1,5x10^3 CFU/ml	1,0x10^3 CFU/ml	**Confirmed**
Staphylococcus aureus	1,3x10^6 CFU/ml	8,6x10^5 CFU/ml	**Confirmed**
Pseudomonas aeruginosa	1,5x10^6 CFU/ml	1,0x10^5 CFU/ml	**Confirmed**

2.3.4 Bacterial Filtration Efficiency (BFE)

The HMEs filter, being a filtering device to help patients with breathing difficulties, can frequently come into contact with bacterial microorganisms potentially pathogenic, especially in a hospital environment. After having determined the bacterial filtration capacity and the bacteriostatic activity of the HME N filter of bacterial suspensions in liquid culture, it was

equally important to evaluate the bacterial filtration efficiency (BFE) of the filter under examination through the use of a bacterial suspension in the aerosol of Staphylococcus aureus. In detail, the optimized HME (sample N) were tested with a bacterial aerosol of *Staphylococcus aureus* according to EN 14683:2019

The EN 14683:2019 standard indicates the requirements and the appropriate method for in vitro determination of bacterial filtration efficiency to try the ability to retain the bacterial load in aerosols of a medical device, eliminating or reducing the risks of infection as much as possible. The sample N tested an average filtration capacity of 66.7% ± 1,66 against a bacterial aerosol of *Staphylococcus aureus*, confirming the filtration capacity of the bacterial suspension, that the optimized HME filter is able to block and retain the bacteria on its surface and inside it.

2.3.5 Validation in hospital environment

In this work, further field trials were carried out validating the effectiveness of HME filter in a real healthcare environment with the aim of confirming the results of in vitro research. In detail, the tests were carried out directly on hospital instrumentation inside the Montecatone Rehabilitation Hospital (Bologna, Italy) without the presence of the patient. The optimized HME filter N was compared with a commercial one normally used in hospitals, placed in parallel between an AMBU (Auxiliary Manual Breathing Unit) respirator bag and the machine connected to the medical gas line. Two tests were carried out in the field, one keeping the two filters connected to an AMBU flask coming from a positive patient for *Acinetobacter species* and *Klebsiella species (KCP)* for 4 hours, the other instead connecting to a flask coming from a positive patient of *KCP NEW DELHI* for 6 hours. The initial bacterial load (T0) was directly quantified from the two infected AMBU bags.

Table 2.4 shows the results obtained with the different HME filters in the two respective tests. Although the commercial filter has a higher filtration efficiency, equal to 99,99% the optimized HME filter N proves to be able to effectively filter the two bacterial strains such as *Acinetobacter* and *Klebsiella (KCP).*

Table 2.4. Bacterial filtration efficiency of HME commercial filter and optimized HME filter (sample N).

Sample	Bacterial suspension	Bacterial concentration T0	Bacterial concentration after filtration	Bacterial filtration efficiency %
Commercial filter	*Acinetobacter species/KCP* After 4 h	$1,7x10^4$ CFU/m^3	$1,2x10^3$ CFU/m^3	93
Commercial filter	*KCP NEW DELHI* After 6 h	$3,0x10^4$ CFU/m^3	$7,2x10^2$ CFU/m^3	98
Sample N	*Acinetobacter species/KCP* After 4 h	$2,0x10^4$ CFU/m3	$6,4x10^3$ CFU/m^3	68
Sample N	*KCP NEW DELHI* After 6 h	$4,5x10^4$ CFU/m3	$1,2x10^4$ CFU/m^3	73

Subsequently, the bacterial filtration efficiency of the optimized HME filter N was tested, in this case placing it between the respiratory mask (in the absence of a patient) and respectively three AMBU respiratory bags that had come into contact with patients infected with different bacterial strains for 4 hours each. The initial bacterial concentration in this case was obtained by calculating the bacterial load present in the commercial HME filter which was connected to the three infected patients. From table 2.5 it is clear that in all three cases there is a good reduction of the bacterial concentration compared to the initial one, which confirms the possibility to use the optimized HME filter in the hospital environment and increase the TRL (Technology Readiness Level) of this product up to 6.

Table 2.5. Bacterial filtration efficiency of optimized HME filter (sample N).

Bacterial suspension	Bacterial concentration T0	Bacterial concentration after filtration	Bacterial filtration efficiency %
Acinetobacter species /KCP	$3,2x10^6$ CFU/m^3	$8,5x10^5$ CFU/ m^3	**73**
Pseudomonas species	$1,9x10^6$ CFU/ m^3	$4,5x10^5$ CFU/ m^3	**76**
Mixed bacterial culture	$1,0x10^7$ CFU/ m^3	$2,7x10^6$ CFU/ m^3	**73**

2.3.6 Stability test

The stability of the HME filter after sterilization at gamma radiation was evaluated allowing to keep and store it for long periods. The optimized filter (sample N) has been tested inside the holder at different time points, precisely 1-3-6-9-12 months, to demonstrate that pressure drops, and moisture exchange measures remain constant over time. From Figure 2.14 it is

clearly visible that both the pressure drops (Figure 2.14 a) and the moisture exchange (Figure 2.14 b) remain constant over time with respect to the values initially obtained. In fact, for all timepoint, sample N shows pressure drops of about 0.7 mbar and moisture exchange of 36 mg H2O/L, which reflect the values measured at t0 in line with the standard specifications. With this evidence, the HME devices can be more easily produced on an industrial scale, sterilized through gamma radiation and stored for long periods before their use, as they maintain their physical and chemical characteristics and therefore their efficiency constant.

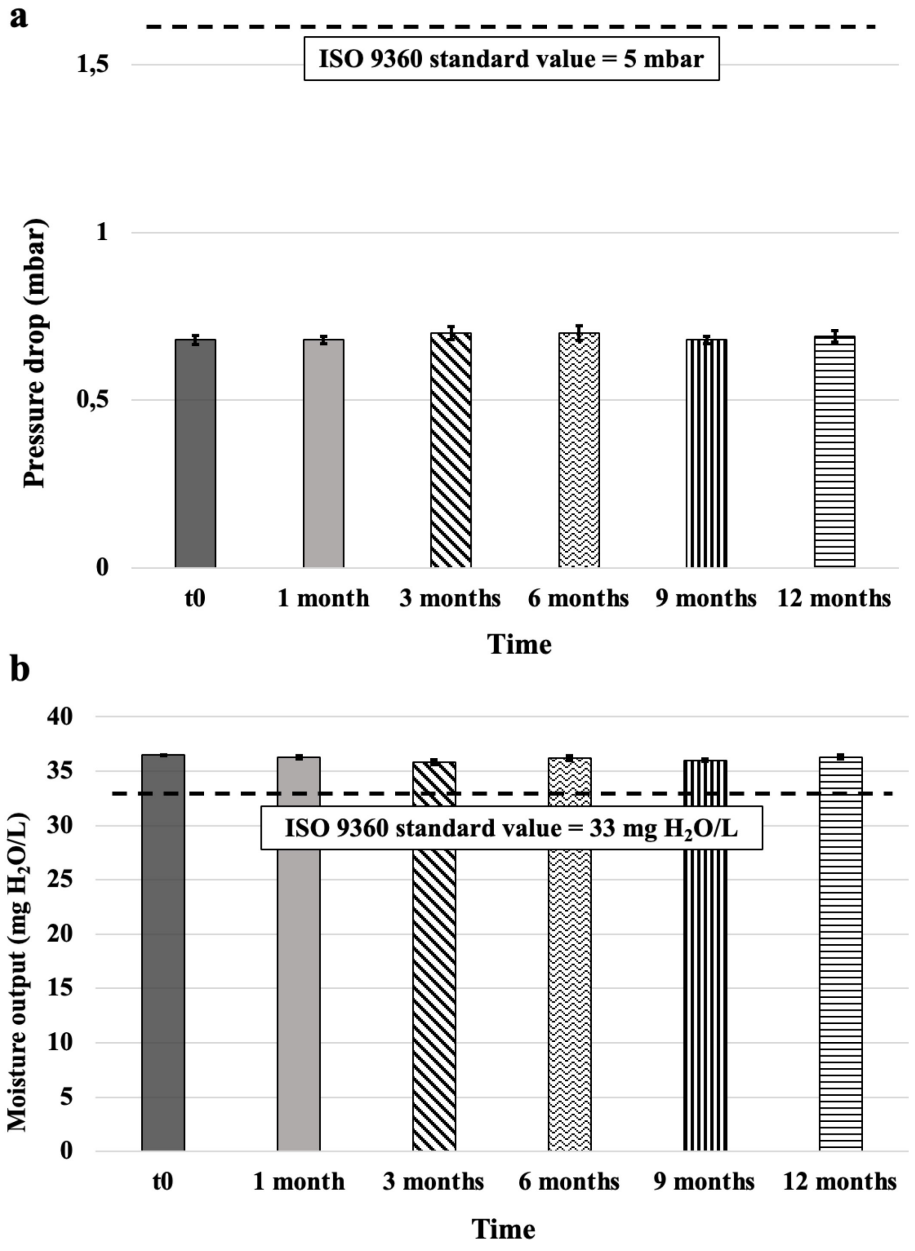

Figure 2.14. Stability test of HME filter validated: a) Pressure drops b) Moisture exchange of sample N at different time point (1, 3, 6, 9 and 12 months).

2.3.7 Diagnostic component (HMEDs filter)

In this work a diagnostic component has been added into HME filter (HMEDs) to promote the de-hospitalization of patients, meaning that moving patients to familiar places to continue the treatments and surveillance. This component, formed by liposomal vesicles of soybean lecithin functionalized with chromatic molecules of Rhodamine-B, allows to visually detect the onset of infections against the main bacterial strains such as *Staphylococcus aureus*, *Pseudomonas aeruginosa* and *Escherichia coli*. In detail, when the liposomes inside HME device encounter the bacteria[42], cell lysis occurs, releasing the dye which colours all the filter; this allows people to timely recognize the infection without remaining necessarily inside the hospital. Two small sections of optimized HME filter were impregnated with two solutions at different concentrations of liposomes/rhodamine (10:1 and 20:1) and came into contact with a bacterial suspension containing *Staphylococcus aureus*, *Pseudomonas aeruginosa* and *Escherichia coli* via membrane filtration Whatman.

As can be seen from Figure 2.15, following contact between the bacterial suspension and the filters containing the liposomes, only the sample HME_10:1 impregnated with the liposomes/rhodamine solution 10:1 shows a visible high pink/fuchsia colour, while the sample HME_20:1 with solution 20:1 showed no change, probably because it was less concentrated. Sample HME_10:1 highlights a colour change immediately after impregnation with the liposome solution, which seems to intensify after contact with bacteria due to the lysis of the liposomal vesicles.

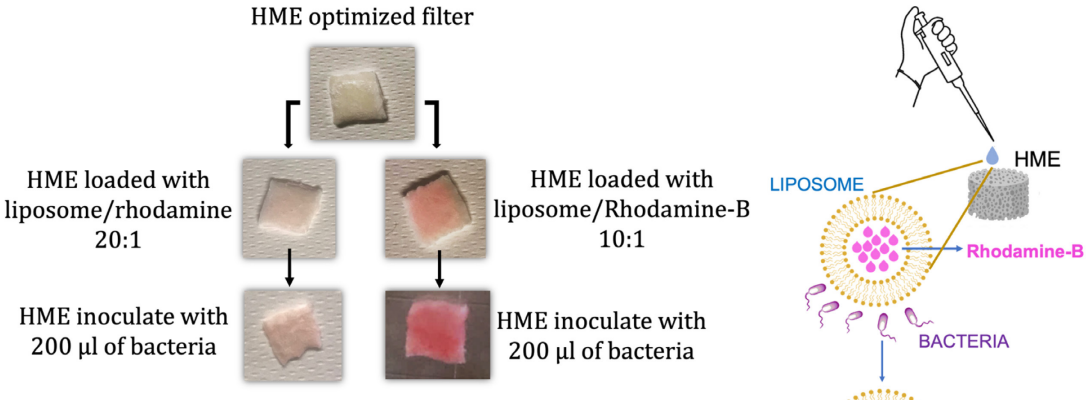

Sample	Bacterial suspension	Visual detection
HME_10:1	200 µL	High pink / fuchsia color (0,5)
HME_20:1	200 µL	No color variation

Legend:
- Negative (no color variation): **0**
-Low pink/fuchsia coloc: **0,2**
-Medium pink/fuchsia color: **0,3**
-High pink/fuchsia color: **0,5**
-Very high pink/fuchsia color:**1**

Figure 2.15. Diagnostic test of HME filter with two solutions of liposome/rhodamine-B.

Taking the legend for the staining intensity as a reference, sample HME_10:1 reported a colour detection equal to 0.5, which denotes a possible potential for the development of the HMED filter with the diagnostic function. This would result in an easier and faster de-hospitalization of patients, reducing hospital costs, but maintaining constant control of the emergence of infections outside the healthcare facility.

2.4 Conclusions

A more effective, eco-sustainable and marketable HME device was successfully developed and validated. Through a green process, we have created a completely biodegradable aerogel composed by gelatin and chitosan, exploiting low-cost raw materials deriving from the recycling of food industry waste. In particular, following a careful raw materials analysis, a 70% reduction in the cost per single HME was highlighted by using low-cost sources of gelatin and chitosan compared to commercial HMEs. Furthermore, the biodegradability of the final device produces practically no environmental impact, as it does not need to dispose of waste by incinerator, limiting the production of CO2. The structure, composition and efficiency of the material remain stable over time; hence it is possible to sterilize the HME prototypes by gamma rays and store them easily for long periods.

The study allows to optimize the process parameters of the freeze-drying and cross-linking, to create a filter with limited pressure drops and effectively exchange of heat and moisture with the inhaled and exhaled air form the patient in compliance with ISO standard 9360, limiting process times and costs. In fact, by simplifying and speeding up the different production steps, the process has been made more easily scalable and close to future industrialisation. Afterwards, thanks to the antibacterial filtration tests, carried out both in vitro and in the hospital environment on medical instruments, it was proved the filtration ability of HME filter against the main nosocomial pathogens that normally affect patients with breathing difficulties. The validation of the filter directly in the clinical environment has made it possible to increase the TRL of the device up to 6, bringing it closer to possible commercialization. Finally, the inclusion of a diagnostic component that changes the colour of the HME in presence of bacteria has highlighted as proof of concept to perform an early diagnosis of infections in the respiratory tract and a more simplified management and de-hospitalization of patients by reducing hospital costs. All these innovations not only offer a more effective and safer HME filter for patients requiring respiratory support, but lead with foresight to a more eco-sustainable, economic, energy-saving process in line with the industrial change of our time.

References

(1) Hurni, J. M; Feihl F.; Lazor R.; Leuenberger P.; Perret C. Safety of Combined Heat and Moisture Exchanger Filters in Long-Term Mechanical Ventilation. *Chest* **1997**, 111, 686-691.

(2) Lee, D.; Minko, T. Nanotherapeutics for Nose-to-Brain Drug Delivery: An Approach to Bypass the Blood Brain Barrier. *Pharmaceutics* **2021**, 13, 2049-2096.

(3) Harkema, J. R.; Carey, S. A.; Wagner, J. G. The Nose Revisited: A Brief Review of the Comparative Structure, Function, and Toxicologic Pathology of the Nasal Epithelium. *Toxicol Pathol* **2006**, 34, 252–269.

(4) Lillehoj, E. P.; Kim, K. C. Airway Mucus: Its Components and Function. *Arch Pharm Res* **2002**, 25, 770-780.

(5) Lillehoj, E. P.; Kato, K.; Lu, W.; Kim, K. C. Cellular and Molecular Biology of Airway Mucins. *International Review of Cell and Molecular Biology* **2013**, 303, 139–202.

(6) Wilkes, A. R. Heat and Moisture Exchangers and Breathing System Filters: Their Use in Anaesthesia and Intensive Care. Part 2 - Practical Use, Including Problems, and Their Use with Paediatric Patients. *Anaesthesia* **2011**, 66, 40–51.

(7) Plotnikow, G. A.; Accoce, M.; Navarro, E.; Tiribelli, N. Humidification and Heating of Inhaled Gas in Patients with Artificial Airway. A Narrative Review. *Revista Brasileira de Terapia Intensiva* **2018**, 30, 86–97.

(8) Awasthi, S. K.; Kumar, M.; Kumar, V.; Sarsaiya, S.; Anerao, P.; Ghosh, P.; Singh, L.; Liu, H.; Zhang, Z.; Awasthi, M. K. A Comprehensive Review on Recent Advancements in Biodegradation and Sustainable Management of Biopolymers. *Environmental Pollution* **2022**, 307, 119600.

(9) Su, S. B.; He, C.; Shu, Y.; Chen, Q. L.; Zhang, B. J. Total Site Modeling and Optimization for Petrochemical Low-Carbon Retrofits Using Multiple CO2 Emission Reduction Methods. *J Clean Prod* **2023**, 383, 135450.

(10) Garnier, M.; Julian, N.; Velly, L. Heat Moisture Exchange/High-Efficiency Particulate Filters and the Risk of Contamination of the Ventilatory Circuit and Patient Environment with SARS-CoV-2: A Brief Report. *Anaesthesia Critical Care and Pain Medicine* **2022,** 41, 101065.

(11) Chen, P.; Liu, L.; Pan, J.; Mei, J.; Li, C.; Zheng, Y. Biomimetic Composite Scaffold of Hydroxyapatite/Gelatin-Chitosan Core-Shell Nanofibers for Bone Tissue Engineering. *Materials Science and Engineering C* **2019**, 97, 325–335.

(12) Campodoni, E.; Artusi, C.; Vazquez Iglesias, B.; Nicosia, A.; Belosi, F.; Vandini, A.; Monticelli, P.; Tampieri, A.; Sandri, M. Nature-Inspired Heat and Moisture Exchanger Filters Composed of Gelatin and Chitosan for the Design of Eco-Sustainable "Artificial Noses." *ACS Appl Polym Mater* **2023**, 5, 3468–3479.

(13) Irastorza, A.; Zarandona, I.; Andonegi, M.; Guerrero, P.; de la Caba, K. The Versatility of Collagen and Chitosan: From Food to Biomedical Applications. *Food Hydrocolloids* **2021**, 116, 106633.

(14) Yu, S.; Sun, J.; Shi, Y.; Wang, Q.; Wu, J.; Liu, J. Nanocellulose from Various Biomass Wastes: Its Preparation and Potential Usages towards the High Value-Added Products. *Environmental Science and Ecotechnology* **2021**, 5, 10077.

(15) Wang, M.; Chen, L.; Zhang, Z. Potential Applications of Alginate Oligosaccharides for Biomedicine – A Mini Review. *Carbohydrate Polymers* **2021**, 271, 118408.

(16) Sethi, S.; Medha; Kaith, B. S. A Review on Chitosan-Gelatin Nanocomposites: Synthesis, Characterization and Biomedical Applications. *Reactive and Functional Polymers* **2022**, 179, 105362.

(17) Campodoni, E.; Montanari, M.; Dozio, S. M.; Heggset, E. B.; Panseri, S.; Montesi, M.; Tampieri, A.; Syverud, K.; Sandri, M. Blending Gelatin and Cellulose Nanofibrils: Biocomposites with Tunable Degradability and Mechanical Behavior. *Nanomaterials* **2020**, 10, 1–18.

(18) Bombaldi de Souza, F. C.; Bombaldi de Souza, R. F.; Drouin, B.; Mantovani, D.; Moraes, Â. M. Comparative Study on Complexes Formed by Chitosan and Different Polyanions: Potential of Chitosan-Pectin Biomaterials as Scaffolds in Tissue Engineering. *Int J Biol Macromol* **2019**, 132, 178–189.

(19) Wang, L. S.; Du, C.; Chung, J. E.; Kurisawa, M. Enzymatically Cross-Linked Gelatin-Phenol Hydrogels with a Broader Stiffness Range for Osteogenic Differentiation of Human Mesenchymal Stem Cells. *Acta Biomater* **2012**, 8, 1826–1837.

(20) Phiri, R.; Mavinkere Rangappa, S.; Siengchin, S.; Oladijo, O. P.; Dhakal, H. N. Development of Sustainable Biopolymer-Based Composites for Lightweight Applications from Agricultural Waste Biomass: A Review. *Advanced Industrial and Engineering Polymer Research* **2023**, 6, 436-450.

(21) O'Brien, F. J.; Harley, B. A.; Yannas, I. V.; Gibson, L. Influence of Freezing Rate on Pore Structure in Freeze-Dried Collagen-GAG Scaffolds. *Biomaterials* **2004**, 25, 1077–1086.

(22) Chen, X.; Fan, M.; Tan, H.; Ren, B.; Yuan, G.; Jia, Y.; Li, J.; Xiong, D.; Xing, X.; Niu, X.; Hu, X. Magnetic and Self-Healing Chitosan-Alginate Hydrogel Encapsulated Gelatin Microspheres via Covalent Cross-Linking for Drug Delivery. *Materials Science and Engineering C* **2019**, 101, 619–629.

(23) Maniglia, B. C.; Lima, D. C.; Matta Junior, M. D.; Le-Bail, P.; Le-Bail, A.; Augusto, P. E. D. Preparation of Cassava Starch Hydrogels for Application in 3D Printing Using Dry Heating Treatment (DHT): A Prospective Study on the Effects of DHT and Gelatinization Conditions. *Food Research International* **2020**, 128, 108803.

(24) Moghaddam, S. Y. Z.; Biazar, E.; Esmaeili, J.; Kheilnezhad, B.; Goleij, F.; Heidari, S. Tannic Acid as a Green Cross-Linker for Biomaterial Applications. *Mini-Reviews in Medicinal Chemistry* **2022**, 23, 1320–1340.

(25) Chang, K. C.; Lin, D. J.; Wu, Y. R.; Chang, C. W.; Chen, C. H.; Ko, C. L.; Chen, W. C. Characterization of Genipin-Crosslinked Gelatin/Hyaluronic Acid-Based Hydrogel Membranes and Loaded with Hinokitiol: In Vitro Evaluation of Antibacterial Activity and Biocompatibility. *Materials Science and Engineering C* **2019**, 105, 110074.

(26) Pinto, R. V.; Gomes, P. S.; Fernandes, M. H.; Costa, M. E. V.; Almeida, M. M. Glutaraldehyde-Crosslinking Chitosan Scaffolds Reinforced with Calcium Phosphate Spray-Dried Granules for Bone Tissue Applications. *Materials Science and Engineering C* **2020**, 109, 110557.

(27) Taheri, P.; Jahanmardi, R.; Koosha, M.; Abdi, S. Physical, Mechanical and Wound Healing Properties of Chitosan/Gelatin Blend Films Containing Tannic Acid and/or Bacterial Nanocellulose. *Int J Biol Macromol* **2020**, 154, 421–432.

(28) Dreyfuss, D.; Djedaïni, K.; Gros, I.; Mier, L.; Le Bourdellés, G.; Cohen, Y.; Estagnasié, P.; Coste, F.; Boussougant, Y. Mechanical Ventilation with Heated Humidifiers or Heat and Moisture Exchangers: Effects on Patient Colonization and Incidence of Nosocomial Pneumonia. *Am J Respir Crit Care Med* **1995**, 151, 986–992.

(29) Giacometti, G.; Marini, M.; Papadopoulos, K.; Ferreri, C.; Chatgilialoglu, C. Trans-Double Bond-Containing Liposomes as Potential Carriers for Drug Delivery. *Molecules* **2017**, 22, 2082-2099.

(30) Campodoni, E.; Heggset, E. B.; Rashad, A.; Ramírez-Rodríguez, G. B.; Mustafa, K.; Syverud, K.; Tampieri, A.; Sandri, M. Polymeric 3D Scaffolds for Tissue Regeneration: Evaluation of Biopolymer Nanocomposite Reinforced with Cellulose Nanofibrils. *Materials Science and Engineering C* **2019**, 94, 867–878.

(31) Balakrishnan, B.; Jayakrishnan, A. Self-Cross-Linking Biopolymers as Injectable in Situ Forming Biodegradable Scaffolds. *Biomaterials* **2005**, 26, 3941–3951.

(32) Vazquez, B.; Monticelli, P.; Nicosia, A.; Santachiara, G.; Belosi, F. Evaluation of Heat and Moisture Exchanger Performance with Two Different Methods in the Same Test Apparatus. *NCSLI Measure* **2015**, 10, 62–65.

(33) Dellamonica, J.; Boisseau, N.; Goubaux, B.; Raucoules-Aimé, M. Comparison of Manufacturers' Specifications for 44 Types of Heat and Moisture Exchanging Filters. *Br J Anaesth* **2004**, 93, 532–539.

(34) UNI EN 14683: 2019. Maschere Facciali Ad Uso Medico - Requisiti e Metodi Di Prova **2019**.

(35) D'Anna, A.; Di Natale, F.; De Falco, G; Di Maio, E.; Tammaro, D.; Quaglia, F.; Ungaro, F.; Cassiano, C.; Salvatore, P.; Colicchio, R.; Scaglione, E.; Pagliuca, C.; Fontana, L; Iavicoli, I. Validazione Di Maschere Chirurgiche Nella Fase Di Emergenza COVID19: L'esperienza Dell'Università Degli Studi Di Napoli Federico II. *G Ital Med Lav Erg* **2020**, 42, 73–81.

(36) Ferreri, C.; Ferocino, A.; Batani, G.; Chatgilialoglu, C.; Randi, V.; Riontino, M. V.; Vetica, F.; Sansone, A. Plasmalogens: Free Radical Reactivity and Identification of Trans Isomers Relevant to Biological Membranes. *Biomolecules* **2023**, 13, 730-747.

(37) Larocca, A. V.; Toniolo, G.; Tortorella, S.; Krokidis, M. G.; Menounou, G.; Bella, G. Di; Chatgilialoglu, C.; Ferreri, C. The Entrapment of Somatostatin in a Lipid Formulation: Retarded Release and Free Radical Reactivity. *Molecules* **2019**, 24, 3085-3097.

(38) Divakar, P.; Yin, K.; Wegst, U. G. K. Anisotropic Freeze-Cast Collagen Scaffolds for Tissue Regeneration: How Processing Conditions Affect Structure and Properties in the Dry and Fully Hydrated States. *J Mech Behav Biomed Mater* **2019**, 90, 350–364.

(39) Krishnakumar, G. S.; Gostynska, N.; Dapporto, M.; Campodoni, E.; Montesi, M.; Panseri, S.; Tampieri, A.; Kon, E.; Marcacci, M.; Sprio, S.; Sandri, M. Evaluation of Different Crosslinking Agents on Hybrid Biomimetic Collagen-Hydroxyapatite Composites for Regenerative Medicine. *Int J Biol Macromol* **2018**, 106, 739–748.

(40) Chen, C.; Yang, H.; Yang, X.; Ma, Q. Tannic Acid: A Crosslinker Leading to Versatile Functional Polymeric Networks: A Review. *RSC Advances* **2022**, 12, 7689–7711.

(41) Salvatore, L.; Calò, E.; Bonfrate, V.; Pedone, D.; Gallo, N.; Natali, M. L.; Sannino, A.; Madaghiele, M. Exploring the Effects of the Crosslink Density on the Physicochemical Properties of Collagen-Based Scaffolds. *Polym Test* **2021**, 93, 106966.

(42) Pornpattananangkul, D.; Zhang, L.; Olson, S.; Aryal, S.; Obonyo, M.; Vecchio, K.; Huang, C.-M.; Zhang, L. Bacterial Toxin-Triggered Drug Release from Gold Nanoparticle-Stabilized Liposomes for the Treatment of Bacterial Infection. *J Am Chem Soc* **2011**, 133, 4132–4139.

CHAPTER 3

Safe-by-Design Approach to Sunscreens: Synthesis and Validation of Biomimetic Hybrid Particles for an Eco-Sustainable UV Protection

Part of the content of this chapter has been published as Campodoni E., Montanari M., Artusi C. et al. "Biomineralization: A New Tool for Developing Eco-Sustainable Ti-Doped Hydroxyapatite-Based Hybrid UV Filters" Biomaterials Advances 2023.

3.1 Introduction

It is well known that the sunlight is essential for human well-being, the exposition to moderate doses of solar radiation is not harmful and have beneficial effects.[1] It is responsible for regulating the internal clock, stimulate the metabolism, the hormonal and the immune systems, it is essential to promote the synthesis of various vitamins and support optimal bone health. Furthermore, thanks to the stimulation to production of serotonin, the sun helps to fight depression. However, in recent years concerns are increasing due to wrong or over-exposition to solar radiations[2], thus, whether we choose to bask in the sunlight for aesthetic or health reasons, it is now well-established that protecting ourselves from solar radiation is of paramount importance. In fact, UV radiation can damage the molecules and structures that make up the skin. They are divided into UVA, UVB and UVC rays, but since the UVC rays are absorbed by the oxygen molecules present in the stratosphere, only the UVA and UVB rays can react with the skin and cause metabolic and biological reactions.[3] In particular, the wavelengths of the UVB region (290-320 nm) are mainly absorbed by the superficial cells of the epidermis causing dermatitis, burns and erythema, while the UVA rays (320-400 nm) penetrate deeply into the skin, reaching dermal fibroblasts and causing the formation of reactive oxygen species (ROS) can cause photoaging, DNA damage up to genetic mutations and melanoma formation (Figure 3.1 a).[4]

In this regard, protecting the skin from damage caused by the sun's rays is really important, especially as it is the body's main barrier against external environmental or biological agents.

The skin in fact, is the largest organ of the human body, with a surface area of about $2m^2$ and is presented as a multilayered tissue, composed of three main layers: epidermis, dermis and hypodermis. The epidermis is the outermost part, with a thickness of about 100 μm and is in

turn made up of four/five sublayers. In particular, among these there is the stratum corneum, which is the one most exposed to infections and atmospheric agents and therefore the one that can be damaged most easily. The dermis, on the other hand, is the thickest (1-4 mm) and vascularized component, capable of supplying nutrients to the epidermis, mainly made up of fibroblasts and immune cells. Finally, the hypodermis, also called adipose layer, formed by a mix of adipocytes, fibroblasts, connective tissue, nerves and arteries (Figure 3.1 b-c).[5,6]

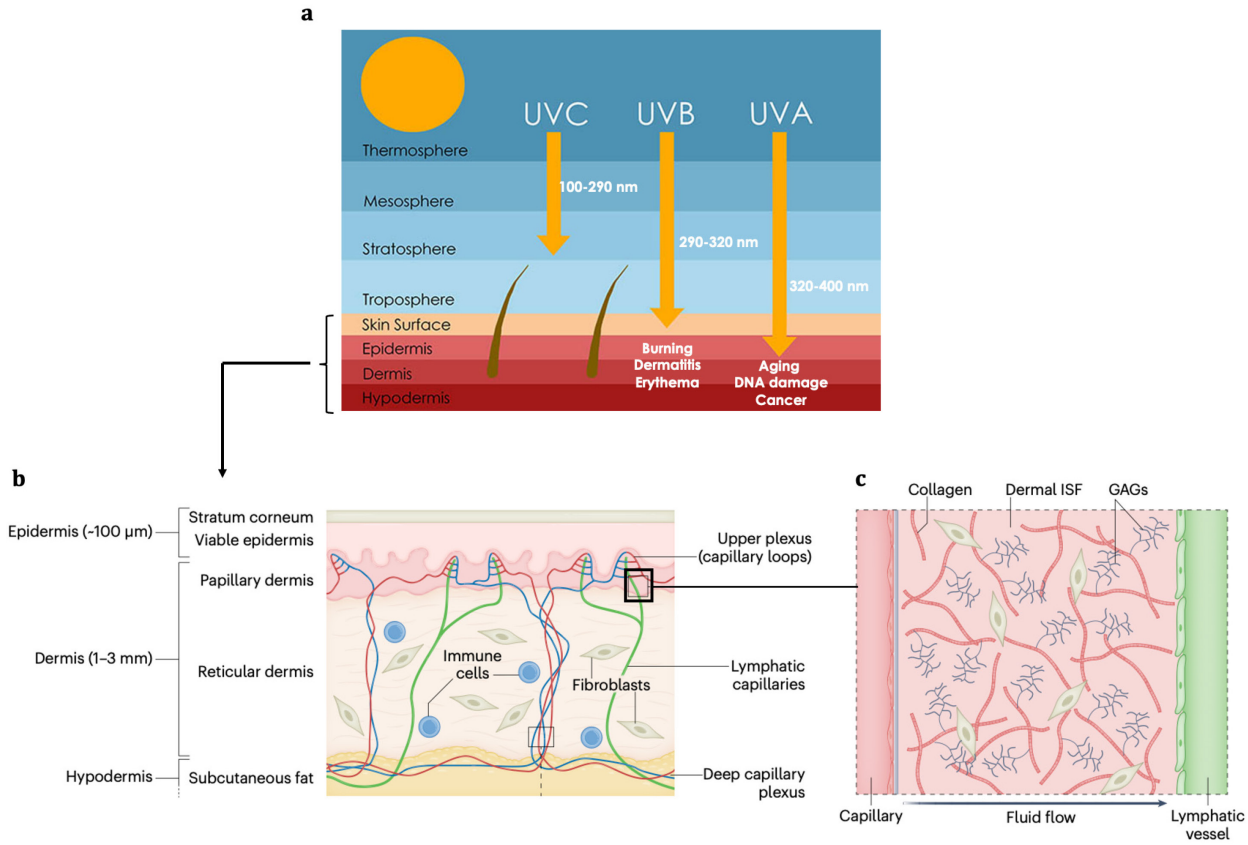

Figure 3.1. a) Schematic representation of the UV radiation composition and their interaction with the skin b) Structure of the skin. c) Microstructure of the mesh-like dermis, where pressure gradients drive flow between capillary blood and lymph.[7]

The skin, being the outermost layer of our body, is particularly vulnerable to damage caused by direct exposure to atmospheric radiation. The combination of air pollution and change in the pattern of sun exposure (even shorter periods but longer overall throughout the day) means that the risk factor for skin diseases is substantially increased. In fact, it is estimated that about one million people are diagnosed with skin cancer every year, and about 10,000 die from malignant melanoma, not to mention others problems due to excessive sun exposure, such are sun burn, photo-aging, hyperpigmentation and spots as well as immune suppression that facilitate the onset of neoplastic forms.[8] Based on these evidences, the repeated application of

effective sunscreens is essential to form a protective barrier on the skin surface against the harmful effects of UV-rays, and in this regard a systematic awareness campaign for consumers has been promoted for years. Indeed, clinical data reveal that regular use of a sunscreen can prevent not only sunburn but also many skin-aging effects such as wrinkles and pigmentation changes.[9]

Commercial sunscreen products are generally composed of organic and/or inorganic filters. Conventional organic filters (i.e Butyl Methoxydibenzoylmethane, Ethylhexyl Methoxycinnamate) absorbing the UV radiation allow to obtain products with high sun protection factor (SPF) values, but often in narrow spectrum range (UVA or UVB), only few filters (i.e. Bis-Ethylhexyloxyphenol Methoxyphenyl Triazine, Methylene Bis-Benzotriazolyl Tetramethylbutylphenol, Benzophenone-3) offer broad band of protection (UVA and UVB) while inorganic filters (TiO_2, ZnO), are able to reflect, deflect and/or absorb the UV radiation in a wide spectrum (UVA and UVB), depending from their particle' size, but with lower SPF.[10,11]

Despite the high efficacy of some commercial sunscreens, which are currently unrivalled in terms of appropriate sun protection, they have drawbacks for both human and environment health.[12,13] Thus, these sunscreen-based filters have been restricted in some tropical paradises, such are Hawaii, the U.S. Virgin Islands and Palau. This approach led to banning the widely used such are Benzophenone-3, Ethylhexyl Methoxycinnamate, Octocrylene, Homosalate, 4-Methylbenzylidene camphor and PABA, while promoting the use of safer but more expensive organic filters (i.e. Diethylamino Hydroxybenzoyl Hexyl Benzoate and Ethylhexyl Triazone) or inorganic filters, such as ZnO and TiO_2.[14] Moreover, some organic UV filters, used in high concentration to achieve high SPF, can penetrate the subcutaneous layers and interfere with the endocrine system as well as causing photosensitivity reactions and pro-carcinogenic activities.[15] In addition, certain organic filters exhibit low stability when exposed to solar radiation, resulting in the formation of by-products and the generation of free radicals that may have adverse effects on the skin.[16] On the other hand, inorganic filters are more stable and do not interact directly with the dermis, but their efficacy also depends on the particles' size: the nano-sized filters are the most effective and easy to be spread, without whitening effect[17], but they have recently raised concerns regarding the potential toxicity associated with the smaller size.[18–20] Additionally, TiO_2 is well known for its high photocatalytic activity, responsible for inducing the generation of ROS under sun exposure, degrading ingredients of the formulation, and also affecting the collagen molecules of the dermis, raising safety concerns.[4,21]

Although, increasing attention is paid to the efficacy and safety of cosmetic products for human health, in recent years, sustainability and low environmental impact are playing an increasingly relevant role on health of people, animals and the environment. It has thus become mandatory to reduce the environmental damage that the persistent use of sunscreens causes.[22] Specifically, in coastal seawater, the presence of organic compounds like Benzophenones, common organic filters, can lead to endocrine disorders in mussels and fish. These compounds can mimic oestrogens, causing disruptions in the hormonal balance of aquatic organisms. Additionally, they can also induce alterations in fecundity, negatively impacting the reproductive capacity of these animals.[23] However, the most widespread and well-known environmental damage concerns the emerging phenomenon of coral bleaching that gave rise to a recent generation of the so-called "reef safe" sunscreens (Figure 3.2).[24,25]

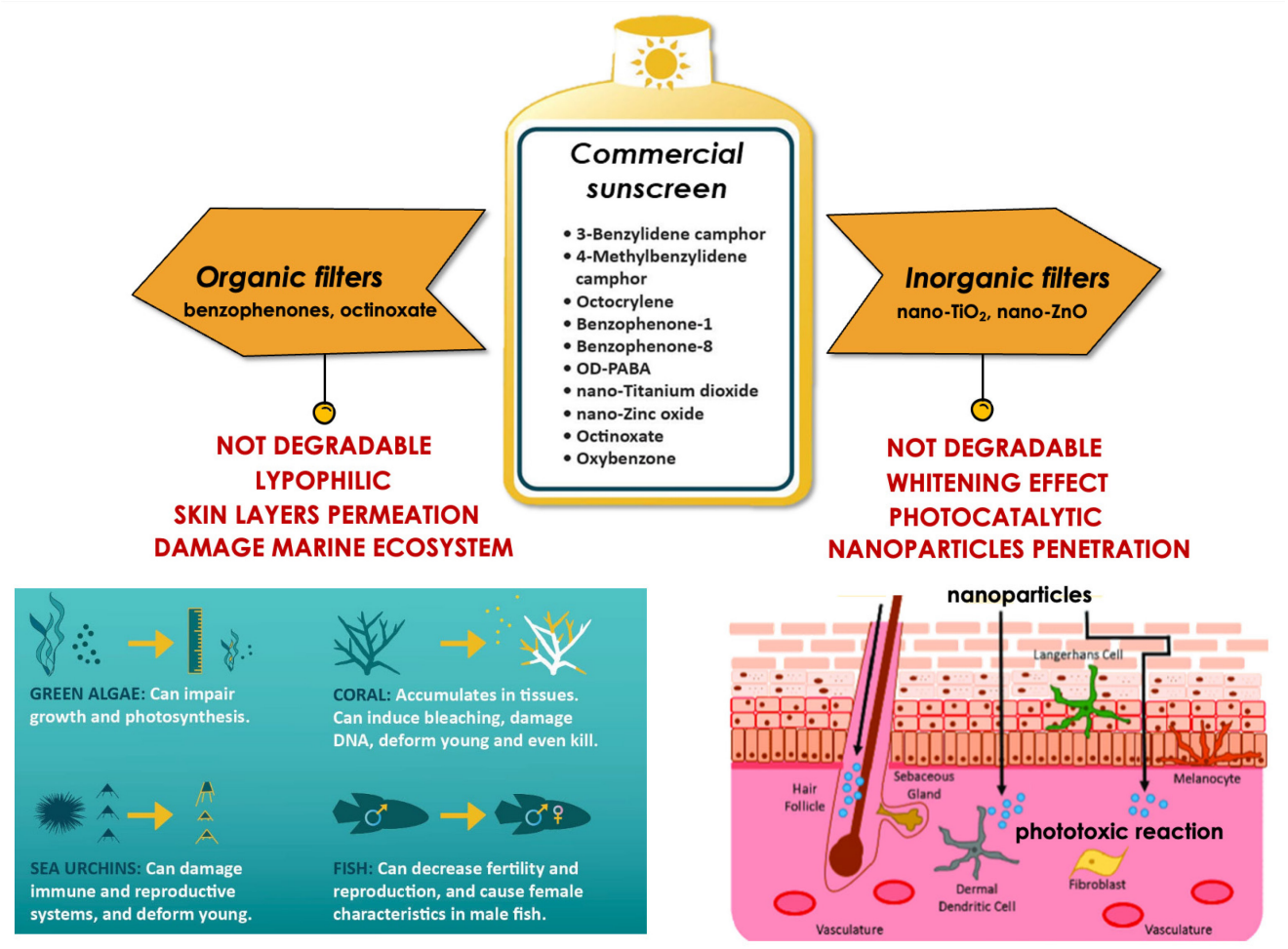

Figure 3.2. Schematic representation of commercial sunscreens and their drawbacks.

Taking this into account, it is clear that there is an increasing demand of safe by design approach for safe and effective sunscreen filters and/or UV filter boosters that consents to decrease the

amount in formulation of the conventional filters.[19,26] As a consequence, it is necessary to reduce the use of most harmful solar filters by partially replacing them with other more biocompatible and non-potentially dangerous compounds. Therefore, the research in the field has moved toward the development of novel eco-friendlier and at the same time more effective sunscreen. It is an example the investigation as SPF booster of calcium phosphate-based particles derived from various natural sources (e.g. coral, fish bone) also modified with the introduction of doping ions.[27] Their effectiveness is quite low and also their integration in sunscreen formulations is often critical, furthermore the extraction from animal sources is not well accepted in the cosmetics industry for ethical reasons. Within this work, this aspect has been addressed by engineering mineral particles by a safe-by-design approach, synthetized through a nature-inspired biomineralization process[28], able to increment the efficiency, the safety and the eco-sustainability of sunscreen formulations. The hybrid particles designed and examined in this study consist of a nanostructured mineral phase called hydroxyapatite (HA). HA is chosen for its remarkable biocompatibility, biomimetic properties, and absence of toxicity[29], that was grown, during the synthesis process, on the organic matrix of alginate (Alg), natural polymer derived from brown algae[30], that it was selected given the preference of the cosmetic field towards vegetable derived ingredients rather than those of animal origin (like gelatin), as well as to facilitate the solar formulation between the various ingredients.[31]

In addition, to confer UV shielding properties, hydroxyapatite particles were doped during the synthesis with titanium ions Ti(IV), given its excellent reflective property.[32] In fact, knowing the high refractive index of titanium in the form of oxide (TiO_2), this ion, inserted in the crystalline lattice of hydroxyapatite is able to create a reflective screen against visible light, avoiding the problems related to the use of TiO_2 in sunscreens.[33]

The hybrid phase obtained by the biomineralization of Ti-doped HA onto Alg molecules (AlgTiHA), has been characterized in its physico-chemical properties and investigated for its stability upon irradiation and also toward the marine environment. Furthermore, it was formulated alone and in association with commercial organic and inorganic filters, and the obtained sunscreen formulations were validated in vitro and in vivo in terms of stability, safety and efficacy as UV shielding. Finally, given the paramount importance of developing environmentally safe yet effective sunscreens for skin protection, AlgTiHA was formulated with a particularly harmful organic filter, Benzophenone-3, to evaluate its stabilization inside the sunscreen thanks to the interaction with the hybrid particles. This organic filter, as previously described, is one of the most powerful UV filters in terms of SPF, but has the reputation of being

extremely harmful if released into the environment and especially when in contact with the skin it easily penetrates the deepest layers of the dermis interacting with cells of the endocrine system.[34,35] In this regard, a formulation with Benzophenone-3 was developed and tested ex vivo to show the ability of AlgTiHA to retain the organic filter inside the sunscreen and prevent it from penetrating under the skin.[36–38]

AlgTiHA hybrid particles, obtained by a safe-by-design approach, demonstrate to be a promising eco-friendly compound provided with SPF boosting capabilities. In this way an effective eco-sustainable and safe sunscreen was developed, able to protect the skin from the sunrays damage and containing a reduced quantitative of commercial filters potentially aggressive to the marine ecosystem.

3.2 Materials&Methods

3.2.1 Chemicals and reagents

Alginic acid sodium salt (Alg) from brown algae, phosphoric acid (H_3PO_4, 85 wt%), calcium hydroxide ($Ca(OH)_2$, 95 wt%), titanium (IV) isopropoxide ($Ti(iOPr)_4$, 97 wt%) and isopropanol (C_3H_8O) were purchased from Sigma Aldrich, (USA). Solaveil XTP1 (INCI name: titanium dioxide (80 wt.%), stearic acid and alumina) in form of round nanoparticles with a diameter of about 50 nm, were purchased from Croda, (UK). Coco-Caprylate, Dicaprylyl Carbonate, Ethylhexyl Triazone, Bis-Ethylhexyloxyphenol Methoxyphenyl Triazine and Diethylamino Hydroxybenzoyl Hexyl Benzoate granular were purchased from BASF S.r.l (Italy). Glicerin, Vegetable squalene, Cetearyl alcohol, Citric acid and Panthenol solution 75 W were purchased from Acef S.p.A (Italy). The emulsifier Cetearyl Alcohol and Coco Glucoside was purchased from Seppic S.r.l. (Italy), the preservative mixture Euxyl K900 was purchased from Schülke & Mayr GmbH (Germany), the mixture Sclerotium Gum (and) Xanthan Gum was purchased from Univar S.p.A (Italy), the preservative mixture Dermofeel PA3 was purchased from Evonik Dr. Straetmans GmbH (Germany), Tocopheryl Acetate was purchased from DSM Nutritional Products Ltd (Swiss). Benzophenone-3 were purchased from Sigma Aldrich, (USA).

3.2.2 Synthesis of alginate titanium-doped hydroxyapatite (AlgTiHA)

Preparation of hybrid AlgTiHA nanocrystals, through heterogeneous nucleation on alginate (Alg) matrix was carried out by means of a neutralization reaction performed as follows. A basic solution of $Ca(OH)_2$ (4.72 g in 100 mL H_2O) and an acid phosphate solution (4.15 g in 30 mL H_2O) were prepared. In the meantime, a titanium solution was prepared by adding 1.90 g $Ti(iOPr)_4$, in 15 mL of isopropanol under argon flux to guarantee and anhydrous environment and hamper the formation of TiO_2. The basic solution was heated up to 45 °C under vigorous blades stirring for 30 minutes. Afterwards, the phosphate and titanium solutions were transferred separately in two cylindrical dropping funnels and slowly and simultaneously added dropwise to the basic solution, at 45°C, under vigorous mechanical stirring. During the dripping, it is possible to observe the solution turning increasingly white. Immediately once finished the dripping, Alg solution (4 g in 100 ml H_2O) was slowly added to the suspension in order to avoid particles agglomeration and it was kept under stirring at 45 °C for 2 hours, then left to rest without stirring and RT for 1 hour. Finally, the product was centrifuged at 11000

rpm for 10 minutes. The pellet obtained was rinsed with double-distilled water for three times and then freeze-dried. A controlled freeze-drying process was applied setting the cooling temperature at −40 °C and the heating ramp at 5 °C min^{-1} up to −5 °C and 2 °C min^{-1} up to 15 °C under a pressure of 0.086 mbar until the obtainment of a disaggregated dried powder. As a last step, a micronizer was used to reduce the particles to a micrometric size and facilitate the dispersion of the powder within the formulation (Figure 3.3).

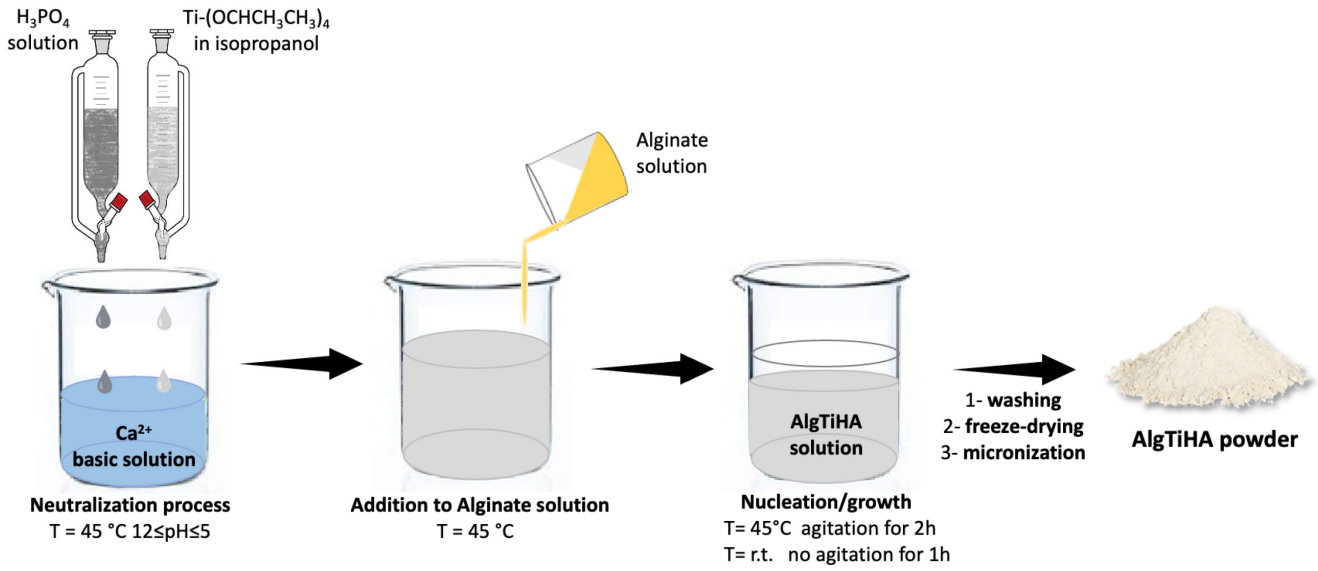

Figure 3.3. Schematic representation of the steps for the synthesis of AlgTiHA hybrid particles.

3.2.3 Sunscreen formulations

In the first part of the study, five different oil in water (O/W) formula containing increasing amounts of AlgTiHA, respectively 0, 3, 5, 10 wt%, and labelled F0, F1, F2, F3 have been developed. Each formulation was made by warming-up the water-based emulsion phase A ingredients, at 70 °C and incorporating the predefined amounts of AlgTiHA micronized powder under vigorous stirring with a turboemulsifier for ten minutes in order to obtain a fluid and completely homogeneous phase. Subsequently, the emulsification phase was carried out by combining and homogenizing the aqueous phase A with the oily phase B, at 70° C. The mixture was then cooled to room temperature and phase C was added into phase A plus B under continuous mixing until homogeneity. This procedure was repeated to prepare samples F0, F1, F2 and F3. Analogously was obtained the reference formula F4 by adding the 5 wt % of TiO_2 based-product (Solaveil XTP1) instead of AlgTiHA. The detailed composition of the base emulsion and formulas F0, F1, F2, F3 and F4 is reported in Table 3.1.

Table 3.1. Ingredients of base emulsion, formulas with (F0) AlgTiHA 0 wt%, (F1) AlgTiHA 3 wt%, (F2) AlgTiHA 5 wt%, (F3) AlgTiHA 10 wt% and (F4) Solaveil XTP1 5 wt%.

Phase	Ingredient (INCI name)	Base emulsion F0	Emulsion + AlgTiHA 3 wt% F1	Emulsion + AlgTiHA 5 wt% F2	Emulsion + AlgTiHA 10 wt% F3	Emulsion + Solaveil XTP1 5 wt% F4
A	Water-based phase					
A1	Aqua	q.b.	q.b.	q.b.	q.b.	q.b.
A2	Sodium phytate,	0,1	0,1	0,1	0,1	0,1
A3	Glycerin	3,0	3,0	3,0	3,0	3,0
A4	Sclerotium gum, Xanthan gum	0,50	0,50	0,50	0,50	0,50
A5	Alginate titanium hydroxyapatite AlgTiHA	-	3,0	5,0	10,0	-
B	Oily phase					
B1	Cetearyl alcohol, Coco-glucoside	2,5	2,5	2,5	2,5	2,5
B2	Cetearyl alcohol	1,0	1,0	1,0	1,0	1,0
B3	Coco-caprylate	4,0	4,0	4,0	4,0	4,0
B4	Dicaprylyl carbonate	3,0	3,0	3,0	3,0	3,0
B5	Squalane	2,0	2,0	2,0	2,0	2,0
B6	Titanium Dioxide, Stearic Acid, Alumina (Solaveil XTP1)	-	-	-	-	5,0
C						
C1	Benzyl alcohol, Ethylhexylglycerin	1,0	1,0	1,0	1,0	1,0

Subsequently, other two different sunscreen formulations have been developed (F6 in Table 3.2 and F9 in Table 3.3), one oil in water emulsion containing a mixture of organic UVA/UVB filters (Bis-ethylhexyloxyphenol, Methoxyphenyl triazine; Ethylhexyl triazone; Diethylamino hydroxybenzoyl hexyl benzoate) and 5 wt% of AlgTiHA to test it as booster of SPF (F6, Table 3.2) and one water in oil emulsion containing inorganic UV filters (mixture of TiO_2 and ZnO) and 5 wt% of AlgTiHA as SPF booster (F9 in Table 3.3). Furthermore, as a comparison, the same sunscreen emulsions without the booster compound (F5 and F8, Table 3.2 and 3.3) and one functionalized with 5 wt% of a commercial hydroxyapatite (HA) instead of AlgTiHA (F7, Table 3.2) were developed.

Each formulation (F5, F6, F7) of Table 3.2 was made by heating phase A ingredients, at 70 °C and taking care to disperse the powders in order to obtain a fluid and homogeneous phase. Phase B, at 70 °C, after mixing to obtain a dispersion as homogeneous as possible, was then added to phase A and mixed until complete dispersion. The mixture was then cooled to room temperature and phase C was added into phase A plus B under continuous mixing until homogeneity.

On the other hand, each formulation (F8, F9) of Table 3.3 was made by melting phase B ingredients, at 70 °C, in the main flask and by mixing to obtain a dispersion as homogeneous as possible. Phase A, taking care to disperse the powders in order to obtain a fluid and completely homogeneous phase, was then added to phase B very slowly, at 70° C and mixed until completely dispersed.

Table 3.2. Ingredient of base emulsion with (F5) organic filters, formulas with (F6) AlgTiHA 5 wt% and with (F7) commercial HA 5 wt%.

Phase	**Ingredient (INCI name)**	**Base emulsion F5**	**Emulsion + AlgTiHA 5 wt% F6**	**Emulsion + commercial HA 5 wt% F7**
A	Water-based phase			
A1	Aqua	q.b.	q.b.	q.b.
A2	Sodium phytate, Aqua, Alcohol	0,1	0,1	0,1
A3	Panthenol, Aqua	0,5	0,5	0,5
A4	Glycerin	3,0	3,0	3,0
A5	Sclerotium gum, Xanthan gum	0,5	0,5	0,5
A6	Alginate titanium hydrxyapatite AlgTiHA	-	5,0	-
A7	Hydroxyapatite (HA)	-	-	5,0
B	Oily phase			
B1	Cetearyl alcohol, Coco-glucoside	2,5	2,5	2,5
B2	Cetearyl alcohol	3,0	3,0	3,0
B3	Coco-caprylate	4,0	4,0	4,0
B4	Dicaprylyl carbonate	3,0	3,0	3,0
B5	Squalane	2,0	2,0	2,0
B6	Bis-ethylhexyloxyphenol, Methoxyphenyl triazine	3,5	3,5	3,5
B7	Ethylhexyl triazone	4,5	4,5	4,5
B8	Diethylamino hydroxybenzoyl hexyl benzoate	3,5	3,5	3,5
C				
C1	Tocopheryl acetate	0,5	0,5	0,5
C2	Benzyl alcohol, Ethylhexylglycerin	1,0	1,0	1,0

Table 3.3. Ingredient of base emulsion with (F8) inorganic filters and formulas with (F9) AlgTiHA 5wt%.

Phase	Ingredient (INCI name)	Base emulsion F8	Emulsion + AlgTiHA 5 wt% F9
A	Water-based phase		
A1	Aqua	q.b.	q.b.
A2	Magnesium sulfate	0,7	0,1
A3	Benzyl alcohol, Ethylhexylglycerin	0,6	0,5
A4	-	-	5,0
B	Oily phase		
B1	Polyglyceryl-3 ricinoleate	2,5	4,0
B2	Glyceryl dibehenate	3,0	1,0
B3	Dicaprylyl ether	4,0	4,0
B4	Squalane	3,0	1,0
B5	Dicaprylyl carbonate	2,0	8,0
B6	Tocopheryl acetate	3,5	0,5
B7	Titanium dioxide, Silica, Jojoba esters	4,5	8,0
B8	Zinc oxide, Caprylic/capric triglyceride, Polyhydroxystearic	3,5	30,0

Finally, using the same ingredients and the same mixing process of formulation F6 (Table 3.2), two formulations were prepared (F10, F11) containing a different organic UV filter, Benzophenone-3 (5 wt%), compared to the previous ones and in F11 AlgTiHA (5 wt%) was also added.

3.2.4 Characterization of AlgTiHA powder

3.2.4.1 Morphological characterization

The sample morphology was examined by scanning electron microscopy (Field Emission Gun Scanning Electron Microscope, FEI, Quanta 200, USA - FEG-SEM) for high resolution images at high magnification. The specimens were previously mounted on aluminum stubs by means of carbon tape and platinum/palladium coated using a coating unit Polaron Sputter Coater E5100 (Polaron Equipment, Watford, Hertfordshire, UK). The dimensional analysis was performed by means of ImageJ software.

3.2.4.2 Chemico-physical characterization

The crystal structure of the composites was established by powder **X-Ray Diffraction (XRD)** analysis. The D8 Advance diffractometer model (Bruker, Karlsruhe, Germany) working with Bragg-Brentano configuration was employed, equipped with a LINXEYE position-sensitive detector (CuKα radiation, λ=1.5418Å) generated at 40 kV and 40 mA. The XRD patterns were recorded in the 2θ range 10°-80°, scan step 0.02° and step time 0.5 seconds.

The thermal behaviour of the composites was determined using the **Simultaneous Thermal Gravimetric Analyzer (TGA)** STA 409C Netsch (Germany). The experiment was carried out in the temperature range of 10-1100 °C using a heating rate of 10 K/min in air flow. For the analysis, 20 mg of sample and Al_2O_3 crucible were employed.

The **Fourier-Transform Infrared (FTIR)** spectra were collected by a Thermo Nicolet-Avatar 320 iD7 ATR FT-IR (Thermo Fisher Scientific Inc., Waltham, MA, USA). All the spectra are the average of 64 spectra, collected at room temperature in the wavelength range of 400-4000 cm^{-1} at a resolution of 4 cm^{-1}.

To perform the analysis of different ions present in AlgTiHA powder, an **Inductively Coupled Plasma – Optical Emission Spectroscopy ICP-OES** Liberty 200 Varian (Clayton South, Australia) was employed. Samples were prepared by dissolving 20 mg of each in 2 mL of nitric acid (HNO_3) and then making them up to 100 mL volume with deionized water after 30 minutes of sonication. Standard solutions of the element of interest were used as reference and an equally diluted solution of nitric acid as blank.

An **Ultraviolet/Visible-NIR spectrophotometer (UV-Vis)** Lambda 750, (Perkin Elmer Instrument, USA) was used to perform absorbance measurements. The powders were suspended in distilled water with a concentration of 10 mg L^{-1} and sonicated for 10 minutes with a sonication probe. The absorbance spectra of the AlgTiHA was recorded from 250 to 700 nm and compared with the TiO_2-based commercial product (Solaveil XTP1). The same spectrophotometer was used to analyse the reflection properties of the sample. The powders were loaded on a sample holder and the spectrum was recorded from 280 nm to 780 nm.

Photodegradation tests were carried out to evaluate the degradation of Blue Acid 9 (42090 Color Index catalog, USA) in contact with each compound after subjecting it to UV radiation.[39] Both light and dark conditions are evaluated, with the aim of reducing the absorption

contribution of the dye on the surface of the adduct materials. 10 mg of powder were added in 100 mL of two different Blue Acid 9 solutions (6 mg/L). The first solution is subjected to UV radiation (OSRAM, L BLUE UVA 18 W/78, radiated power 4.7 W, UVA range 315-400 nm, intensity 7800cd); while the second is stirred in the dark. This step lasts 1 hour for both, followed by a time of 3 hours to reach an absorption/de-absorption equilibrium. Before proceeding to the UV-Vis analysis at 630 nm, 2 mL of each sample are centrifuged at 14.5 rpm for 5 minutes and then filtered (0.45 μm). The AlgTiHA sample was compared with the TiO_2-based commercial product (Solaveil XTP1).

The results were expressed in the form of "photocatalytic efficiency (%)", in accordance with the Lambert-Beer law in which the absorbance is proportional to the concentration of Blue Acid 9. Specifically, the photocatalytic efficiency indicates the ratio between the amount of consumed reagent and the amount of initial reagent in the reaction environment, determined with the following equation:

$$\boldsymbol{Photocatalytic\ efficiency}\ (\%) = \frac{\boldsymbol{A0-At}}{\boldsymbol{A0}}\ \boldsymbol{x\ 100} \qquad \textbf{Eq. 3.1}$$

where A0 is the initial absorbance of Blue acid 9 and At is the absorbance after one hour of irradiation.

3.2.4.3 Degradation test in marine and lake-like environment

To evaluate the possible degradation of AlgTiHA and the release of titanium in the form of TiO_2 in the water, we recreated the environmental conditions present in the aquatic environment.[40] 3.5 g of NaCl were dissolved in 100 mL of milliQ water (3.5% salinity) to imitate the marine environment and 0.05 g of NaCl in 100 mL of milliQ water (0.05% salinity) to simulate fresh water from rivers and lakes. Subsequently, 1 g of AlgTiHA powder was suspended into 40 mL of saltwater and freshwater respectively and placed at both room temperature and 37 °C under stirring. At different time points (3, 7, 14, 21, 28 days) the sample was withdrawn and the mixture was centrifuged to separate the powder form the supernatant that was analysed at ICP-OES (Liberty 200, Varian) to quantify the content of ions. The powder and the supernatant were freeze-dried and analysed with XRD (D8 Advance diffractometer model, Bruker, Karlsruhe, Germany) to exclude the formation of TiO_2. At each time point, 40 mL of fresh and salt water were added to the remaining powder.

3.2.4.4 In vitro evaluation of antimicrobial activity

Determining the minimum inhibitory concentration (MIC) is a quantitative measure of the activity of a substance against defined bacteria.[41] It is reported as the lowest concentration of a substance capable of inhibiting visible bacterial growth. In the purpose of this study, the MIC of AlgTiHA was determined against both Propionibacterium acnes and Staphylococcus aureus. As shown in Table 3.4, 10 mL of stock solution containing AlgTiHA (10 mg/mL) and its respective diluted solutions (2 mL for each sample) were prepared.

Table 3.4. Concentration values of AlgTiHA diluted suspensions.

AlgTiHA suspensions	Suspensions concentration (µM)
1	1000
2	100
3	10
4	1
5	0.1

Bacterial inoculum was then prepared by dissolution of a bacterial culture in 5 mL of TS broth and incubation overnight at 35 °C. The optical density (OD) of the inoculum was measured using a UV-Vis spectrophotometer at 600 nm. The number of bacteria present was calculated using the following equations:

$$0{,}1\ OD600 : 1 \times 10^6\ cells/ml = sample\ OD600 : X\ (cells/ml) \qquad \textbf{Eq. 3.2}$$

$$X\ (cells/ml) = sample\ OD600 \times 10^6 / 0{,}1 \qquad \textbf{Eq. 3.3}$$

Depending on the calculated concentration of bacteria, a dilution of 1 x 106/5 cells/ml was prepared to form the appropriate inoculum. Each tube corresponding to a different dilution was then inoculated and incubated at 35 °C for a period of 16 to 24 hours with stirring. Bacterial growth was then measured by reading the absorbance of the tubes to determine the MIC.[42]

3.2.5 Sunscreen formulations efficacy and safety assessment

3.2.5.1 In vitro SPF and UVA test

Irradiation of each formulation was carried out using the Atlas SUNTEST CPS + solar simulator, equipped with a Xenon lamp, an optical filter to cut off wavelengths shorter than 290 nm and an IR-block filter to avoid thermal effect, and set to operate between 40-200 W/m^2 in accordance to ISO 24443:2012 guidelines.[42]

Instrumental determinations of the UV absorbance (calculated from transmittance) were carried out using a Shimadzu UV-2600 spectrophotometer, provided of integrating sphere ISR 2600 60 mm and coupled with an SPF determination software, with emission of wavelength from 290 nm to 400 nm and 1 nm increment. This test is informative for the determination of two significant parameters: the critical lambda and the SPF label/UVAPF ratio. Critical lambda describes the amplitude of the protection across all the UV spectra (280-400 nm). It is the wavelength at which 90% of the area under the absorbance curve (AUC) is reached starting from 290 nm. SPF label/UVAPF ratio relies on the ability of the formula to specifically protect in the UVA range, in relation to the global SPF value declared on the label. Similarly, to the Critical Lambda, this ratio provides an evaluation of the amplitude of the protection across the UV spectra without considering the amount of the filtering activity. Values near to 1 are indicative of a broad-spectrum activity. EC 647/2006 suggests that all solar products have a critical lambda value greater than 370 nm and a UVAPF value of at least 1/3 of the SPF value declared on the label (SPF label).

In vitro SPF was calculated as follows:

$$\boldsymbol{In\ vitro\ SPF} = \frac{\int_{\lambda=290nm}^{\lambda=400nm} \boldsymbol{E(\lambda)I(\lambda)d(\lambda)}}{\int_{\lambda=290nm}^{\lambda=400nm} \boldsymbol{E(\lambda)I(\lambda)10^{-A(\lambda)}d(\lambda)}} \qquad \textbf{Eq. 3.4}$$

E (λ)= erythema action spectrum (CIE-1987) at a wavelength λ.

I (λ)= spectral irradiance received from the UV source at a wavelength λ.

A (λ)= a monochromatic absorbance of the test product layer at a wavelength d (λ), wavelength step (1 nm).

The UVA protection factor UVAPF0 has been calculated for each non-irradiated plate individually with the equation 3.5:

$$UVAPF0 = \frac{\int_{\lambda=320nm}^{\lambda=400nm} P(\lambda)I(\lambda)d(\lambda)}{\int_{\lambda=320nm}^{\lambda=400nm} P(\lambda)I(\lambda)10^{-A(\lambda)C}d(\lambda)} \qquad \textbf{Eq. 3. 5}$$

P (λ) = Persistent Pigment Darkening (PPD) action spectrum.

I (λ) = spectral irradiance received from the UV source (UVA 320–400 nm for PPD testing).

A (λ) = Mean monochromatic absorbance of the test product layer.

C = Coefficient of adjustment.

dl = Wavelength step (1 nm).

The evaluation of SPF in vitro was conducted following the ISO 244431 guideline and the European Commission recommendation EC 647/2006 relating to the efficacy of sunscreen products.[43]

The protocol used consents to instrumentally predict the SPF and UVAPF of a cosmetic product, by a spectrophotometric technique, before and after a period of controlled UV irradiation. The substrate chosen for the test consists of PMMA plates with transmittance and roughness characteristics predefined.[4]

3.2.5.2 In vivo SPF test

Preliminary tests for the evaluation of the sun protection factor (SPF) in vivo on sunscreen formulations with 5wt% of AlgTiHA with organic/inorganic filters were conducted on five volunteers in accordance to ISO 24444:2019 guidelines.[42] The SPF in vivo test method utilizes a xenon arc lamp solar simulator (or equivalent) of defined and known output to determine the protection provided by sunscreen products on human skin against erythema induced by solar ultraviolet rays. The test is restricted to the area of the back of selected human subjects. A control area of each subject's skin is exposed to ultraviolet light without protection, and another (test section) is exposed after application of the sunscreen product under test. One further section is exposed after application of an SPF reference sunscreen formulation which is used for the procedure validation. To determine the sun protection factor, an incremental series of delayed erythema responses are induced on several small sub-sites on the skin. These responses are visually assessed for presence of redness from 16 h to 24h after UV radiation, by the judgment of an expert evaluator. The minimal erythematous dose (MED) for unprotected skin (MEDu) and the MED obtained after application of the sunscreen product (i.e. MEDp) is

determined on the same subject on the same day. An individual sun protection factor (SPFi) for each subject tested is calculated as the ratio of individual MED on protected skin divided by the individual MED on unprotected skin (i.e. MEDp/MEDu). The sun protection factor for the product (SPF) is the arithmetic mean of all valid SPFi results from each subject in the test.

3.2.5.3 Safety test (patch test)

To evaluate the safety of AlgTiHA, a patch test was performed on a base emulsion with high concentration (10 wt%) of sample.[44,45] The test was conducted on 20 healthy volunteers of both sexes, who have given a written consent to the experimentation. Samples were poured into aluminium Finn chambers and applied to the skin of the forearm protected by self–sticking tape. The cosmetic products were left in contact with the skin surface for 24 hours. Removal of the Finn chamber and cleaning of the skin area from residual cosmetic products was carried out by experimenters. The evaluation of skin reactions was made 15 min and 24 hours after removal of the Finn chambers by an expert evaluator. The sum of erythema and edema scores is defined as the "irritation index".

3.2.5.4 Stability test

The stability test of sunscreen emulsions has been conducted in parallel in a glass jar at room temperature and at 40 ± 2°C for six months. At selected intervals (1 week, 1 month, 2 months, 3 months, 6 months), samples were picked up and evaluated for physical-chemical (pH, viscosity) and organoleptic characteristics (appearance, colour, odor) to monitor changes.

3.2.5.5 Ex vivo release test

To evaluate the ability of AlgTiHA to act as a stabilizer and therefore prevent organic/inorganic filters release from the formulation that can penetrate under the skin, an ex vivo release test was performed on human skin explants using OFM (Open Flow Microperfusion) equipment at Institute for Biomedical Research and Technologies - Joanneum Research in Austria (Graz). In details, a formulation with AlgTiHA and Benzophenone-3 as organic filter was analysed.
OFM is a system of thin flexible probes with a permeable exchange area, which inserted under the skin at the level of the dermis allows continuous monitoring of the permeation of substances in the form of creams applied to the skin. The probes are connected to a push-pull pump system, i.e. two peristaltic pumps which guarantee the continuous flow inside the probes of a sterile

and biocompatible perfusate which mimics the dermal interstitial fluid, normally present inside our tissues and which allows the exchange of substances between cells and blood. The speed of the flow can be varied according to the needs and will affect the volume of sample collected inside the vial, from which it is possible to evaluate the concentration of substance released under the skin (Figure 3.4).[37]

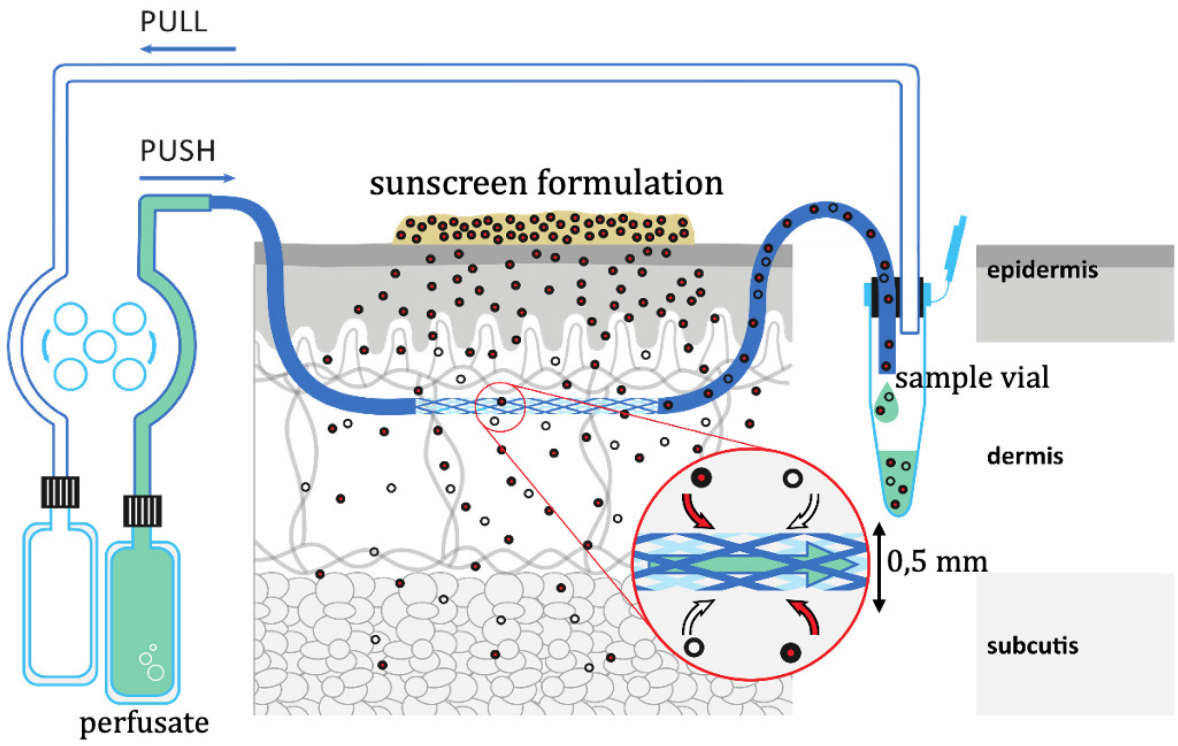

Figure 3.4. Schematic drawing of a dOFM sampling system.

In this test a skin explant frozen at -20°C from the abdomen of a female donor was used. After having disinfected the explant using gauze soaked with water and marked the area for probe insertion and application of the formulation with a felt-tip pen, 12 dOFM probes (MS0200401 type, Joanneum Research) CE certified with 15 mm braided (stent -like) sampling section (outer diameter 0.5 mm), were inserted under the skin using cannula needles (0.9x70 mm) as a guide. Two probes in triplicate were used for each formulation tested (Figure 3.5).

The skin explant was then placed inside a climatic chamber at 32.5 °C with 40-60% of relative humidity to carry out the experiment under the same temperature conditions as the skin. Subsequently, each probe was connected through capillary tubes, entering with a 10 mL bag of perfusate (9 ml ELOMEL isoton, Fresenius Kabi Austria, with 1 mL Human Serum Albumin, Octapharma, Vienna, Austria) and exiting to sample vials 0.2 mL bottle for collecting samples.

All connected with the push-pull pump system (MPP102PK type, Joanneum Research) with a pump rate of 0.5 µL/min. All accessories and equipment used are CE certified for human use. For each formulation (F10, F11) to be tested, 55 mg were applied with a spatula and spread on the appropriate previously marked areas and the perfusate solution was started to flow inside the probes. At different time points every 4 h for 24 consecutive hours the samples were collected and frozen at -80 °C to subsequently carry out the quantification of the released Benzophenone-3 by High Performance Liquid Chromatography (HPLC) analysis.[46]

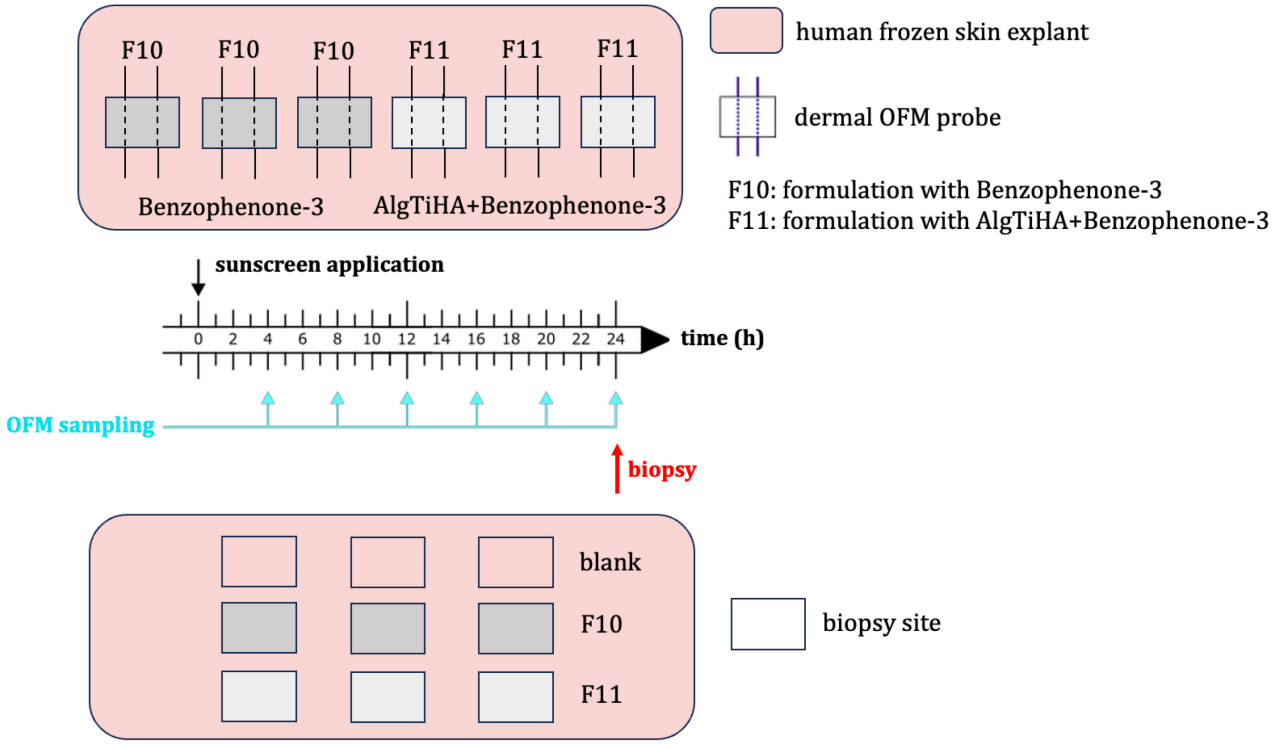

Figure 3.5. Schematic representation of ex vivo study set-up and sampling schedule.

Each collected sample was prepared as follows for HPLC analysis.

10 µL of collected sample was mixed with 200 µL of 90:10 Ethyl-acetate/Hexane solution and centrifuged for 2 min at 13000 rpm to perform a solid-phase extraction. Subsequently the supernatant was transferred into a PCR plate and evaporated to dryness with nitrogen. Finally, the residue obtained was resuspended with 50 µL of Acetonitrile solution (20%) and vortexed for 1 minute, thus ready for HPLC analysis.

The sample analysis was performed with an Ultimate 3000 HPLC (Thermo Fisher Scientific, Waltham, MA, USA) with ACQUITY-UPLC-HSS-T3 C18 reverse phase column (1,8 µm, 2,1x100

mm) using an isocratic method with a methanol/water (95:5 v/v%) mobile phase, a flow rate of 300 μL/min and an injection volume of 3 μL. The ultraviolet detector was set at 287 nm.[36]

Simultaneously with the OFM release test, another skin explant from the same donor was disinfected and used to perform the biopsy and obtain specimens for histological analysis (Figure 3.5).
After having marked the areas with a felt-tip pen on which to apply the formulations, for each sunscreen sample 80 mg were spread, in addition to the control blank. Subsequently, the skin explant was placed for 24 hours in a climatic chamber at 32.5 °C with 40-60% of relative humidity to carry out the experiment under the same temperature conditions as the skin.
After the pre-established hours, the explant was cleaned of excess residual cream and the skin samples (2x2 cm) were taken with a scalpel, in triplicate for each formulation. A deep cut was performed in order to obtain a sample volume with all layers (epidermis, dermis and hypodermis) clearly visible for histological analysis.[47]

3.2.5.6 Histological analysis

- Fixation

For the histological analysis, the three different biopsy samples of skin explants were fixed in 4% buffered formalin (KalteK 1609). Briefly, the explants were washed in Phosphate Buffered Saline solution 1X (PBS 1X) once and incubated 20 minutes in the fixative solution. The explants were washed twice with PBS 1X for 5 minutes and store at 4°C until dehydration process for paraffin embedding.[48]

- Dehydration and paraffin embedding

The fixed samples were put in plastic supports and dehydrated by direct immersion in an increasing scale of ethanol solutions (from 70 to 100% v/v) and cleared in xylene reagent (Sigma) in order to prepare the samples to the paraffin embedding. Indeed, the paraffin is a wax-like substance composed of a mix of saturated hydrocarbons that it's solid at room temperature and its melting point is close to 60 °C. As paraffin is not miscible with water but tissues and fixatives are mostly water, the aqueous component must be removed from the samples before they are infiltrated with liquid paraffin and this is done by dehydration of tissues with ethanol for a good embedding.[49] Briefly, the samples were incubated for 1 hours with each ethanol solution (70%, 80%, 95% and 100%) under vacuum conditions, followed by

a second overnight incubation with 100% ethanol. After dehydration, the samples must be transferred to an intermediary liquid, like xylene, which is miscible with both ethanol and paraffin. These are called clearing substances, and the immersion in the intermediary liquid must not be long to avoid samples hardening.[49] After clarification, various changes in liquid paraffin are recommended in order to completely replace the intermediary liquid with paraffin. In our case, the samples were cleared twice in xylene for 1 hour's incubation and also pre-conditioned twice in liquid paraffin (Histo-line laboratoties) at 65 °C for 1 hour's incubation, under vacuum conditions. For the embedding, the samples were removed from the plastic support and they were put transversally in a metal cell. The liquid paraffin was poured over the sample to cover it and to completely fill the cell. The paraffin was allowed to solidify at room temperature until sectioning.

- Sectioning, deparaffinization, hydration/dehydration and mounting of sections

The embedded explants were dissected in 10 μm sections by using a semi-automatic rotary microtome (Histo-line laboratories). The obtained sections were put in a 45°C water bath to allow them to stretch before being collected on Polylysine coated slides (25 x 75 x 1 mm), Histo-line laboratories). Before the histological staining, the collected sections were partly deparaffinised for about 10 minutes' incubation at 59 °C and left them dried at room temperature. The paraffin was totally removed by clearing the sections twice in xylene for 5 minutes. Then, the sections were hydrated in a decreasing scale of ethanol solutions in order to make the sections suitable for water soluble staining; specifically, the sections slides were incubated twice with 100% and 80% ethanol solutions for 5 minutes, followed by rinsing in MilliQ water until histological staining was performed.

After the histological staining, an increasing scale of ethanol solutions was used to dehydrate the sections for the mounting. In detail, the sections slides were incubated twice with 80%, 95% and 100% ethanol solutions for 5 minutes and they were finally cleared twice in xylene for 5 minutes. Then, the sections slides were mounted by using a specific histological mount (Histo-line Laboratories) and a cover glass in order to preserve the morphological status of the sample in long term. The histological mount was dropped on the sections avoiding the creation of bubbles and the cover glass was carefully placed on top and left them dried at room temperature.[48]

- Haematoxylin and Eosin staining

For all the explants groups, the Haematoxylin of Mayer and Eosin (Histo-Line Laboratories) (H&E) staining was performed to highlight cellular morphology and the reagents were prepared as follows. In detail, both staining solutions were prepared in the lab, following the manufacturer's instructions. Briefly, Haematoxylin (0.75 g, Fluka, Sigma Aldrich), potassium alum (25 g, $KAl(SO_4)_2 12H_2O$), sodium iodate (0.1 g, $NaIO_3$) and MilliQ water were mixed to obtain 500 mL of Haematoxylin of Mayer. The Eosin solution was used as counterstaining for cell nuclei identification and it was prepared in the lab by mixing 100 mg Eosin Y (Sigma) with 100% ethanol and acetic acid in order to obtain an 1% aqueous eosin Y. The H&E staining is the most commonly used histological analysis that allows the qualitative detection of cell nuclei and the cytoskeleton in violet and pink, respectively. Specifically, the haematoxylin is a positively charged dye that is able to interact with the negatively charged histone proteins of the chromatin in cell nuclei; on the other hand, the eosin is an anionic dye which interact with different cellular components such as the cytoplasm, the collagen etc., giving them a pink colour. After the clarification and hydration process reported in the previous section, the protocol of H&E staining was performed following the manufacturer's instructions. Briefly, the Haematoxylin of Mayer was added with acetic acid at 1 mL per 100 mL of total solution and both dyes were filtered before the use to remove any deposits. Then, the sections were incubated with Haematoxylin of Mayer for 7 minutes at room temperature followed by rinsing in running spring water for 10 minutes. The sections were washed in MilliQ water and incubated with Eosin Y for 3 minutes at room temperature. The excess dye was removed by washings in MilliQ water before the dehydration, the clarification in xylene and the mounting of sections as reported in the previous section. The images were acquired at the optical microscope (Nikon) at various magnifications.[48]

3.3 Results&Discussion

3.3.1 Synthesis and characterization of AlgTiHA powder

Physical filters, such as titanium dioxide (TiO_2) and zinc oxide (ZnO) are able to shield the skin from both UVA and UVB radiation, however, they have some important limitations, especially regarding their critical size and, in the case of TiO_2, photocatalytic properties and further associated risk of bioaccumulation in marine environment due to insolubility. In detail, the recent sunscreen products contain mineral particles with nanometric dimensions that allow to decrease the undesired whitening effect, however nano-size increase overall potential reactivity. Furthermore, TiO_2 is known for its high photocatalytic activity, generating reactive oxygen species (ROS), which can also interact with formulation, raising safety concerns.[14] In the other hand, the main problem regarding some often-used organic UV-filters, is that being mainly used on the seaside, the components of the formulation are released in sea water, and the marine environment can be damaged, causing coral bleaching and bioaccumulation in the fauna. Considering all these issues, attention is shifting towards the development of effective and safer UV filters for both human and environment, evaluating the possibility to modify the current commercial filters formulation by replacing, totally or partially, those carrying the above stated side effects, with the ultimate goal of producing more eco-sustainable and safer sunscreen formulations.

To face this challenge, this research has been focused on the development of new eco-friendly formulations, designed following the safe-by-design approach, and characterized by a safe and biocompatible UV filters, obtained through the biomineralization process, i.e. the natural process by which organisms generate hybrid nanostructured materials hierarchically organized from the nano to the macroscopic scale exhibiting unusual behaviour.[28,29,50]

In this process the selected organic matrix strictly controls the nucleation and growth of inorganic crystals featured by low crystallinity, which results in a higher solubility, and with a strong interaction with the organic template, achieving a hybrid structure. The flexibility of this process and the low crystallinity of the mineral phase obtained, also allows the introduction of different dopant ions inside the crystalline lattice, with the generation of new further functions. The biomimetic approach utilized in this study has proven to be effective in developing a safer inorganic filter. By mineralizing titanium-doped hydroxyapatite (TiHA) nanocrystals onto Alginate (Alg) molecules, the essential features necessary for creating an innovative, eco-sustainable sunscreen in compliance with cosmetic regulations have been achieved.[28] In Figure

3.6 we summarized the chemical-physical characterizations carried out to confirm the successful synthesis and efficacy of AlgTiHA hybrid particles. Starting from physical-chemical characteristics, the XRD profile (Figure 3.6 A) indicate the presence of a mineral phase with low crystallinity that can be identified as an apatite-like structure according to the PDF cards #09-0432.

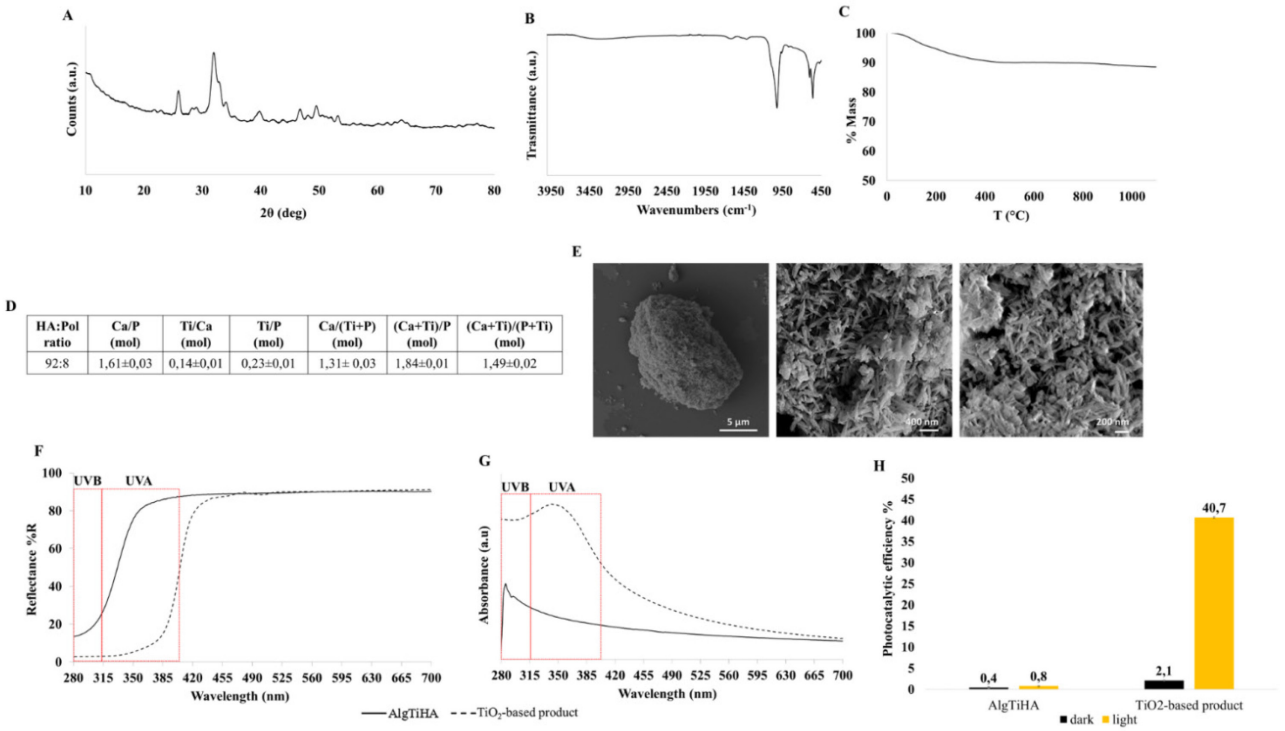

HA:Pol ratio	Ca/P (mol)	Ti/Ca (mol)	Ti/P (mol)	Ca/(Ti+P) (mol)	(Ca+Ti)/P (mol)	(Ca+Ti)/(P+Ti) (mol)
92:8	1,61±0,03	0,14±0,01	0,23±0,01	1,31± 0,03	1,84±0,01	1,49±0,02

Figure 3.6. The panel summarizes all the characterizations of the synthetized AlgTiHA powder also in comparison with a TiO_2-based commercial product: A) XRD spectra highlighting the low crystallinity of the TiHA mineral phase; B) FTIR spectra showing the typical signal of HA; C) thermal decomposition profile (TGA) of AlgTiHA; D) table reporting the inorganic/organic ratio and the chemical composition of TiHA evaluated by ICP; E) SEM-FEG images of AlgTiHA micro-aggregates and at higher magnification the nucleated TiHA elongated nanocrystals; F) reflectance spectra in the UVA-UVB range; G) absorption in the UVA-UVB range; H) photocatalytic efficiency evaluated as induction of the degradation of Blue Acid 9 solution.

The presence of the apatite-like phase was confirmed by both XRD analysis and FTIR spectra, as shown in Figure 3.6 B. In particular, the signal at 1036 cm^{-1} corresponds to the asymmetric stretching of PO_4 groups of HA, while, peaks at 602 and 562 cm^{-1} are related to the bending of the PO_4 group of the HA.[51] From Figure 3.6 C, TGA profile revealed two different weight loss consisting first in the adsorbed water loss and then in polymer degradation, in line with what reported in the literature.[52]

In detail, Alg:TiHA ratio is lower than the theoretical one (20:80), the observed decrease in the organic phase can be attributed to the strong affinity between the Ca^{2+} ions of TiHA and Alg, facilitating the immediate interaction between the newly formed hydroxyapatite and Alg. As a result, the residual Alg was effectively removed during the washing step.

The chemical composition of the mineral phase was measured by ICP quantitative analyses (Figure 3.6 D), confirming the effective partial substitution of both Ca^{2+} ions and PO_4^{3-} ions in the HA lattice by, respectively, Ti^{4+} and TiO_4^{4-} ions. Furthermore, titanium ions are incorporated within the calcium-phosphate crystalline structure, not in the form of oxide (TiO_2), thus avoiding any photocatalytic properties, point of weakness, of the currently used TiO_2 and ZnO.[14,32]

AlgTiHA, thanks to the presence of organic phase, appears as disaggregated hybrid micro-particles completely covered of hydroxyapatite nanoparticles as it is clearly visible through SEM-FEG (Figure 3.6 E). AlgTiHA sample consists of needle-like crystals of, respectively, 305 ± 55 nm and 277 ± 76 nm length (n=30), with a high tendency to aggregate. The direct nucleation onto polymeric matrices, allow to create hybrid clusters thought to avoid the penetration of the epidermal layers, thus providing a safe-by-design feature associated with the use of nanomaterials in dermocosmetic formulations.[53]

As regards the absorption and reflectance capacities of AlgTiHA powder, two different behaviours were observed. The reflectance profile (Figure 3.6 F) revealed that AlgTiHA is able to reflect the UV radiation more than the TiO_2-based commercial product, mostly in UVA range (315-400 nm) where an increase of value is observed until a plateau of 90% at the edge of the visible range (400 nm) confirming the good reflection properties of these hybrid composite. On the other hand, AlgTiHA show lower absorption (Figure 3.6 G) than the TiO_2-based commercial product. This is partially explainable by the content of above the 48 wt% of Ti(IV) in the TiO_2-based commercial products, while in AlgTiHA it is present in the percentage of 10 wt%.

Finally, the absence photocatalytic activity in AlgTiHA, essential requirement for a safe sunscreen, was evaluated in dark and UV light conditions. Through the photodegradation test of an aqueous solution of Blue Acid 9 absorbed on the surface of the compound[54], no photocatalytic effect was detected for AlgTiHA (Figure 3.6 H) both dark and UV light conditions, sign that there is no degradation of the compound with the formation of radicals and/or reactive species under irradiation and highlighting its potential use for safer sunscreens. On the contrary, the TiO_2-based commercial product showed photocatalytic efficiency inducing the

degradation of Blue Acid 9. The specific description of the characterizations of AlgTiHA hybrid particles was reported by Campodoni et al.[28]

Summarizing the results obtained following the characterization of the AlgTiHA powders, we can state that:

- XRD and FTIR spectra confirm the crystal and chemical structure typical of apatite.
- TGA profile denotes the weight loss of the polymeric and inorganic components, demonstrating the successful synthesis with an Alg:TiHA ratio of 8:92.
- SEM images show the presence of microaggregates and not nanoparticles.
- AlgTiHA exhibits an effective reflective power especially in the UVA range.
- Photocatalytic activity is absent for AlgTiHA under both light and dark conditions.

3.3.2 Degradation test in marine and lake-like environment

Given the photocatalytic activity of TiO_2-based products and the potential damage to the marine (i.e. coral bleaching[24,55]) and non-marine environments by the release of their degradation by-products, it is crucial to identify and characterize the degradation behaviour of AlgTiHA under specific environmental conditions. To achieve this, the study replicated the conditions of seawater using saltwater (Salt) and freshwater conditions resembling those of a lake or river (Fresh). Two different temperatures were considered: 37 °C and room temperature (RT). The degradation of AlgTiHA and the formation of degradation by-products were evaluated at various time points (3, 7, 14, 21, and 28 days) to monitor the degradation process in these simulated environmental conditions (Figure 3.7).

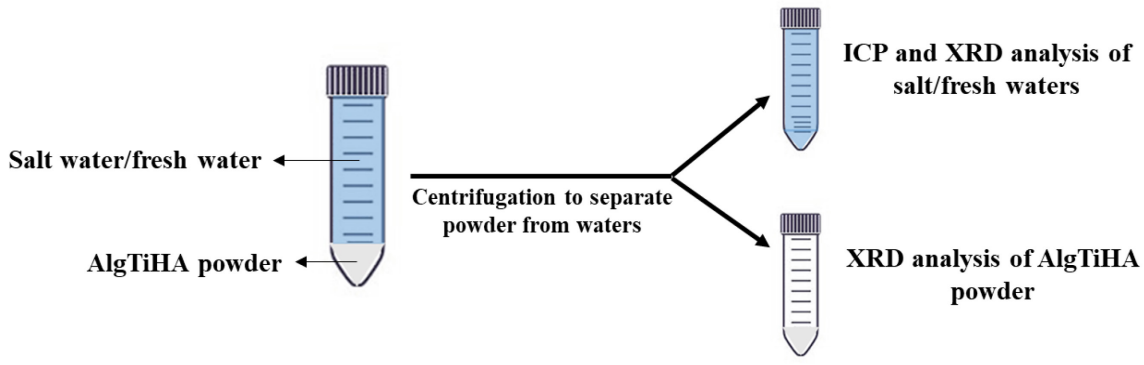

Figure 3.7. Schematic representation of analysis for AlgTiHA degradation test.

The XRD analysis carried out on the residual powder and the supernatant, show the results after 28 days of degradation (Figure 3.8). XRD results for the earlier time points (3, 7, 14, and

21 days), showing spectra equal to those obtained after 28 days, have not been included in the work.

From Figure 3.8 it can be observed that both the Supern_Salt_RT, Supern_Salt_37, Supern_Fresh_RT, and Supern_Fresh_37 samples obtained from the freeze-drying of supernatants do not exhibit the characteristic peaks of titanium dioxide, indicated in the spectra with the red dots.

On the other hand, the XRD spectra of the residual powders (AlgTiHA_salt_RT, AlgTiHA_salt_37, AlgTiHA_fresh_RT, AlgTiHA_fresh_37) tested in the two different mediums show a similar profile to that of the initial AlgTiHA sample.

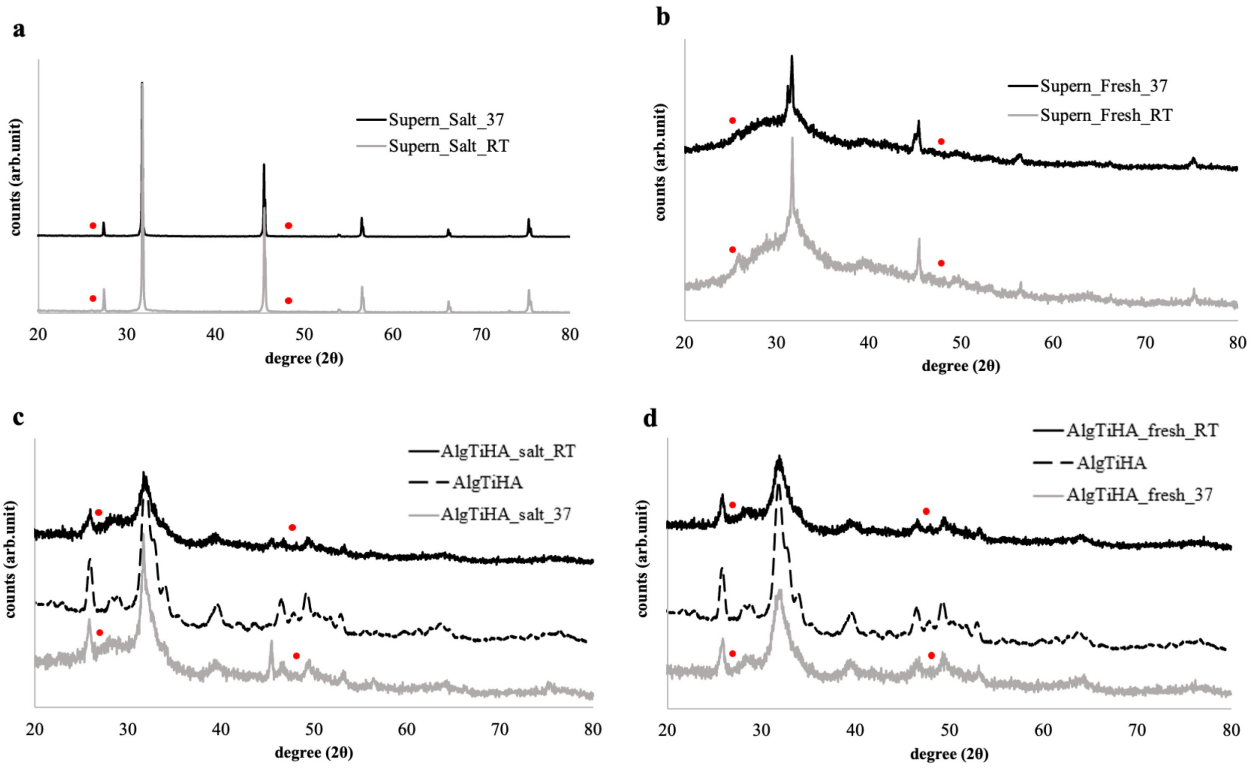

Figure 3.8. XRD spectra of a) Salt water after 28 days at room temperature and 37 °C (Supern_Salt_RT, Supern_Salt_37); b) Fresh water after 28 days at room temperature and 37 °C (Supern_Fresh_RT, Supern_Fresh_37); c) Powders withdrawn from salt water after 28 days at room temperature and 37 °C (AlgTiHA_salt_RT, AlgTiHA_salt_37) compared to AlgTiHA spectrum; d) Powders withdrawn from fresh water after 28 days at room temperature and 37 °C (AlgTiHA_fresh_RT, AlgTiHA_fresh_37) compared to AlgTiHA spectrum. Red dots refer to the most intense typical TiO_2 signals.

In order to have a more precise evaluation of the chemical species corresponding to the XRD spectra obtained, a quantitative phase analysis was carried out through the Rietveld method. Observing Table 3.5 below, Supern_Salt_RT and Supern_Salt_37 after 28 days showed only the presence of NaCl (Halite mineral phase), while in Supern_Fresh_RT and Supern_Fresh_37,

despite the poor resolution and low intensity of the XRD patterns, Halite and a small percentage of Apatite (26-22 Wt%) have been identified.

In the powders, instead, as already highlighted by the XRD profile, the presence of apatite is mainly recovered, but in AlgTiHA_salt_RT and AlgTiHA_salt_37 a low percentage of Halite is present, probably precipitated over the days. As for the XRD spectra, also in this case the other time points at 3, 7, 14 and 21 days showed similar behaviour and for this reason they are not present in the work.

Table 3.5. Quantitative phase analysis of supernatant in salt water (Supern_Salt_RT, Supern_Salt_37), and fresh water (Supern_Fresh_RT, Supern_Fresh_37), powders in salt water (AlgTiHA_salt_RT, AlgTiHA_salt_37) and powders in fresh water (AlgTiHA_fresh_RT, AlgTiHA_fresh_37) after 28 days through Rietveld method.

Sample name	Apatite Wt%	Halite Wt%	Anatase Wt%
Supern_Salt_RT	0	100	0
Supern_Salt_37	0	100	0
Supern_Fresh_RT	22	78	0
Supern_Fresh_37	26	74	0
AlgTiHA_salt_RT	93	7	0
AlgTiHA_salt_37	93	7	0
AlgTiHA_fresh_RT	100	0	0
AlgTiHA_fresh_37	100	0	0

Subsequently, an ICP analysis was conducted on the aliquots from the different time points (3, 7, 14, 21, 28 days) of the two different mediums to assess the presence of ions in the water and determine the degradation of AlgTiHA over time. As anticipated, the ions comprising AlgTiHA, namely Ca, P, and Ti, were detected in the samples. The release percentage trend of these ions over time was obtained and is presented in Figure 3.9.

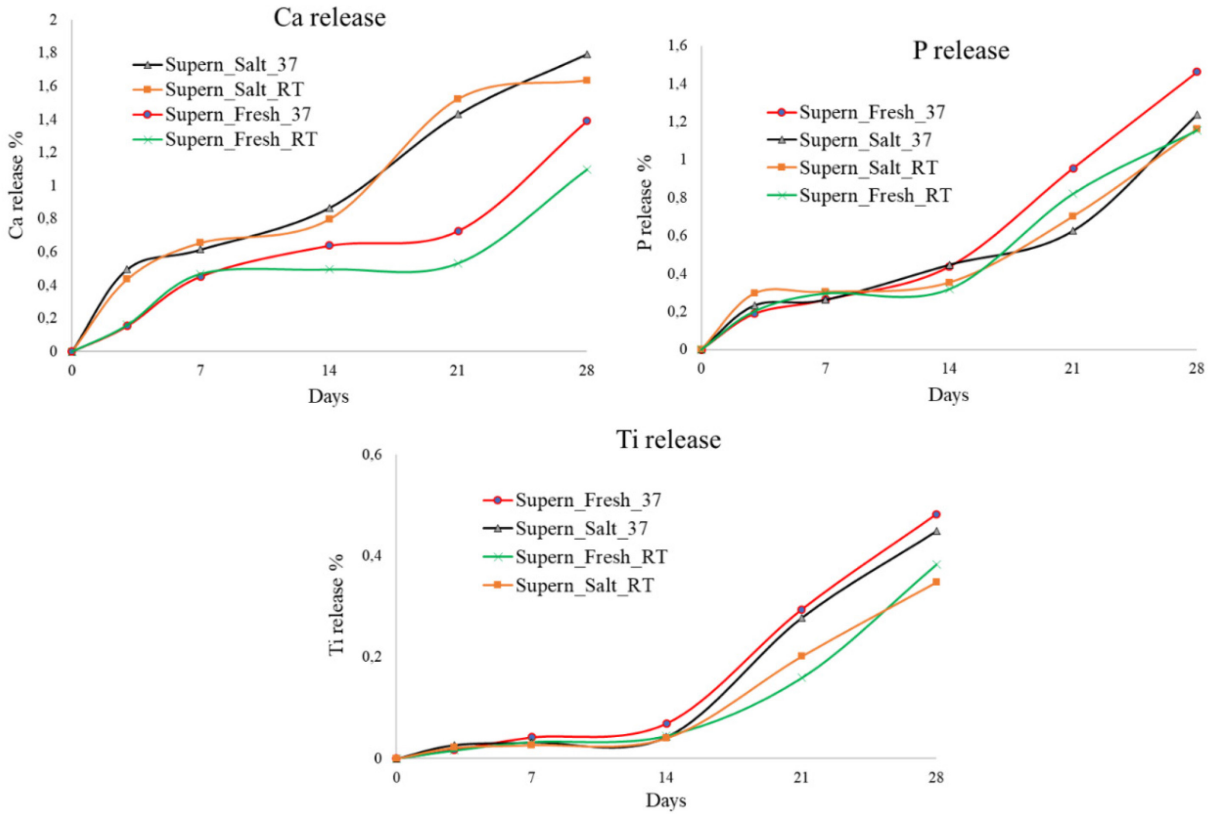

Figure 3.9. Release trend of Ca, P and Ti ions in salt and fresh water at room temperature (RT) and 37 °C monitored for 28 days through ICP analysis.

ICP quantitative analysis allowed to evaluate the percentage of Ca, P and Ti ion released in the fresh (Supern_Fresh_RT. Supern_Fresh_37) or salt (Supern_Salt_RT, Supern_Salt_37) water at the different time points as reported in Figure 3.9. In detail, Ca ion in Supern_Salt was released faster and in greater quantities (1.5 - 1.8% after 28 days) than P and Ti ions, probably also because it is the prevailing ion within the apatites. On the contrary, in Supern_Fresh, at room temperatures, the quantity released is less. Regarding P ions, the different mediums does not seem to influence its release, only the sample in Supern_Fresh$_{37}$ has a higher percentage on the 28th day compared to the initial value. Ti, on the other hand, being one doping ion, shows the least quantity released (about 0,3-0,4% after 28 days) and has a more static trend, which increases only after 14 days, not being influenced by the different medium, but more by the temperature. With this evidence, therefore, it can be deduced that AlgTiHA has a slow degradation in both fresh and salt water (given the low percentage of ion release in 28 days), slightly increased by the rise in temperature.

Considering the significant environmental pollution and the accumulation of harmful by-products in both sea and freshwater, longer-term degradation tests were conducted for a duration of 2, 2,5, and 3 months. These tests involved the saltwater samples (Supern_Salt_37

and AlgTiHA_salt_37) as well as the freshwater samples (Supern_Fresh_37 and AlgTiHA_fresh_37) at 37 °C.

Figure 3.10 displays the XRD results for the 90-day time point (3 months) for both Supern_Salt_37 and Supern_Fresh_37 samples. It is evident that only the same peaks observed in the previous time points are visible, with the absence of titanium dioxide peaks (indicated by red dots in the graphs). Conversely, the XRD analysis conducted on the powders obtained from the different mediums (AlgTiHA_salt_37 and AlgTiHA_fresh_37) exhibits a spectrum similar to that of the initial AlgTiHA sample.

The other time points, for both water and powders at 60 and 75 days (2 and 2,5 months), are highlighted the same results, therefore it was not considered relevant to show them.

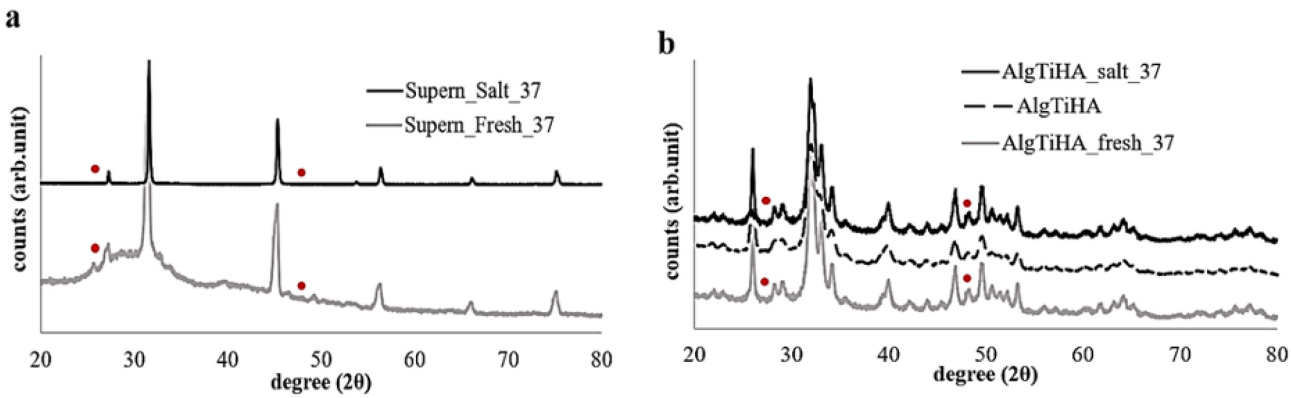

Figure 3.10. XRD spectra of a) salt and fresh water after 90 days at 37 °C (Supern_Salt_37, Supern_Fresh_37); b) powders withdrawn from salt and fresh water after 90 days at 37 °C (AlgTiHA_salt_37, AlgTiHA_fresh_37) compared to AlgTiHA spectrum. Red dots refer to TiO_2 highest intensity peaks.

As presented above, a quantitative phase analysis of XRD spectra obtained after 90 days was carried out through the Rietveld method. Observing Table 3.6, Supern_Salt_37 and Supern_Fresh_37 showed only the presence of NaCl (Halite mineral phase).

In powders (AlgTiHA_salt_37, AlgTiHA_fresh_37) instead, as already highlighted by the XRD profile, the presence of apatite is mainly recovered. The fundamental aspect, however, is that the Rietveld analysis also confirmed that TiO_2 (Anatase phase) was not present in any of the samples. The quantitative phase analysis after 60 and 75 days show a similar behaviour and as for XRD analysis they are not display.

Table 3.6. Quantitative phase analysis of salt water (Supern_Salt_37), fresh water (Supern_Fresh_37) and powders in salt water (AlgTiHA_salt_37) and powders in fresh water (AlgTiHA_fresh_37) after 90 days through Rietveld method.

Sample name	Apatite Wt%	Halite Wt%	Anatase Wt%
Supern_Salt_37	0	100	0
Supern_Fresh_37	14	86	0
AlgTiHA_salt_37	92	8	0
AlgTiHA_fresh_37	100	0	0

Through ICP analysis (Figure 3.11) the percentage of Ca, P and Ti ions released in the two different mediums (Supern_Salt_37 and Supern_Fresh_37) was evaluated after 60, 75 and 90 days, as for the other time points.

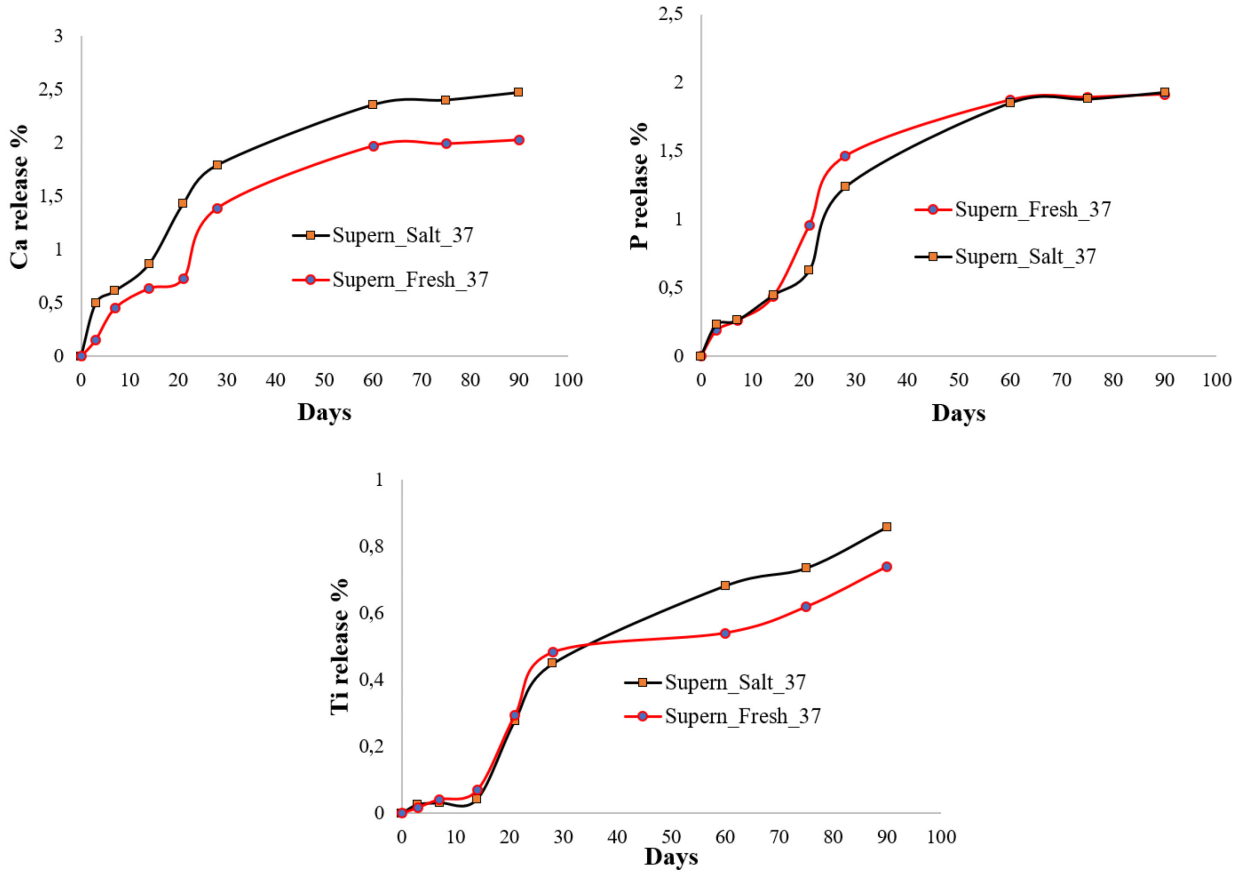

Figure 3.11. Release trend of Ca, P and Ti ions from salt water and fresh water at 37 °C (Supern_Salt_37, Supern_Fresh_37) monitored through ICP analysis after 60, 75 and 90 days.

For all three ions, there is an increasing percentage of release in both solutions compared to the previous time points. In particular, the release of Ca and P ions seems to reach a plateau point

after about 60 days, while Ti ion increase its release in salt water as compared to fresh water, but always confirming the slow degradation of AlgTiHA over time in both mediums.

The XRD and ICP analyses, confirmed the absence of TiO_2 in both, the supernatant (Supern_Fresh, Supern_Salt), and the residual powders of AlgTiHA_salt and AlgTiHA_fresh undergoing degradation, despite the use of two different mediums and the temperature variation, which further denotes the safety of this material for both human and environmental health.

Summarising the results obtained:

- XRD spectra show no typical TiO_2 peaks in both fresh and salt water, also confirmed by Rietveld analysis.
- The ICP confirms the slow degradation of AlgTiHA by releasing only the ions of which it is composed that are safe for humans and the environment.

3.3.3 In vitro evaluation of antimicrobial activity

While the cytocompatibility of AlgTiHA has been already assessed by *Campodoni et al.* showing as AlgTiHA do not compromise the cell viability[28], the antimicrobial effect of this material had not been tested before. MIC test was performed using bacterial cultures of Propionibacterium acnes and Staphylococcus aureus. The results in Table 3.7 showed that, for both strains, the minimum inhibitory concentration is close to 1 mg/mL concentration (1000 μM), considering that, at the concentration of 0.1 mg/mL, AlgTiHA induced a significant reduction in bacterial growth. This pattern is very promising indicating potential multifunctional activity for our newly synthesized compound. Indeed, multifunctionality is quite appreciated in modern formulations because it consents to reduce the number of ingredients and thus potential side effects.

Table 3.7. Antimicrobial efficacy of AlgTiHA through MIC test.

Solutions concentration (μM)	Staphylococcus aureus	Propionibacterium acnes
CTRL	0,421	0,103
1000 μM	0,012	0,003
100 μM	0,121	0,056
10 μM	0,432	0,102
1 μM	0,440	0,098
0.1 μM	0,428	0,106

3.3.4 Sunscreen formulations efficacy and safety assessment

Over the past two decades, there has been significant progress in sun protection technology. With increased awareness among consumers regarding the harmful effects of UV radiation on the skin, and the enhanced understanding of dermatologists regarding the mechanisms of such damage, there has been a growing demand for more effective sunscreen formulations, leading to numerous innovations in this field.

When formulating sun care products, the selection of ingredients involves considering various factors, including ease of use, cost, stability, and safety. Additionally, specific factors related to the efficacy of the active ingredients must be considered, such as seeking synergy between UV filters and ensuring their photostability.

In this context, our aim was to evaluate the photoprotective capabilities of AlgTiHA and its potential as a booster for Sun Protection Factor (SPF). We incorporated AlgTiHA into different cosmetic formulations, both alone and in combination with other organic and inorganic filters. Initially, three formulations were developed with increasing concentrations of AlgTiHA (3%, 5%, and 10%). Subsequently, an in vitro test was performed to determine the SPF value of these formulations, following a protocol that was previously developed by some members of our team.

The results of this study contribute to the understanding of AlgTiHA's photoprotective properties and its potential for enhancing the SPF of sunscreen formulations.[56]

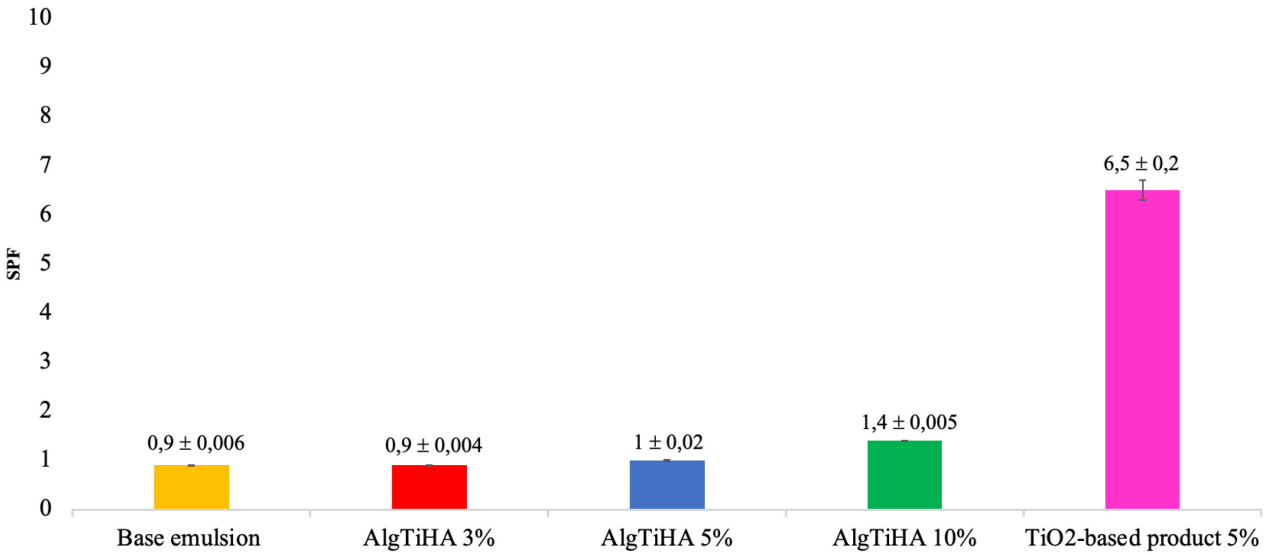

Figure 3.12. In vitro SPF value of emulsions with different AlgTiHA concentration.

During the investigation, it was observed that the presence of AlgTiHA in the emulsions did not have an impact on the SPF value measured in vitro. The SPF values obtained and presented in Figure 3.12 were comparable to those of the base emulsion without hydroxyapatite, indicating that AlgTiHA does not function as an effective inorganic UV filter. In contrast, the same emulsion formulated with a traditional TiO_2-based product (Solaveil XTP1) demonstrated an SPF value of 6.5. These findings suggest that AlgTiHA does not possess inherent SPF boosting capabilities as observed in previous studies involving organic and inorganic molecules.[4] Based on these observations, we proceeded to develop two distinct formulations, one containing organic filters and the other containing inorganic filters, to assess the SPF boosting capabilities of AlgTiHA. Figure 3.13 demonstrates the results of the in vitro test conducted on these formulations. In the case of the organic filter-based formulation, it is evident that the inclusion of AlgTiHA leads to a substantial increase in the SPF value (+64.5%). This increase is notably higher compared to the formulation containing just hydroxyapatite (HA), which resulted in an SPF boost of only 38%.

Regarding the formulation with inorganic filters, exhibited SPF values lower than those obtained with organic filters, but always showing an enhancement following the addition of AlgTiHA particles (+68%).

These findings demonstrate that AlgTiHA possesses notable SPF booster capabilities when combined with organic and inorganic filters, particularly in formulations containing organic filters. This highlights the potential of AlgTiHA as an effective ingredient for enhancing the sun protection properties of sunscreen formulations.

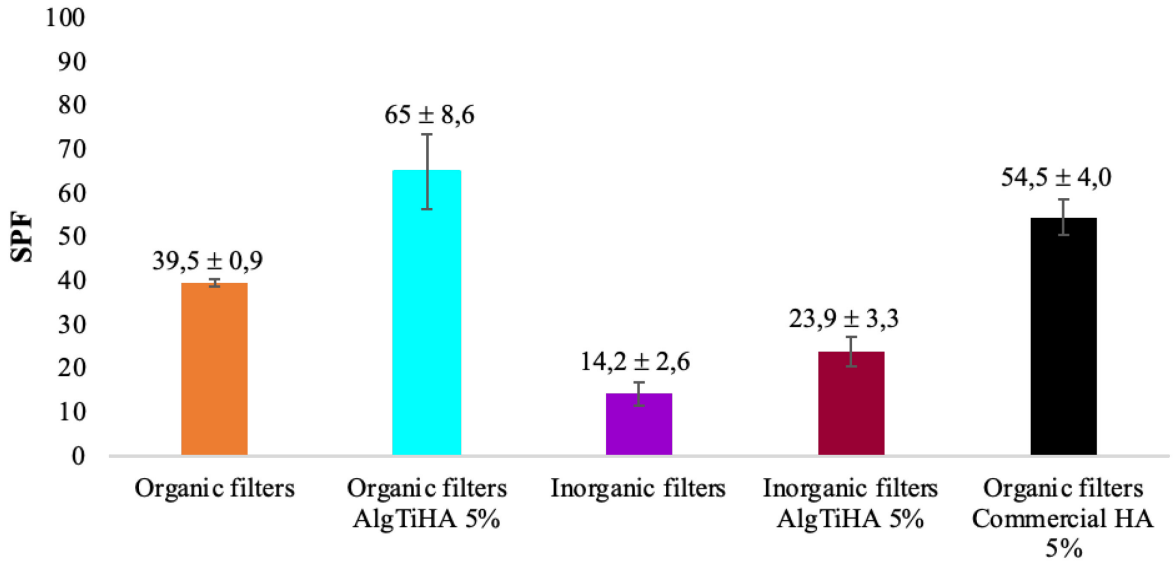

Figure 3.13. In vitro SFP values of emulsions with organic/inorganic filters and AlgTiHA.

Given the results obtained from in vitro tests for both emulsions with organic and inorganic filters, it can be deducted that AlgTiHA does not work as a filter itself but as a potent booster of both kind of filters. This function is important as that of the filters because it consents to reduce the quantity of filters in the formulation with improved safety profile for humans and the environment.

Although not mandatory in Europe the confirmation of the SPF value should be conducted on human volunteers according to the ISO 24444:2019. In other countries is even mandatory (i.e. USA) being classified over-the-counter drugs and thus definitely strongly recommended also in EU. In absence of an ISO regulation for the in vitro tests each laboratory may develop a more or less predictive procedure to guide the R&D process. On the other hand, UVA-PF should be conducted only in vitro due to ethical issues.[57]

In detail, a preliminary test carried out on 5 volunteers, showed that, in vivo, SPF data of the emulsion with organic filters, although proportionally lower than the in vitro values, showed a higher sun protection factor in the presence of AlgTiHA, confirming its booster activity. The average SPF value of the functionalized emulsion shown in Figure 3.14 is approximately 31, corresponding to a value 30% higher than that of the sunscreen with only organic filters.

Regarding emulsions with inorganic filters, also in this case the in vivo SPF data were lower than those in vitro, but still indicated a higher SPF for the emulsion containing AlgTiHA compared to that with only the inorganic filters (Figure 3.14). In particular, the average SPF value of the functionalized product is 16,7, corresponding to a value 33% higher than that of the formulation without AlgTiHA. This further confirmed the ability of this new molecule to act as a booster.

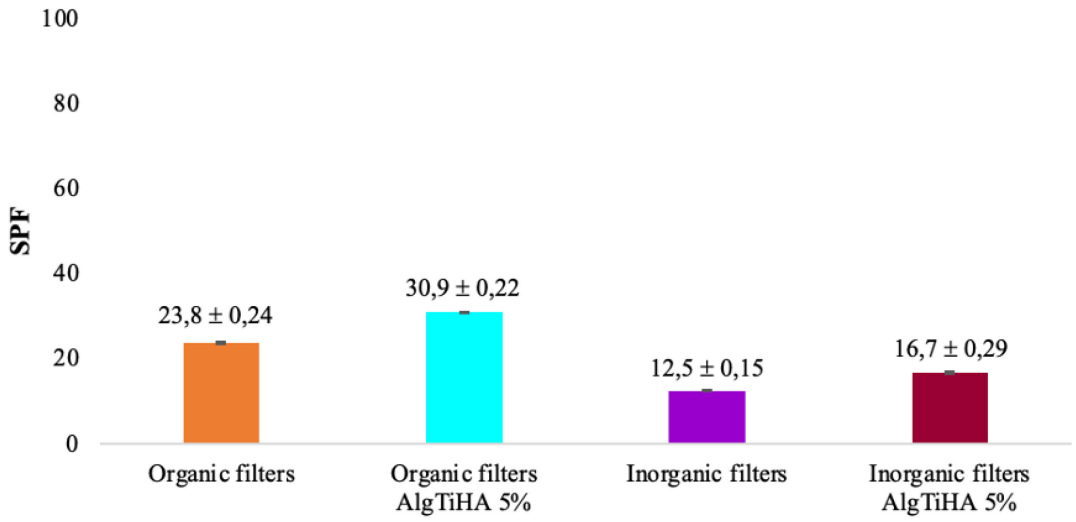

Figure 3.14. In vivo SFP values of emulsions with organic/inorganic filters and AlgTiHA.

From the results collected from the in vivo tests, the booster effect found is lower than that obtained with the in vitro test, but it is still consistent and confirms the effectiveness of AlgTiHA as a booster in sunscreen containing organic and/or inorganic filters. Thus, AlgTiHA designed as a safe ingredient for the use in sun damage protection, consented to obtain effective sunscreens without irritation even at the highest concentration tested (10%) (Figure 3.15).

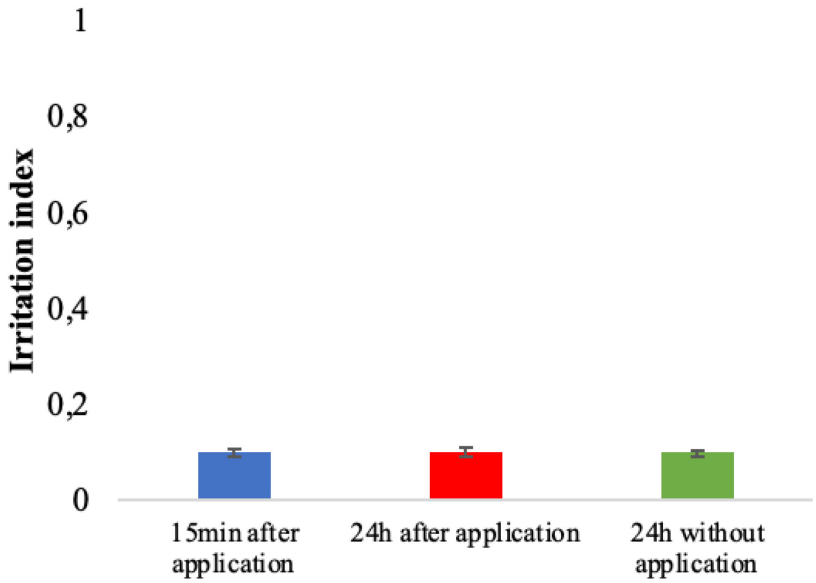

Figure 3.15. Safety test for the evaluation of the irritation index of sunscreen with the 10% AlgTiHA concentration.

Finally, having selected the two formulations containing 5% of AlgTiHA with organic and/or inorganic filters as the most effective and safest, their stability was evaluated both at room temperature and at 40 °C ± 2 at different time intervals up to 6 months, observing the possible changes to physical-chemical and organoleptic properties. Both sunscreen formulations showed maintenance of structural stability at all time points until 6 months neither at room temperature nor at 40°C, no oozing or significant change in the reference olfactory note.

Summarizing the results obtained from the in vitro and in vivo SPF and safety tests, it can be state that:

- The SPF power of AlgTiHA as a physical filter alone is not appreciable.
- AlgTiHA formulated with commercial organic and inorganic filters has an effective booster effect both in vitro and in vivo.
- It shows no signs of irritation on contact with the skin.

3.3.5 Ex vivo release and histological analysis

It is now known that, despite having significant disadvantages, there is still no possibility of giving up the use of commercial filters, especially organic ones that have a high SPF. Therefore, the development of new sunscreens containing more eco-sustainable and biocompatible UV filters, which can reduce the quantity of the most harmful commercial ones, is the focal point of this research. In fact, as demonstrated by the previous tests, the innovative UV filter formed by AlgTiHA hybrid particles formulated together with a reduced quantity of commercial organic/inorganic filters has led to the development of an eco-friendly, safe and effective sunscreen on the skin.

Based on these results, a sunscreen containing AlgTiHA was formulated together with a commercial organic filter, Benzophenone-3, known to have high SPF, but also numerous environmental and human health concerns. In this way, the possibility of using Benzophenone-3 in minimum quantities was evaluated, exploiting its UV protective capabilities and at the same time blocking, thanks to the AlgTiHA particles, its penetration under the skin.

To evaluate the real effectiveness of the combination of Benzophenone-3 and AlgTiHA, an ex vivo test was performed with OFM instrumentation. Using a human skin explant, the subcutaneous release of Benzophenone-3 at the dermis level for 24h at 32,5 °C from two formulations was analysed, one containing only the organic filter (F10) as control and the other instead mixed together with AlgTiHA (F11), simultaneously observing the ability of AlgTiHA to stabilize Benzophenone-3 and preventing its penetration under the skin.

As can be seen from Figure 3.16, following the HPLC analysis of the releases collected every 4 h, a concentration trend of Benzophenone-3 released over time by the two formulations was obtained.

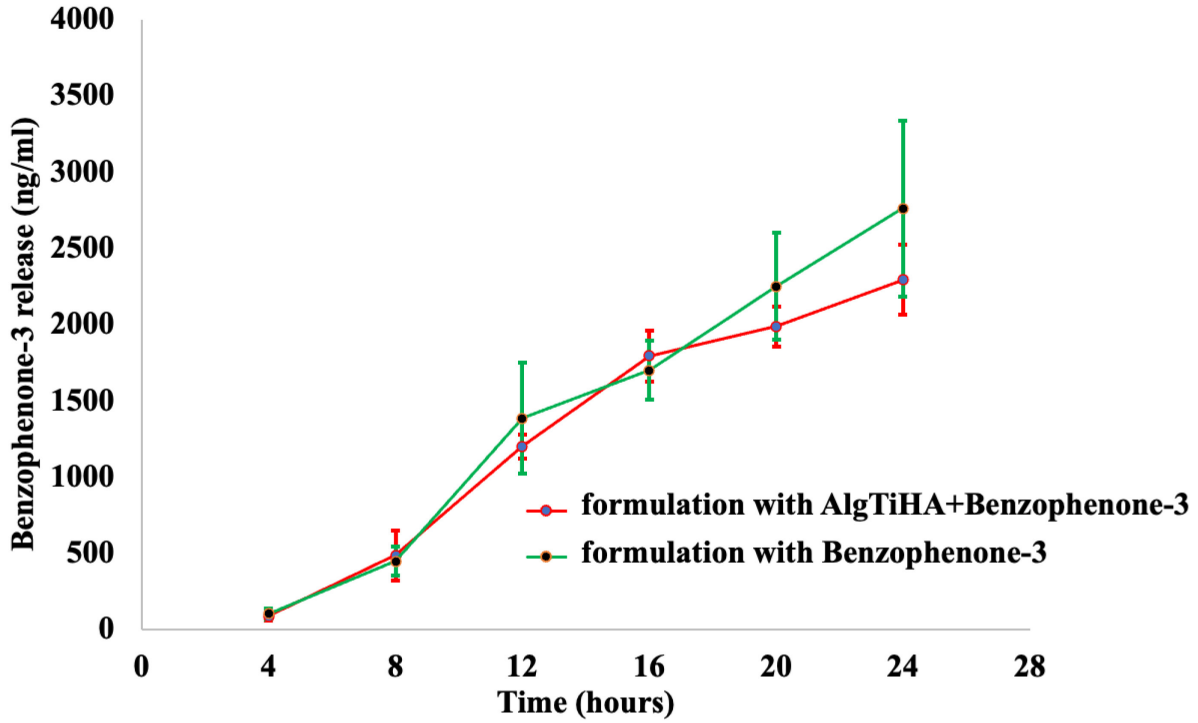

Figure 3.16. Release concentration trend of Benzophenone-3 from formulation F10 (only Benzophenone-3) and formulation F11 (AlgTiHA+Benzophenone-3) in human skin explant through HPLC analysis for 24h at 32,5 °C.

The results obtained show that the presence or absence of AlgTiHA in the sunscreen does not prevent the release of Benzophenone-3 under the skin, in fact the two formulations have a similar concentration trend, increasing over time. It is probably not possible to establish an interaction between the hybrid particles and the organic filter such as to stabilize the latter within the formulation, avoiding its penetration and therefore its possible harmful effect on the dermis.

After ex vivo release test, histological analysis was carried out on skin samples taken through biopsy to evaluate possible morphological differences in the epithelia tissue following the release of Benzophenone-3. From the images shown in Figure 3.17, no significant differences are shown on morphological level between the tissue in contact with the two formulations containing Benzophenone-3 compared to the control blank. Although Benzophenone-3 manages to penetrate the dermis, no signs of inflammation of the cellular tissue were observed, attributable to the low quantity of organic filter released, which is not sufficient to induce cytotoxic reactions in the dermis.

Although Benzophenone-3 has excellent shielding properties against UV radiation, its mixing in sunscreen with AlgTiHA particles does not prevent its penetration into the dermis and therefore the possible risk of inflammatory reactions in contact with the tissue.

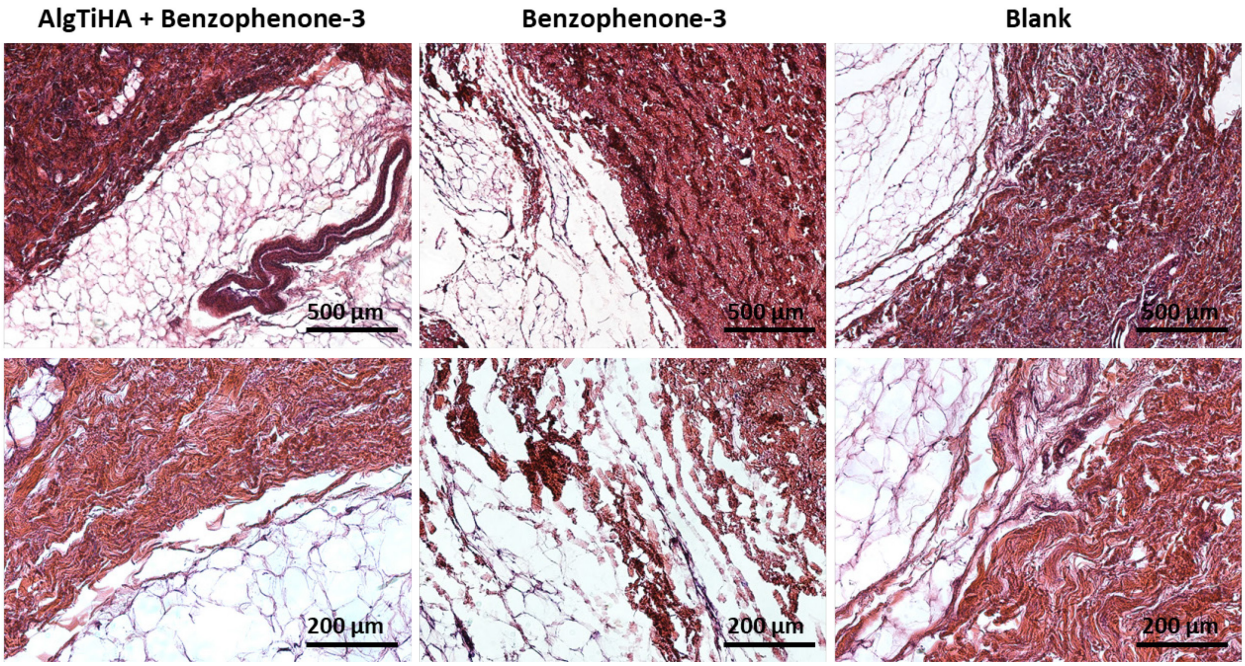

Figure 3.17. The Haematoxylin and Eosin staining of the samples is reported. Cell nuclei in violet, cytoplasm in pink.

Summarising the results obtained through ex vivo release tests and histological analysis:

- AlgTiHA particles mixed within the formulation with Benzophenone-3 are unable to stabilise the organic filter preventing its possible penetration into the dermis.
- Histological analysis of the tissues showed no particular differences between the formulations with Benzophenone-3 and the control blank, attributable to the low release of the organic substance under the skin not being sufficient to trigger an inflammatory reaction.

3.4 Conclusions

This study represents a significant advancement in the development of an eco-friendly sunscreen formulation using the novel hybrid Ti-doped hydroxyapatite UV-filter (AlgTiHA). Through an in-lab biomineralization process, we successfully created a sunscreen formulation that is more environmentally sustainable.

One of the key advantages of this formulation is the low degree of crystallinity of the hydroxyapatite, which results in limited chemical stability in aqueous environments. Over time, the hydroxyapatite gradually dissolves, releasing calcium and phosphate ions. These ions are non-toxic and naturally present in body fluids and the environment. This dissolution process contributes to the environmentally friendly nature of the formulation.

Furthermore, by incorporating titanium in the form of Ti (IV) ions rather than TiO_2, we have addressed concerns related to the photocatalytic effect and the accumulation of harmful substances in water. This choice reduces potential risks and ensures the formulation's safety for both users and the environment. Upon production, the final sunscreen formulation exhibited a higher SPF compared to formulations containing only commercial organic/inorganic filters. The hybrid AlgTiHA particles effectively boosted the SPF value, allowing for a reduction in the amount of organic/inorganic filters typically required to achieve similar levels of sun protection. This reduction in filter content is desirable for both efficacy and environmental reasons. The composition of the formulation demonstrated excellent stability over a period of six months, without any phase separation or alteration of its chemical-physical properties. In addition, the formulation exhibited antibacterial properties, inhibiting the growth of bacteria. Importantly, the complete sunscreen formulation underwent thorough testing on human volunteers and did not cause any irritation. This confirms its efficacy and safety in vivo, further supporting its potential as a promising, safer, and more environmentally friendly sunscreen product. To conclude, although AlgTiHA particles are able to reduce the use of organic/inorganic filters within the formulations, making them effective and safe as well as more eco-sustainable, some particularly protective but at the same time harmful UV filters, such as Benzophenone-3, are still dangerous. In fact, this organic filter even if formulated with AlgTiHA, is easily released from sunscreen, penetrating under the skin and demonstrating that the hybrid particles are capable of decreasing its quantity but not stabilizing it. Evidently, only the mixing in cream between the AlgTiHA particles and the Benzophenone-3 does not create such a strong interaction as to prevent its penetration into the dermis, but we will investigate the anchoring of the organic filter directly on the mineral phase during biomineralization.

References

(1) Passeron, T.; Bouillon, R.; Callender, V.; Cestari, T.; Diepgen, T. L.; Green, A. C.; van der Pols, J. C.; Bernard, B. A.; Ly, F.; Bernerd, F.; Marrot, L.; Nielsen, M.; Verschoore, M.; Jablonski, N. G.; Young, A. R. Sunscreen Photoprotection and Vitamin D Status. *British Journal of Dermatology* **2019**, 181, 916–931.

(2) Lindqvist, P. G.; Epstein, E.; Landin-Olsson, M. Sun Exposure - Hazards and Benefits. *Anticancer Research*. **2022**, 42, 1671–1677.

(3) Burnett, M. E.; Hu, J. Y.; Wang, S. Q. Sunscreens: Obtaining Adequate Photoprotection. *Dermatol Ther* **2012**, 25, 244–251.

(4) Battistin, M.; Dissette, V.; Bonetto, A.; Durini, E.; Manfredini, S.; Marcomini, A.; Casagrande, E.; Brunetta, A.; Ziosi, P.; Molesini, S.; Gavioli, R.; Nicoli, F.; Vertuani, S.; Baldisserotto, A. A New Approach to UV Protection by Direct Surface Functionalization of TiO2 with the Antioxidant Polyphenol Dihydroxyphenyl Benzimidazole Carboxylic Acid. *Nanomaterials* **2020**, 10, 231-250.

(5) Jepps, O. G.; Dancik, Y.; Anissimov, Y. G.; Roberts, M. S. Modeling the Human Skin Barrier - Towards a Better Understanding of Dermal Absorption. *Advanced Drug Delivery Reviews* **2013**, 65, 152–168.

(6) Groeber, F.; Holeiter, M.; Hampel, M.; Hinderer, S.; Schenke-Layland, K. Skin Tissue Engineering - In Vivo and in Vitro Applications. *Advanced Drug Delivery Reviews* **2011**, 63, 352–366.

(7) Friedel, M.; Thompson, I. A. P.; Kasting, G.; Polsky, R.; Cunningham, D.; Soh, H. T.; Heikenfeld, J. Opportunities and Challenges in the Diagnostic Utility of Dermal Interstitial Fluid. *Nat Biomed Eng* **2023**.

(8) Sambandan, D. R.; Ratner, D. Sunscreens: An Overview and Update. *Journal of the American Academy of Dermatology* **2011**, 64, 748–758.

(9) Gilchrest, B. A. A Review of Skin Ageing and Its Medical Therapy. *British Journal of Dermatology 1996* **1996**, 135, 867–875.

(10) Matsui, M. S.; Hsia, A.; Miller, J. D.; Hanneman, K.; Scull, H.; Cooper, K. D.; Baron, E. Non-Sunscreen Photoprotection: Antioxidants Add Value to a Sunscreen. In *Journal of Investigative Dermatology Symposium Proceedings* **2009**, 14, 56–59.

(11) Narayanan, D. L.; Saladi, R. N.; Fox, J. L. Ultraviolet Radiation and Skin Cancer. *International Journal of Dermatology* **2010**, 49, 978–986.

(12) Vuckovic, D.; Tinoco, A. I.; Ling, L.; Renicke, C.; Pringle, J. R.; Mitch, W. A. Conversion of Oxybenzone Sunscreen to Phototoxic Glucoside Conjugates by Sea Anemones and Corals. *Science* **2022**, 376, 644-648.

(13) Antoniou, C.; Kosmadaki, M. G.; Stratigos, A. J.; Katsambas, A. D. Sunscreens - What's Important to Know. *Journal of the European Academy of Dermatology and Venereology* **2008**, 22, 1110–1119.

(14) Battistin, M.; Pascalicchio, P.; Tabaro, B.; Hasa, D.; Bonetto, A.; Manfredini, S.; Baldisserotto, A.; Scarso, A.; Ziosi, P.; Brunetta, A.; Brunetta, F.; Vertuani, S. A Safe-by-Design Approach to "Reef Safe" Sunscreens Based on ZnO and Organic UV Filters. *Antioxidants* **2022**, 11, 2209-2224.

(15) Schlumpf, M.; Cotton, B.; Conscience, M.; Haller, V.; Steinmann, B.; Lichtensteiger, W. *In Vitro and in Vivo Estrogenicity of UV Screens* **2001**, 109, 239-244.

(16) Miura, F.; Enomoto, Y.; Dairiki, R.; Ito, T. Amplification-Free Whole-Genome Bisulfite Sequencing by Post-Bisulfite Adaptor Tagging. *Nucleic Acids Res* **2012**, 40, e136.

(17) Rabani, I.; Lee, S. H.; Kim, H. S.; Yoo, J.; Hussain, S.; Maqbool, T.; Seo, Y. S. Engineering-Safer-by Design ZnO Nanoparticles Incorporated Cellulose Nanofiber Hybrid for High UV Protection and Low Photocatalytic Activity with Mechanism. *J Environ Chem Eng* **2021**, 9, 105845.

(18) Tortini, G.; Ziosi, P.; Cesa, E.; Molesini, S.; Baldini, E.; De Lucia, D.; Rossi, C.; Durini, E.; Vertuani, S.; Manfredini, S. Criticisms in the Development of High-Protection and Broad-Spectrum "Natural/Organic" Certifiable Sunscreen. *Cosmetics* **2022**, 9, 56-84.

(19) Baldisserotto, A.; Baldini, E.; Ravarotto, S.; Cesa, E.; De Lucia, D.; Durini, E.; Vertuani, S.; Manfredini, S.; Michniak-Kohn, B. B. Expert Systems for Predicting the Bioavailability of Sun Filters in Cosmetic Products, Software vs. Expert Formulator: The Benzophenone-3 Case. *Pharmaceutics* **2022**, 14, 1815-1834.

(20) Labille, J.; Catalano, R.; Slomberg, D.; Motellier, S.; Pinsino, A.; Hennebert, P.; Santaella, C.; Bartolomei, V. Assessing Sunscreen Lifecycle to Minimize Environmental Risk Posed by Nanoparticulate UV-Filters – A Review for Safer-by-Design Products. *Frontiers in Environmental Science* **2020**, 8.

(21) Hanigan, D.; Truong, L.; Schoepf, J.; Nosaka, T.; Mulchandani, A.; Tanguay, R. L.; Westerhoff, P. Trade-Offs in Ecosystem Impacts from Nanomaterial versus Organic Chemical Ultraviolet Filters in Sunscreens. *Water Res* **2018**, 139, 281–290.

(22) Downs, C. A.; Diaz-Cruz, M. S.; White, W. T.; Rice, M.; Jim, L.; Punihaole, C.; Dant, M.; Gautam, K.; Woodley, C. M.; Walsh, K. O.; Perry, J.; Downs, E. M.; Bishop, L.; Garg, A.; King, K.; Paltin, T.; McKinley, E. B.; Beers, A. I.; Anbumani, S.; Bagshaw, J. Beach Showers as Sources of Contamination for Sunscreen Pollution in Marine Protected Areas and Areas of Intensive Beach Tourism in Hawaii, USA. *J Hazard Mater* **2022**, 438, 129546.

(23) Sharifan, H. Alarming the Impacts of the Organic and Inorganic UV Blockers on Endangered Coral's Species in the Persian Gulf: A Scientific Concern for Coral Protection. *Sustainable Futures* **2020**, 2, 100017.

(24) Slomberg, D. L.; Catalano, R.; Bartolomei, V.; Labille, J. Release and Fate of Nanoparticulate TiO2 UV Filters from Sunscreen: Effects of Particle Coating and Formulation Type. *Environmental Pollution* **2021**, 271, 116263.

(25) Danovaro, R.; Bongiorni, L.; Corinaldesi, C.; Giovannelli, D.; Damiani, E.; Astolfi, P.; Greci, L.; Pusceddu, A. Sunscreens Cause Coral Bleaching by Promoting Viral Infections. *Environ Health Perspect* **2008**, 116, 441–447.

(26) Burnett, M. E.; Wang, S. Q. Current Sunscreen Controversies: A Critical Review. *Photodermatology Photoimmunology and Photomedicine* **2011**, 27, 58–67.

(27) Righi, S.; Prato, E.; Magnani, G.; Lama, V.; Biandolino, F.; Parlapiano, I.; Carella, F.; Iafisco, M.; Adamiano, A. Calcium Phosphates from Fish Bones in Sunscreen: An LCA and Toxicity Study of an Emerging Material for Circular Economy. *Science of the Total Environment* **2023**, 862, 160751.

(28) Campodoni, E.; Montanari, M.; Artusi, C.; Bergamini, L.; Bassi, G.; Destro, E.; Fenoglio, I.; Panseri, S.; Tampieri, A.; Sanson, A.; Sandri, M. Biomineralization: A New Tool for Developing Eco-Sustainable Ti-Doped Hydroxyapatite-Based Hybrid UV Filters. *Biomaterials Advances* **2023**, 151, 213474.

(29) Campodoni, E.; Montanari, M.; Artusi, C.; Bassi, G.; Furlani, F.; Montesi, M.; Panseri, S.; Sandri, M.; Tampieri, A. Calcium-Based Biomineralization: A Smart Approach for the Design of Novel Multifunctional Hybrid Materials. *Journal of Composites Science* **2021**, 5, 278-302.

(30) Liu, J.; Yang, S.; Li, X.; Yan, Q.; Reaney, M. J. T.; Jiang, Z. Alginate Oligosaccharides: Production, Biological Activities, and Potential Applications. *Comprehensive Reviews in Food Science and Food Safety* **2019**, 18, 1859–1881.

(31) Romanhole, R. C.; Fava, A. L. M.; Tundisi, L. L.; Macedo, L. M. de; Santos, É. M. dos; Ataide, J. A.; Mazzola, P. G. Unplanned Absorption of Sunscreen Ingredients: Impact of Formulation and Evaluation Methods. *International Journal of Pharmaceutics* **2020**, 591, 120013.

(32) Adamiano, A.; Sangiorgi, N.; Sprio, S.; Ruffini, A.; Sandri, M.; Sanson, A.; Gras, P.; Grossin, D.; Francès, C.; Chatzipanagis, K.; Bilton, M.; Marzec, B.; Varesano, A.; Meldrum, F.; Kröger, R.; Tampieri, A. Biomineralization of a Titanium-Modified Hydroxyapatite Semiconductor on Conductive Wool Fibers. *J Mater Chem B* **2017**, 5, 7608–7621.

(33) Chavda, V. P.; Acharya, D.; Hala, V.; Daware, S.; Vora, L. K. Sunscreens: A Comprehensive Review with the Application of Nanotechnology. *Journal of Drug Delivery Science and Technology* **2023**, 86, 104720.

(34) Li, C. C.; Lin, Y. T.; Chen, Y. T.; Sie, S. F.; Chen-Yang, Y. W. Improvement in UV Protection Retention Capability and Reduction in Skin Penetration of Benzophenone-3 with Mesoporous Silica as Drug Carrier by Encapsulation. *J Photochem Photobiol B* **2015**, 148, 277–283.

(35) *Scientific Committee on Consumer Products SCCP OPINION ON Benzophenone-3 COLIPA N° S38*; **2008**. http://ec.europa.eu/health/ph_risk/risk_en.htm.

(36) Songkro, S.; Lo, N.; Tanmanee, N.; Maneenuan, D.; Boonme, P. *In Vitro Release, Skin Permeation and Retention of Benzophenone-3 from Microemulsions (o/w and w/o)*. Journal of Drug Delivery Science and Technology **2014**, 24, 703-711.

(37) Bodenlenz, M.; Aigner, B.; Dragatin, C.; Liebenberger, L.; Zahiragic, S.; Höfferer, C.; Birngruber, T.; Priedl, J.; Feichtner, F.; Schaupp, L.; Korsatko, S.; Ratzer, M.; Magnes, C.; Pieber,

T. R.; Sinner, F. Clinical Applicability of DOFM Devices for Dermal Sampling. *Skin Research and Technology* **2013**, 19, 474–483.

(38) Eirefelt, S.; Hummer, J.; Basse, L. H.; Bertelsen, M.; Johansson, F.; Birngruber, T.; Sinner, F.; Larsen, J.; Nielsen, S. F.; Lambert, M. Evaluating Dermal Pharmacokinetics and Pharmacodymanic Effect of Soft Topical PDE4 Inhibitors: Open Flow Microperfusion and Skin Biopsies. *Pharm Res* **2020**, 37, 243-255.

(39) Paz, C. V.; Ung, F.; Zárate, J.; Cortés, J. A. Evaluation of Surface Phenomena Involved in Photocatalytic Degradation of Acid Blue 9 by TiO2 Catalysts of Single and Mixed Phase – A Theoretical and Experimental Study. *Appl Surf Sci* **2020**, 508, 145114.

(40) Levine, A. Sunscreen Use and Awareness of Chemical Toxicity among Beach Goers in Hawaii Prior to a Ban on the Sale of Sunscreens Containing Ingredients Found to Be Toxic to Coral Reef Ecosystems. *Mar Policy* **2020**, 117, 103875.

(41) Andrews, J. M. Determination of Minimum Inhibitory Concentrations. *Journal of Antimicrobial Chemotherapy* **2001**, 48, 5–16.

(42) Tortini, G.; Ziosi, P.; Cesa, E.; Molesini, S.; Baldini, E.; De Lucia, D.; Rossi, C.; Durini, E.; Vertuani, S.; Manfredini, S.; Criticisms in the Development of High-Protection and Broad-Spectrum "Natural/Organic" Certifiable Sunscreen. *Cosmetics* **2022**, 9, 56.

(43) COMMISSION RECOMMENDATION of 22 September 2006 on the Efficacy of Sunscreen Products and the Claims Made Relating Thereto. *Official Journal of the European Union* **2006**.

(44) The SCCS Notes of Guidance for the Testing of Cosmetic Ingredients and Their Safety Evaluation, 11th Revision, 30-31 March 2021, SCCS/1628/21. *Regul Toxicol Pharmacol* **2021**, 127, 105052.

(45) Tan, Y. M.; Barton, H. A.; Boobis, A.; Brunner, R.; Clewell, H.; Cope, R.; Dawson, J.; Domoradzki, J.; Egeghy, P.; Gulati, P.; Ingle, B.; Kleinstreuer, N.; Lowe, K.; Lowit, A.; Mendez, E.; Miller, D.; Minucci, J.; Nguyen, J.; Paini, A.; Perron, M.; Phillips, K.; Qian, H.; Ramanarayanan, T.; Sewell, F.; Villanueva, P.; Wambaugh, J.; Embry, M. Opportunities and Challenges Related to Saturation of Toxicokinetic Processes: Implications for Risk Assessment. *Regulatory Toxicology and Pharmacology* **2021**, 127, 105070.

(46) Bodenlenz, M.; Tiffner, K. I.; Raml, R.; Augustin, T.; Dragatin, C.; Birngruber, T.; Schimek, D.; Schwagerle, G.; Pieber, T. R.; Raney, S. G.; Kanfer, I.; Sinner, F. Open Flow Microperfusion as a Dermal Pharmacokinetic Approach to Evaluate Topical Bioequivalence. *Clin Pharmacokinet* **2017**, 56, 91–98.

(47) Hofmann, E.; Fink, J.; Eberl, A.; Prugger, E.-M.; Kolb, D.; Luze, H.; Schwingenschuh, S.; Birngruber, T.; Magnes, C.; Mautner, S. I.; Kamolz, L.-P.; Kotzbeck, P. A Novel Human Ex Vivo Skin Model to Study Early Local Responses to Burn Injuries. *Sci Rep* **2021**, 11, 364-377.

(48) Bassi, G.; Panseri, S.; Dozio, S. M.; Sandri, M.; Campodoni, E.; Dapporto, M.; Sprio, S.; Tampieri, A.; Montesi, M. Scaffold-Based 3D Cellular Models Mimicking the Heterogeneity of Osteosarcoma Stem Cell Niche. *Sci Rep* **2020**, 10, 22294.

(49) Megías M, Molist P, Pombal MA. Atlas of Plant and Animal Histology. *http://mmegias.webs.uvigo.es/index.html*.

(50) Tampieri, A.; D'Alessandro, T.; Sandri, M.; Sprio, S.; Landi, E.; Bertinetti, L.; Panseri, S.; Pepponi, G.; Goettlicher, J.; Bañobre-López, M.; Rivas, J. Intrinsic Magnetism and Hyperthermia in Bioactive Fe-Doped Hydroxyapatite. *Acta Biomater* **2012**, 8, 843–851.

(51) Luz, G. M.; Mano, J. F. Mineralized Structures in Nature: Examples and Inspirations for the Design of New Composite Materials and Biomaterials. *Compos Sci Technol* **2010**, 70, 1777–1788.

(52) Kuzema, P. O.; Stavinskaya, O. N.; Laguta, I. V.; Kazakova, O. A. Thermogravimetric Study of Water Affinity of Gelatin Materials. In *Journal of Thermal Analysis and Calorimetry* **2015**, 122, 1231–1237.

(53) Zhao, X.; Ng, S.; Heng, B. C.; Guo, J.; Ma, L.; Tan, T. T. Y.; Ng, K. W.; Loo, S. C. J. Cytotoxicity of Hydroxyapatite Nanoparticles Is Shape and Cell Dependent. *Arch Toxicol* **2013**, 87, 1037–1052.

(54) Caudillo-Flores, U.; Muñoz-Batista, M. J.; Kubacka, A.; Zárate-Medina, J.; Cortés, J. A.; Fernández-García, M. Measuring and Interpreting Quantum Efficiency of Acid Blue 9 Photodegradation Using TiO2-Based Catalysts. *Appl Catal A Gen* **2018**, 550, 38–47.

(55) He, T.; Tsui, M. M. P.; Mayfield, A. B.; Liu, P.-J.; Chen, T.-H.; Wang, L.-H.; Fan, T.-Y.; Lam, P. K. S.; Murphy, M. B. Organic Ultraviolet Filter Mixture Promotes Bleaching of Reef Corals upon the Threat of Elevated Seawater Temperature. *Science of The Total Environment* **2023**, 876, 162744.

(56) Dimitrovska Cvetkovska, A.; Manfredini, S.; Ziosi, P.; Molesini, S.; Dissette, V.; Magri, I.; Scapoli, C.; Carrieri, A.; Durini, E.; Vertuani, S. Factors Affecting SPF in Vitro Measurement and Correlation with in Vivo Results. *Int J Cosmet Sci* **2017**, 39, 310–319.

(57) *Guidelines on Technical Definitions and Criteria for Natural and Organic Cosmetic Ingredients and Products-Part 1: Definitions for Ingredients ISO 16128-1:2016*; Geneva, Switzerland, **2016**.

CHAPTER 4

Conclusions

The need for a new generation of biomaterials that follow the principles of the circular economy, applicable to different fields, is one of the key points of our century. In particular, it is essential to be able to eliminate the use of non-renewable raw materials wherever possible, replacing them with biodegradable materials derived from industrial waste or natural sources, which can then be recycled, avoiding excessive costs and damage to the environment and the human health.

Based on these concepts, the aim of this research work, was to design and develop innovative ad eco-sustainable biomaterials for the healthcare sector. More specifically, two completely different biomaterials have been developed, one a porous and fully polymeric 3D device with high potential in the field of mechanical ventilation of patients and the other, a biohybrid particulate which has highlighted considerable interest for cosmetics, both designed in the concept of eco-sustainable processes (green chemical synthesis and waste recycling) and with low environmental impact. In order to achieve this goal, the following crucial steps were taken. First of all, the characteristics of each product were carefully considered and evaluated in order to select the most suitable biomaterial, i.e. the biocompatible and biodegradable material suitable for the purpose. As regards the HME filter, natural polymers such as gelatin and chitosan, by carefully studying the respiratory system, were chosen because they are able to mimic the chemical composition of the nasal mucosa, following the principles of biomimetics. Furthermore, these biopolymers coming from food industry waste, were selected to make the final polymeric compound completely eco-sustainable and limit raw materials costs. Subsequently, the prototyping, i.e. the freeze-drying and cross-linking processes, was optimized to obtain the 3D filter construct with the appropriate porosity, low pressure drop, structural stability and desired wettability, limiting the process costs and the environmental impact for its industrialization. Once the device had been created, in-depth characterization was carried out on several fronts up to validation with a ventilation device in a hospital environment. This made it possible to highlight the effectiveness of the HME device in terms of microbial filtration and heat and moisture exchange, as well as the main obstacles they had to overcome.

Moving on to the biomaterial with cosmetic application, a hybrid compound in form of micro-particulate was developed, consisting of biomimetic and environmental friendly hydroxyapatite nanoparticles nucleated on alginate matrix through a nature-inspired biomineralization process. Thanks to the versatility of its crystalline lattice and of the synthesis process, the hydroxyapatite was doped with titanium ions (Ti^{4+}) to confer to the hybrid particles (AlgTiHA) reflective properties and a SPF booster effect, thus, to be involved for the development of more eco-sustainable products for UV protection. In fact, compared to the inorganic TiO_2 filter typically used in commercial sunscreen, this new physical filer exploits shielding capacity, eliminating the risk of photocatalytic effect and environmental pollution associated instead with the dioxide. In addition, the organic matrix makes the compound more biodegradable, easier to formulate in sunscreen and, being of plant origin, more appreciated by the cosmetic sector. A sunscreen formulation was then developed and carefully characterized leading to in vivo testing that prove its efficacy as a safe and environmentally friendly sunscreen product. In this regard, its SPF booster capacity was highlighted by reducing the amount of commercial filters normally present in sunscreens and the environmental damage associated with their use. Furthermore, being composed entirely of natural and biocompatible materials, its release into the water does not cause damage to the marine ecosystem or to human health.
Both biomaterials developed in this work, exploiting natural resources and green processes, have made it possible to obtain eco-sustainable, but at the same time safe and effective products, in one case to assist patients in intensive care or anesthetized subjected to mechanical ventilation and in the other as cosmetic product for sun protection, more respectful for the skin and the environment.

Acknowledgments

I would like to thank all the partners who collaborated for the creation and carrying out of the two research projects, **MEDFil** and **ProtecTHA**, which were the founding aim of my PhD research activity: Pollution S.r.l, the Institute of Atmospheric Sciences and Climate (ISAC-CNR), the Institute for Organic Synthesis and Photoreactivity (ISOF-CNR), Montecatone Hospital, Consorzio Futuro in Ricerca (CFR), Joanneum Research Institute, AmbrosiaLab S.r.l.